APPLICATIONS OF BIONANOTECHNOLOGY

by

Christophe Pejoux

A dissertation submitted to the Graduate Faculty in Chemistry in partial fulfillment of the

requirements for the degree of Doctor of Philosophy,

The City University of New York.

2011

© 2011

Christophe Pejoux

All Rights Reserved

This manuscript has been read and accepted for the Graduate Faculty in Chemistry in satisfaction for the dissertation requirement for the degree of Doctor of Philosophy.

Dr. Hiroshi Matsui

January 28, 2011 _____
Chair of Examining Committee

Dr. Mahesh Lakshman

January 28, 2011 _____
Executive Officer

Dr. Charles Michael Drain
Dr. Lynn C. Francesconi
Dr. Harry D. Gafney
Supervisory Committee

THE CITY UNIVERSITY OF NEW YORK

Abstract

Applications of Bionanotechnology

by

Christophe Pejoux

Adviser: Dr. Hiroshi Matsui

The aim of nanotechnology is to devise technologies at the crossroads of chemistry, physics and biology to shape matter at the atomic scale to form nanosized functional objects and to arrange them into intricate assemblies to elaborate new devices. Today, its biological aspect is largely emphasized to tackle biomedical issues such as pathogen identification, disease diagnosis and treatment. In this respect, interdigitated electrodes were employed to monitor the presence of harmful bacteria, then to attempt to detect human PC3 carcinoma prostate cells as well as the size variation of stimulus-responsive hydrogel beads designed for drug delivery. Our second project aimed at demonstrating the potential use of TiO_2-labeled antibodies as substitute for horse-radish peroxidase-labeled antibodies for Enzyme-Linked ImmunoSorbent Assays (ELISA). Our last project revolved around harnessing the enzymatic activity of urease to grow silver-sulfide nanoparticles.

Acknowledgments

I would like to thank my advisor Dr. Hiroshi Matsui for offering me the opportunity to conduct research in his laboratory without any money constraint and for guiding me along the years.

I am sincerely grateful to Dr. Charles Michael Drain (Hunter College), Dr. Lynn C. Francesconi (Hunter College) and Dr. Harry D. Gafney (Queens College) for their pertinent comments and valuable advice as well as their time, knowing their busy schedule.

I am especially indebted to Dr. Roberto de la Rica (formerly at Hunter College), with whom I had the privilege to work. Roberto did not only teach me a lot about interdigitated electrodes and proteins, the main subjects of my thesis, but was also a real source of inspiration and a model to follow.

I would like to express my gratitude to MengLu Shi (Matsui lab, Hunter College) for having taken an active role in the continuation of the cancer-cell project and I wish her the best to bring it to a successful completion. MengLu also worked on the hydrogel-bead and the TiO_2-labeled antibody projects.

I am really grateful to Dr. Sebastian Thompson (formerly at Hunter College) and M.D. He Liu (Cornell University) to have taught me how to culture and stain cells from scratch.

I would like to thank the entire Foster lab (Hunter College) for the unlimited access to their tissue-culture room as well as their tips related to cell culturing.

I am grateful to Dr. Jorge Morales (Manager of the Electron Microscopy, City College) and to Dr. Chu-Min Feng (City College) for providing me guidance and assistance when I had to use the TEM and the SEM, and for giving me the JCPDS and teaching me how to utilize a glove box, respectively.

I would like to express my gratitude to Zhichen Zu (Suskivishli lab, Stevens Institute of Technology, New Jersey) and to Dr. Louise Birchall (Ulijn lab, University of Strathclyde, Scotland) for their generous gift (hydrogel beads).

I would like to thank Dr. Raquel Perez-Castillejos (New Jersey Institute of Technology), M.D Neil H. Bander (Cornell University), and Dr. Antonio Baldi (Instituto de Microelectronica de Barcelona, Spain) for taking the time to answer my questions.

I would like to express my gratitude to the current and past members of Matsui lab (Prerna Kaur, Luona Anjia, Hanying Bai, Kristina Fabijanic, Dr. Gao Xueyun, Amit Haboosheh, Parminder Kaur, Dr. Jung-Sun Lim, Dr. Nurxat Nuraje, Dr. Yoshiaki Maeda, Wei Su and Zengyan Wei.) as well as to the whole Department of Chemistry of Hunter College for their assistance in the daily life at Hunter College.

I am also grateful to Dr. David Fidock (Columbia University) to have lent me a laptop, allowing me to write my thesis at home, in other words in the best possible conditions.

I am fully indebted to my Family, which includes my fiancée Dr. Sophie Adjalley (Columbia University), for their strong moral support.

Table of Contents

List of Tables

Lists of Figures

Introduction.

One aim of nanotechnology is to devise technologies at the crossroads of chemistry, physics and biology, able on one hand, to shape matter at the atomic scale (where it exhibits novel properties) to form nanosized functional objects and on the other hand to arrange them into intricate architectures to elaborate new devices. The difficulty of those tasks lies in the direct limitation of our human sight and physical grasp, which are not suited for manipulating and positioning atoms.

Although those operations appear extremely challenging, history has already recorded several successes well before the word nanotechnology was even coined. For instance, gold and silver nanoparticles have already been synthesized by medieval craftsmen to create vibrant-ruby and bright-yellow colors of stained glass, respectively.[1] Their plasmon-polariton absorption stemming from their very small size, the interparticle spacing and their close chemical environment, determine the color exhibited by the stained glass. In addition, the steel of a Damascus sabre from the seventeenth century is believed to contain brittle cementite (Fe_3C) nanowires encased in carbon nanotubes, whose extraordinary mechanical properties reflect in the exceptional qualities of the blade.[2] Through annealing and forging, catalytic elements present in the wootz[1] (Appendix 10) segregate in layers, promote the formation of carbon nanotubes, which in turn induce the growth of cementite nanowires, and finally results in the banding pattern of Damascus-sabre blades. A more recent field perfectly exemplifies nanotechnology by assembling various nanostructures to create a light sensor as well as a hard-copy image display: silver-halide based photography.[3] J-aggregates of dye

molecules and chemical-sensitization centers such as $(Ag_2S)_2Au$, are grown on the surface of silver-halide microcrystals. Subjected to light exposure, the former ones photogenerate electron/hole pairs whose negative elements are directly injected into the silver-halide microcrystals, while the latter ones trap them permitting their reaction with interstitial silver ions (originated from the microcrystals), resulting in the formation of atomic silver clusters, called latent images. In the presence of a reducing agent, the latent images catalyze the reduction of exposed silver-halide microcrystals into silver, allowing the discrimination between exposed and unexposed microcrystals, leading to the formation of an image.[3]

In the past, the field of applications of nanotechnology was exclusively confined to the synthesis of functional materials and their integration into devices. Today, nanotechnology aims at tackling biomedical issues such as pathogen identification, disease diagnosis and treatment. To do so, nanotechnology intends to establish in vivo diagnostics and treatment systems, which could benefit the development of tools capable of shedding light on the biology of living organisms and to design highly-sensitive portable high-throughput screening diagnostics technologies.

To enter the biomedical realm, nanotechnology has to combine the properties (absorption, fluorescence, magnetism, uptake of "skillful" molecules, etc…) of nanoparticles with the recognition ability of biomolecules (antibodies, aptamers, peptides, biotin/avidin, etc…) by covalently attaching them to create nanoparticle/biomolecule hybrids. In vivo, these hybrids are expected to mediate the imaging of abnormal cells[2], their repair or their degradation. There are several ways to degrade abnormal cells: either by locally generating heat [4] or reactive oxygen species [5, 6], or by releasing nearby

drugs displayed on the nanoparticle surface (covalent bonds ruptured by heat [7]) or encapsulated in the nanoparticle [8, 9]. In the last example, the drug delivery is triggered by the nanoparticle-conformation change induced by an external stimulus. Here are some examples of promising hybrids for in vivo applications.

Xie Jin, Chen Kai, Lee Ha-Young, Xu Chenjie, Hsu Andrew R., Peng Sheng, Chen Xiaoyuan and Sun Shouheng have successfully and easily synthesized cyclic-RGDyK-peptide-coated Fe_3O_4 nanoparticles able to specifically target integrin $\alpha_v\beta_3$-rich tumor cells (implanted in mice) and to make them visible via Magnetic Resonance Imaging by drastically enhancing their contrast.[10] These hybrids were able to travel through the blood stream of the animals, to likely cross their blood brain barrier (the mice were sacrificed four hours after the hybrids injection) thanks to their small size (8.5nm) and a significant number of them did reach their target while avoiding the uptake by macrophages and the deposition in liver, spleen and kidneys.

Using cobalt nanoparticles as sacrificial templates, Schwartzberg Adam M., Olson Tammy Y., Talley Chad E. and Zhang Jin Z. prepared hollow gold nanoshells, whose surface-plasmon band-absorption peak was tuned between 550 and 820nm by controlling their inner diameter and thickness.[11] Then, Melancon Marites P., Lu Wei, Yang Zhi, Zhang Rui, Cheng Zhi, Elliot Andrew M., Stafford Jason, Olson Tammy, Zhang Jin Z., Li Chun employed them in photothermal-ablation therapy [4]: they conjugated 30nm hollow gold nanoshells (strongly absorbing in the NIR) with anti-EGFR[3] monoclonal antibody (functionalized in turn with a ligand able to bind the γ emitter ^{111}In), and afterwards coated them with thiolated PEG. Those nanoshells were shown to preferentially accumulate within EGFR-rich cells (such as tumor cells) via

EGFR-mediated endocytosis. When exposed to NIR irradiation, they appear to promote in vitro and in vivo the death of EGFR-rich cells by locally producing heat. Two other strings were added to the bow of those nanoshells: they permit the in vitro imaging of tumors by light-scattering dark-field optical microscopy and the determination of their distribution within the tissues of a mouse by measuring the radiotracer emission intensity. Moreover, they do not contain any cytotoxic elements like CTAB[4] or silica.

Rozhkova Elena A., Ulasov Ilya, Lai Barry, Dimitrijevic Nada M., Lesniak Maciej S. and Rajh Tijana labeled anti-IL13R2R[5] antibodies with 5nm DOPAC[6]-coated TiO_2 nanoparticles and were able to specifically photokill cells affected by glioblastoma multiforme, a primary brain cancer form, via the photogeneration of reactive oxygen species.[5] The importance of DOPAC lies in the fact that it shifts the absorption of pure TiO_2 into the visible (up to the NIR) by the formation of a ligand-to-particle charge-transfer and to provide a carboxylic group on which the EDC/NHS[7] method could be used to attach an antibody.

The ideal pursued by nanotechnology in the biomedical field is to craft versatile nanoplatforms like Kopelman Raoul, Koo Yong-Eun Lee, Philbert Martin, Moffat Bradford A., Reddy G. Ramachandra, McConville Patrick, Hall Daniel E., Chenevert Thomas L., Swaroop Bhojani Mahaveer, Buck Sarah M., Rehemtulla Alnawaz and Ross Brian D. did.[6] Their NanoPEBBLEs[8] did photokill brain-tumor cells (from mice) in vivo and allowed their imaging through MRI. They are (30-60 nm) polyacrylamide nanoparticles displaying cyclic RGD-based peptides and PEG on their surface to specifically interact with integrin $\alpha_v\beta_3$-rich tumor cells, to reduce non-specific adsorption and increase their plasma residence time, respectively. They encapsulate iron-

oxide nanoparticles and Photofrin®, a commercial photodynamic agent, to mediate the visualization of tumor cells through MRI and to produce reactive oxygen species lethal to them, respectively. Furthermore, their positioning at the surface of the tumor cells circumvents the natural mechanisms of defense expressed by the latter ones such as multi-drug resistance[9].

Besides those hybrids, tremendous efforts are invested on nanoparticles to deliver drugs when exposed to external stimulus. They might, in the future, be tethered to biorecognition entities to improve their efficiency.

Samsam Bakhtiari Amir Bahman, Hsiao Dennis, Jin Guoxia, Gates Byron D. and Branda Neil R. figured out that heat could be used not only for photothermal-ablation therapy, but also to command the release of poisonous or therapeutic agents attached covalently on nanoshells by selective bond cleavage.[7] To prove their concept, they prepared a would-be fluorescent molecule: they fused (via a Diels-Alder reaction) a fluorescein molecule displaying a furan moiety to a long aliphatic chain terminated by an imide function and a mercapto group (which allows the attachment of the would-be fluorescent dye on the gold nanoshells). The NIR absorption by the gold nanoshells increased the temperature nearby and activated the retro-Diels-Alder reaction, bringing about the release of the modified fluorescein, while leaving the long aliphatic connected to the gold-nanoshell surface. The freed modified fluorescein molecules do fluoresce and there are no free thiols, which could trigger side reactions.

An alternative approach relies on hydrogel nanoparticles that encapsulate drugs whose release is activated by external parameters like temperature. Temperature

tunes the affinity of the hydrogel polymer chains towards water molecules.[12] Below the lower critical solution temperature, hydrogel nanoparticles adopt an extended conformation, useful to retain drugs and above it a collapsed one, which frees them. For instance, Li Dongxiang, He Qiang, Cui Yue, Wang Kewei, Zhang Xiaoming and Li Jumbai succeeded in growing a copolymer made of NIPAM[10] and MBAA[11] on gold nanoparticles.[8] Those polymer/gold nanoparticles could load tiny free gold nanoparticles by decreasing the temperature and could certainly release them by elevating it. (A laser could be used to increase the temperature using the surface plasmon absorption of the gold nanoparticles.) The drug delivery could also be triggered by an enzyme, which irreversibly cuts the hydrogel polymer chains.[13]

Kong Won-Ho, Sung Dong-Kyung, Shim Yong-Ho, Bae Ki Hyun, Dubois Philippe, Park Tae Gwan, Kim Jin-Hoon and Seo Soo-Won took another route to deliver their drug, siRNA[12], which silences the expression of given genes. The genes targeted are the ones responsible for diseases or crucial to the life of cells. siRNA could consequently repair cells or program their death. Nevertheless, if provided as it is, siRNA is easily degraded by nucleases from the serum and its cellular uptake is low. They blended negatively-charged siRNA strands with positively-charged PDMAEMA[13] to form nanoparticles (within which siRNA strands are condensed), then electrostatically wrapped them with an optimum quantity of palm-tree positively-charged PDMAEMA-b-PMAPEG[14] to harness the abilities of PEG without having it interacting with siRNA.[9] These siRNA-containing nanoparticles protected their precious payload, penetrated the cells and gradually exuded it.

Nanoparticle/biomolecule hybrids can be utilized for in vitro applications as well, like imaging and diagnostics.

Quantum dots possess several interesting properties for fluorescence imaging: a size-tuned absorption and fluorescence, a narrow and high fluorescence emission and a strong resistance towards photobleaching. In practice, any type of cells could be multi-color imaged, using a single excitation wavelength and quantum dots of different sizes labeled with recognition-oriented biomolecules. Bruchez Marcel Jr., Moronne Mario, Gin Peter, Weiss Shimon and Alivisatos A. Paul succeeded in imaging mouse 3T3 fibroblasts using two types of hybrids emitting at different wavelengths and exposed to a given excitation wavelength.[14] They wrapped fluorescent type I quantum dots into a silica shell to disperse them into aqueous solutions, then derivatized their surface with trimethoxysilylpropyl urea and acetate groups or biotin to specifically bind them to the cell nuclei or to the actin filaments, respectively. Those hybrids could also be precious to extract diagnostics by coloring biopsied tissues.

Regarding in vitro diagnostics, the Mirkin group opted to track DNA strands and proteins affiliated with given diseases by monitoring the surface plasmon absorption of gold-nanoparticle assembly resulting from the interactions between thiolated DNA oligonucleotide-grafted gold nanoparticles and their target.[15-17] The first step consisted in noticing the properties of thiolated DNA oligonucleotide-grafted gold nanoparticles. Compared to bare nanoparticles, they remained dispersed for days in aqueous solutions highly concentrated in salt or subjected to 80°C. By mixing two types of hybrids (differing only in the sequence of their grafted oligonucleotides) in PBS buffer (10mM phosphate, 1M NaCl, pH=7) and a duplex terminated by sticky ends able to

hybridize with each grafted oligonucleotide, Mirkin Chad A., Letsinger Robert L., Mucic Robert C. and Storhoff James J. induced the creation of a gold-nanoparticle assembly and the concomitant color change from red to purple, leading at last to the formation of a pinkish-grey precipitate.[15] By shaking the mixture and fixing the temperature at 80°C, the nanoparticle assembly was dismantled. This could be reversibly reformed and taken apart at wish. The second step was to introduce a solid support (TLC plate) on which a drop of the mixture (two types of hybrids and a given type of free oligonucleotide) is deposited.[16] If the free oligonucleotides exactly represented the fusion of the two DNA oligonucleotides complementary to the grafted ones, then an assembly of gold nanoparticles was produced, materialized by a purple spot on the solid support, which at last became blue. This color stemmed from the drying process on the TLC plate, which increases the aggregation of the preorganized polynucleotide-linked nanoparticles. The thermal dissociation of gold-nanoparticle assemblies depends upon the extent of the sequence similarity between the free oligonucleotide and the grafted ones and happens at a narrow temperature window. One base mismatch occurring on the free oligonucleotide could still be detected by spotting drops of the mixture subjected to different temperatures. The third step was to involve their thiolated DNA oligonucleotide-grafted gold nanoparticles in the recognition of proteins and to show the possibility of multiplex analyses.[17] Two kinds of hapten-labeled DNA oligonucleotides[15] were hybridized with the corresponding thiolated DNA oligonucleotide-grafted gold nanoparticles to target given antibodies and generate gold-nanoparticle assemblies. The thermal behavior of these assemblies and of their mixture were characterized by recording their absorption at 260 nm. The absorption of the assembly mixture had inherited from each assembly

absorption profile (their respective absorption peak being located at 36 and 55ºC). From this method, Nam Jwa-Min, Park So-Yung and Mirkin Chad A. derived a more sensitive one by focusing on the extraction of the biobarcodes[10] (centrifugation, denaturation, centrifugal filtration), followed by their immobilization on a glass slide presenting an array of complimentary half-oligonucleotides and the subsequent "docking" of their complementary half-oligonucleotide grafted gold nanoparticles on their remaining part. The glass slide is then subjected to a photographic development (gold nanoparticles catalyze the reduction of silver) and read by a flat bed scanner. An obvious advantage of this technique is the increased sensitivity brought by photographic development to avoid the use of proteins, which non-specifically adsorb easily on solid surfaces.

Diagnostics devices usually rely on optical or electrical readouts, those being easy to process through electronics. That is the reason why Park So-Yung, Taton T. Andrew and Mirkin Chad A. coupled the use of microelectrodes and the thiolated DNA oligonucleotide-grafted gold nanoparticles to sense DNA targets.[18] The microelectrode gap was functionalized with half-oligonucleotides complementary to a part of the target DNA oligonucleotides, whereas their other part was able to hybridize with thiolated DNA oligonucleotide-grafted gold nanoparticles. By putting a drop of the mixture composed of target DNA oligonucleotides and thiolated DNA oligonucleotide-grafted gold nanoparticles in between the gap, an array of gold nanoparticles is built, then connected to each other via a photographic development to form a metallic nanowire joining the two microelectrodes. Its resistance is monitored to sense target DNA oligonucleotides. By washing the electrodes (before the photographic development) with PBS buffer of lower salt concentration, they were able to discriminate with ease a single-base mismatch on the

oligonucleotides attached on the solid support from a perfect match, the ratio of their respective resistance being 10^5. Multiplexing is at reach by employing microelectrode arrays, announcing the incoming venue of commercial lab-on chips, the grail of the in vitro diagnostic tools: small quantities of a sample are carried through microfluidics to several analyzing microareas, in which they are subjected to given tests whose readouts are optical and/or electrical.

The hybrids illustrated earlier represent only a tiny piece of the visible part of the iceberg. There is a plethora of biomolecules and nanoparticles, thus an even greater amount of hybrids are possible to make, whose versatile aspect is more and more emphasized to accomplish several tasks in vivo as well as in vitro, where some of them will be integrated into lab-on chips. Before lab-on chips become a commercial reality, detection schemes have to be implemented leading to electrical or optical outputs. In this respect, we employed interdigitated electrodes to detect pathogenic bacteria such as *Escherichia coli* and *Salmonella typhi* and to determine their potential when it comes to sense the presence of human PC3 prostate carcinoma cells, both via impedimetric measurements. We also investigated the possibility to monitor the size change of hydrogel beads exposed to external stimulus with those interdigitated electrodes. Focusing on the optical outputs, we studied the eventuality to substitute Horse Radish Peroxidase-conjugated antibodies by the following hybrid TiO_2 nanoparticle-labeled antibodies for Enzyme-Linked ImmunoSorbent Assay (ELISA). Finally, we synthesized urease-encapsulated Ag_2S nanoparticles harnessing its enzymatic activity.

Chapter I.

Interdigitated electrodes-based biosensors.

I.1. Introduction.

Interdigitated electrodes (IDEs) are planar microelectrodes used for dielectrophoresis and impedimetric measurements. They are made of two interpenetrating sets of conductive micrometer-sized finger-shaped electrodes, deposited on a substrate (Figure I.1). Their ease of fabrication due to their simple architecture and the well-established CMOS[16] technology, their robustness resulting in their long-term reliability and above all, their electric properties have sparked the interest of the sensor aficionados. They actually display desirable features to design biosensors based on non-faradaic impedimetric measurements: a short penetration depth of their electric-field lines, a low cell constant and a relatively large inter-electrode capacitance.[19]

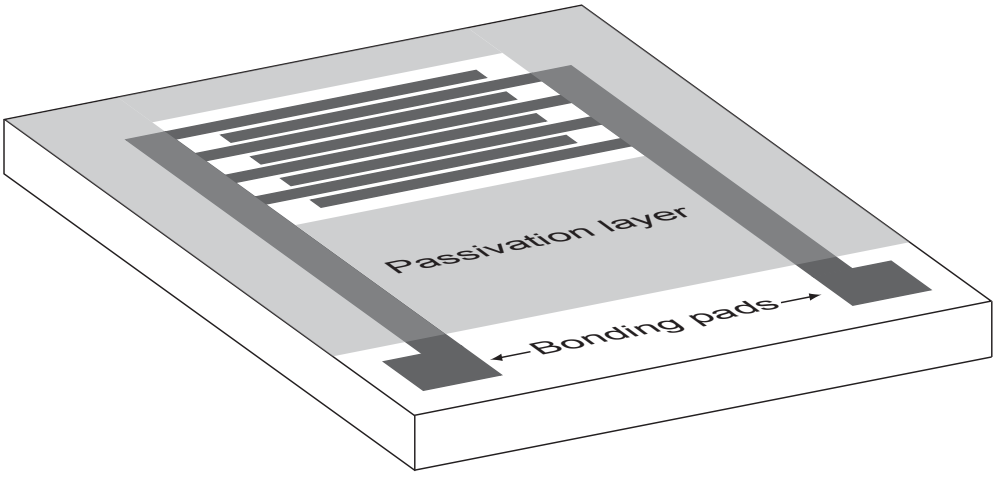

Figure I.1: Schema depicting IDEs (adapted from [20]).

Van Gerwen Peter, Laureyn Wim, Laureys Wim, Huyberechts Guido, Op De Beeck Maaike, Baert Kris, Suls Jan, Sansen Willy, Jacobs P., Hermans Lou and Mertens Robert showed that the immobilization of glucose oxidase on the surface of IDEs dipped in a highly-conductive phosphate buffer solution can be monitored in real-time by visualizing the timewise decrease of the capacitance, resulting from the modification of the double-layer by the covalent attachment of the proteins.[21] Furthermore, de la Rica Roberto, Baldi Antonio, and Fernández-Sánchez César revealed that the production of ions by urease in presence of urea could be detected only if the enzymatic reaction occurs at the electrodes.[22] Those two experiments strongly suggest that the vertical (perpendicular to the IDEs surface) penetration depth of their electric-field lines is so short that IDEs can probe with an acute sensitivity any event occurring some hundreds of nanometers above their surface, while conventional electrodes are sensitive to any change located in an area comprised between 1 um and several millimeters from their surface [21]. IDEs could accordingly monitor the binding of biomolecules (antibody-antigen, complementary DNA strands) if it were functionalized with their complementary ″halves″.[21]

The low cell constant of IDEs allows the measurement of minute conductivity solutions [19] ($\sigma = k/R_{sol}$, refer to page 17), which raises the possibility to sense certain enzyme substrates, targets of enzyme-labeled antibodies as well (i.e. molecules, proteins, microorganisms and potentially materials [23]) and microorganisms. In fact, given enzymes, like urease, catalyze the degradation of their specific substrates into ions. By anchoring those enzymes on the surface of the IDEs, the impedance measured at a given frequency becomes correlated to the concentration of their specific

substrate.[19, 24] The same enzymes could be covalently attached to antibodies. These enzyme-labeled antibodies could then assist the detection of their specific targets physisorbed on the IDEs by the impedimetric transducer, when exposed to their specific substrates.[25] The same enzymes can be synthesized by microorganisms. Their action results in the conductivity increase of the low-conductivity medium in which the microorganisms lie, allowing the real-time assessment of their population.[20]

The inter-electrode capacitance of IDEs is so high compared to the stray capacitance[17] that dielectric permittivity of media becomes accessible [19], which makes the detection of proteins and microorganisms a reality. The high capacitance displayed by the IDEs directly stems from their architecture inherited from the ingenuity of the infamous Nikola Tesla.[26] He fabricated an electrical condenser, a device consisting of a set of rectangular metallic plates arranged in an interdigitated fashion and immersed in an insulating liquid; he actually showed that its capacitance linearly increases with the number of plates.[27] Provided that the capacitance of two coplanar metallic finger-shaped electrodes and the stray capacitance of the leads are of the same order of magnitude, adding a large amount of electrodes permits to obtain a measurable capacitance.[26] The capacitance C obeys the following equation:

$$C = \varepsilon\varepsilon_0 \frac{A}{d}$$

where ε,ε_o, A, and d represent the dielectric constant, the permittivity of the free space, the area of the plates and the distance between them, respectively. Accordingly, any changes in the permittivity of the medium surrounding the IDEs alter the capacitance. Knowing that the permittivity of proteins, antibodies, cell membranes and polymers are

low compared to the one of water [28, 29], all of these elements could be easily detected by the IDEs.

For instance, grafting glucose oxidase on the surface of IDEs is visualized in real-time through the timewise decrease of the capacitance.[21] As well, the binding of antibodies specifically targeting affinity ligands coated upon the surface of the IDEs displaces water molecules and solvated ions away from it, lowering the permittivity constant and accordingly the capacitance.[29] Bacteria deposited on the surface of the IDEs do also reduce the capacitance by decreasing the permittivity of the medium surrounding the IDEs.[28, 30]

Moreover, Fernández-Sánchez César, McNeil Calum J., Rawson Keith and Nilsson Olle were able to conceive an ingenious biosensor based on pH-sensitive polymer coated IDEs, quantifying the two forms of prostate-specific antigens (PSA) present in serum, whose ratio is relevant for prostate-cancer diagnosis.[31] The sample is at first mixed with urease-labeled anti-PSA antibodies to form complexes. These complexes migrate along a nitrocellulose-membrane strip and are immobilized by anti-PSA antibodies anchored on the strip, right below the polymer-coated IDEs. The rapid addition of urea removes any unbound complexes from the strip and triggers the formation of ammonia by urease resulting in the degradation of the polymer and the increase of the capacitance until reaching the value of the double-layer capacitance. The point of using a pH-sensitive polymer is to obtain a difference of capacitance up to four orders of magnitude between the polymer-coated IDEs and the bare IDEs configurations.

Furthermore, some IDEs (the ones made of polysilicon electrodes such as $(IDEs)_2$) are covered by a top silicon-oxide layer, permitting the easy functionalization of their surface through silanization to graft enzymes [22] and antibodies [30]. Silanization could certainly be applied to immobilize phages and aptamers, more affordable alternatives to antibodies [20], to study the electrical behavior of bacteria and cells, respectively.

Additionally, non-faradaic IDEs display a short response time, do not require the use of a reference electrode [20] or redox probes (such as $[Fe(CN)_6]^{3-}$ /$[Fe(CN)_6]^{4-}$) detrimental to the recognition ability of antibodies [32], facilitating their integration into portable devices, are easy to fabricate via the well-established CMOS[16] technologies and can be operated by common people. All of these characteristics are prerequisites for point-of-care testing, nevertheless, to the best of our knowledge, the issues of multiplex analyses and the IDEs reusability have not been addressed yet.

Our goal is to harness the amazing sensing abilities of IDEs in three distinct projects. The first project was aiming at detecting common pathogens utilizing arrays of IDEs to show the feasibility of performing multiplex analyses, while devising a simple detection scheme leading to their complete reusability, bringing the point-of-care testing one step closer to reality. (This project led by Dr. de la Rica allowed me to get acquainted with the characterization of the IDEs and the way they work.) The second project consisted in continuing the pioneer work of de la Rica and colleagues dealing with the label-free impedance-based discrimination of cancer cells from normal cells.[33] Its goal was to examine the eventuality to extend their detection method to other cell types, such as human PC3 carcinoma prostate cells. Finally, the aim of the third project

was to investigate the possibility to monitor the size change of hydrogel beads subjected to an external stimulus (laser or enzyme) via impedimetric measurements. The next section of this chapter will address the characterization of the IDEs, then each of the following sections will be devoted to one of the projects previously mentioned.

I.2. Characterization of the IDEs: cell constant and ν_{rt}.

Two kinds of IDEs, $(IDEs)_1$ and $(IDEs)_2$, were employed during our studies. Both IDEs were fabricated by Dr. Antonio Baldi's team at the *Instituto de Microelectronica de Barcelona* (IMB-CNM, CSIC, Barcelona, Spain) using standard photolithography.

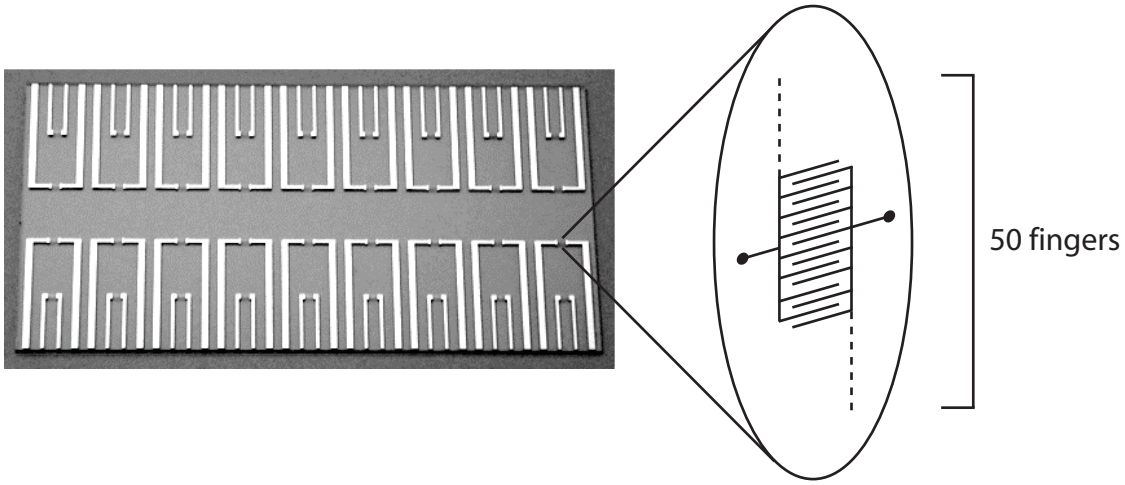

Figure I.2: Arrays of 36 $(IDEs)_1$ adapted from [34].

An array of $(IDEs)_1$ (Figure I.2) made of a triple layer of Ti/Ni/Au (500Å each) is deposited on a 500µm-thick Pyrex wafer. A 1µm-thick silicon-oxide passivation layer covers everything but the IDEs area to collect only their electrical response.[20] $(IDEs)_1$ are composed of 50 fingers, each being 29µm-long, 3µm-wide and 3µm-apart from each other. They were connected to the impedance analyzer through the tips of a probe station.

The array of $(IDEs)_1$ was exclusively employed for the project entitled peptide-nanotube biochips for label-free detection of multiple pathogens (Section I.2 and Appendix 2).

Figure I.3: Pictures of the $(IDEs)_2$.

$(IDEs)_2$ (Figure I.3) are made of 218 polysilicon[18] fingers (1600µm-long, 3µm-wide and 3µm apart from each other), deposited on a 1.5µm-thick layer of SiO_2, itself covering a silicon substrate.[19] A passivation layer composed of 0.3µm of SiO_2 and 0.7µm of Si_3N_4 coats everything but the IDEs area. A 3nm layer of native oxide spontaneously grows on the polysilicon fingers, granting its protection against any further corrosion.[35] The bonding pads of $(IDEs)_2$ are directly interfaced with aligned wires ended by a micropost connector, in which a banana plug perfectly clips to insure the connection to the impedance analyzer.

IDEs are characterized by their geometry, which in turn determines their cell constant *k* defined by the following equation:

$$k = \frac{R_{sol}}{\rho} = \frac{\varepsilon}{C_{sol}}$$

where R_{sol}, ρ, ε and C_{sol} stand for the resistance of the solution, the resistivity of the solution, the permittivity of the solution and the capacitance of the solution, respectively. The resistance of a circuit component refers to the ratio of the voltage applied to the current, which flows through it, and could be expressed in terms of resistivity by taking into account its dimensions. The determination of the cell constant relies on the method

developed by Van Gerwen Peter, Laureyn Wim, Laureys Wim, Huyberechts Guido, Op De Beeck Maaike, Baert Kris, Suls Jan, Sansen Willy, Jacobs P., Hermans Lou and Mertens Robert as well as by de la Rica Roberto, Fernández-Sánchez César and Baldi Antonio.[19, 21] By definition, the cell constant represents the slope of the curve representing R_{sol} against ρ. Those two parameters have thus to be assessed to find out the cell constant.

The conductivity of aqueous salt solutions made of phosphate buffer[19] and KCl of various concentrations was measured at room temperature by a conductivity meter -Seven Easy, Mettler-Toledo- (Appendix 1) to determine the cell constant of $(IDEs)_1$ and $(IDEs)_2$, respectively. Next, a 10µl drop of each aqueous salt solution was deposited on the IDEs connected to an impedance analyzer -model 1260A, Solartron- through their bonding pads (Appendix 1). A 10mV alternating voltage was applied onto the IDEs by the impedance analyzer and its frequency was swept from 1MHz to 10Hz. This low alternative voltage avoids any redox reactions to happen and accordingly chemically maintains our system. The current induced by the voltage change was collected for each frequency and the impedance, the voltage-to-current-intensity ratio, was read by the impedance analyzer controlled via the SMaRT Impedance Measurement software -Solartron- (Appendix 1). After each measurement, the IDEs were rinsed with deionised water and dried with nitrogen gas.

The impedance data obtained were viewed on the Zview software -Scribner Associates-(Appendix 1), which offers the possibility to simultaneously watch their corresponding Bode plot (|Z| vs. frequency), Nyquist plot (Z' vs. Z'') and plot representing the phase angle against the frequency. The data were then fitted (Appendix

1) using an equivalent circuit (Figure I.4) reflecting the system composed of an aqueous solution and given IDEs. From these fittings, are deduced the values of R_{sol} and the cell constant is finally determined.

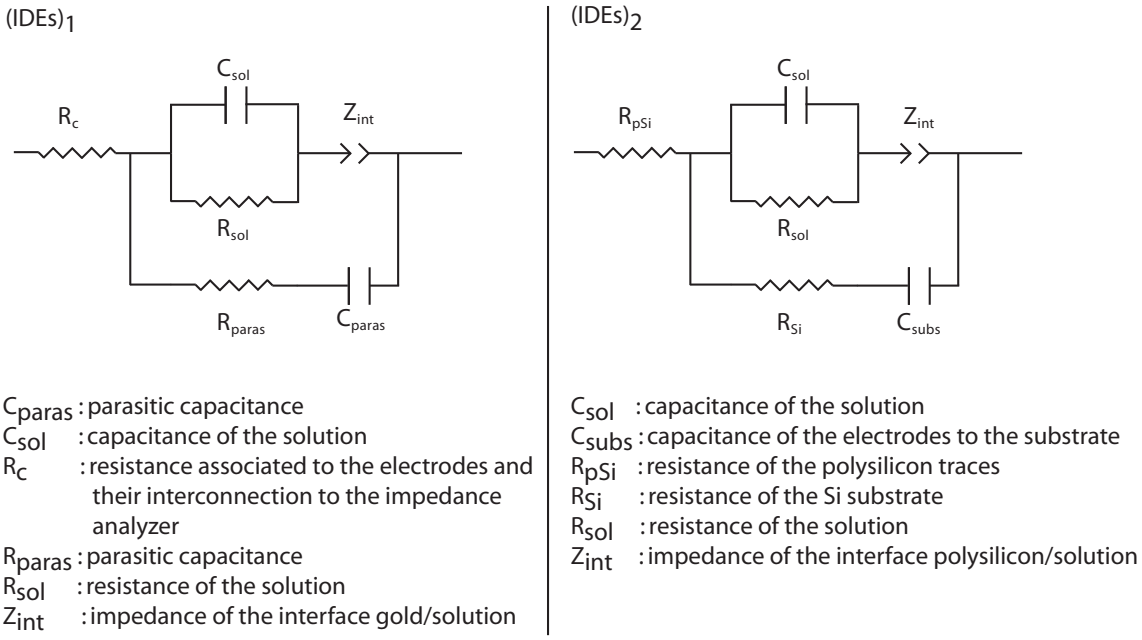

C_{paras} : parasitic capacitance
C_{sol} : capacitance of the solution
R_c : resistance associated to the electrodes and their interconnection to the impedance analyzer
R_{paras} : parasitic capacitance
R_{sol} : resistance of the solution
Z_{int} : impedance of the interface gold/solution

C_{sol} : capacitance of the solution
C_{subs} : capacitance of the electrodes to the substrate
R_{pSi} : resistance of the polysilicon traces
R_{Si} : resistance of the Si substrate
R_{sol} : resistance of the solution
Z_{int} : impedance of the interface polysilicon/solution

Figure I.4: Equivalent circuits of $(IDEs)_1$ and $(IDEs)_2$ immersed in a solution adapted from [19, 34].

The average cell constant of the $(IDEs)_1$ equals to $1.700cm^{-1}$ and its associated standard deviation amounts to 2.5% of its value (Figure I.5). Consequently, those five identical $(IDEs)_1$ can be considered as equivalent. The cell constant of the $(IDEs)_2$ is equal to $0.029cm^{-1}$ (Figure 5), a value of same order of magnitude as the one reported by de la Rica Roberto, Fernández-Sánchez César and Baldi Antonio [19]. The cell constant can also be determined by retrieving C_{sol} values. To do so, IDEs are incubated with different solvents of known dielectric permittivity (water, acetonitrile, ethanol, tetrahydrofuran and hexane) and the data are fitted exploiting the equivalent circuits mentioned earlier.[19]

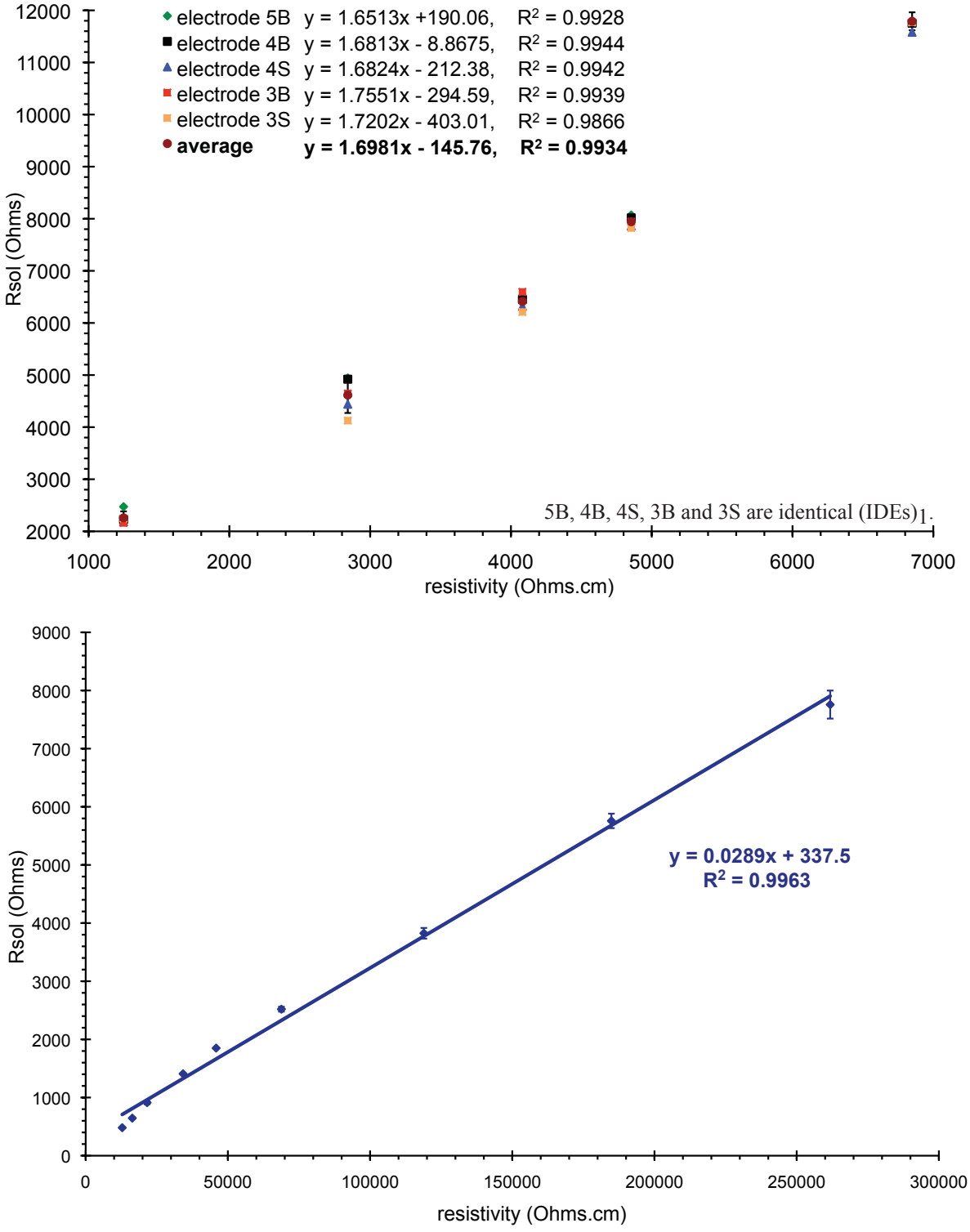

Figure I.5: Graph 1: Determination of cell constants related to five identical $(IDEs)_1$.
Graph 2: Determination of the cell constant of one $(IDEs)_2$.
(Error bars are calculated from five measurements.)

The cell constant of IDEs entirely depends upon their geometry. Any change in the geometry of the IDEs such as the deposition of insulating objects (latex beads, bacteria…) modifies the distribution of the electric-field lines [30, 36] (Figure I.6) and consequently the cell constant. Therefore, given the mathematical relationship between the cell constant and R_{sol} (ρ being a property of the solution, it is not affected by insulating objects), IDEs can sense the attachment of insulating objects through the variations of R_{sol}. The larger the amount of insulating objects in the area probed by the IDEs is, the higher the cell constant and R_{sol} are.[36]

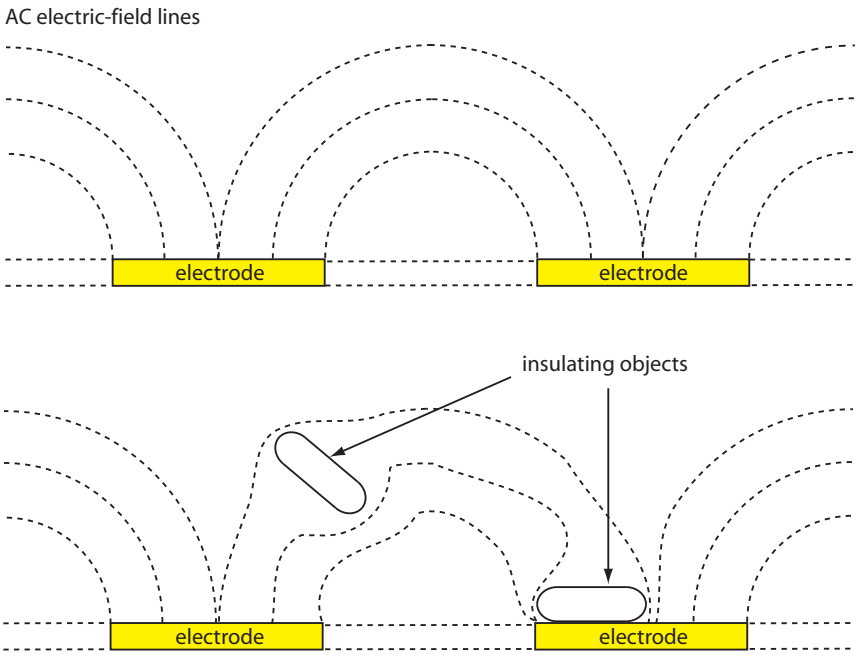

Figure I.6: Schema illustrating the distortion of the AC electric-field lines generated by IDEs while depositing insulating objects (adapted from [20, 30, 34, 36]).

R_{sol}, being a resistance, is contained in the real part of the impedance represented by Z'. At a given frequency, the value of Z' is only determined by the one of R_{sol} in such a manner that Z' equals to R_{sol}. At this unique frequency, R_{sol} is directly accessible through Z', which is measurable. To determine the cell constant, a set of data

(frequency, Z', ρ) was collected. For each frequency, it is possible to plot Z' against ρ and determine its slope. At a precise frequency called ν_{rt}, the slope of Z' vs. ρ matches the cell constant (determined in figure I.5), in other words, Z' is equal to R_{sol}. At ν_{rt}, Z' and R_{sol} can be used indistinguishably. For $(IDEs)_1$ and $(IDEs)_2$, ν_{rt} is equal to 316kHz and 20kHz, respectively.[33, 34]

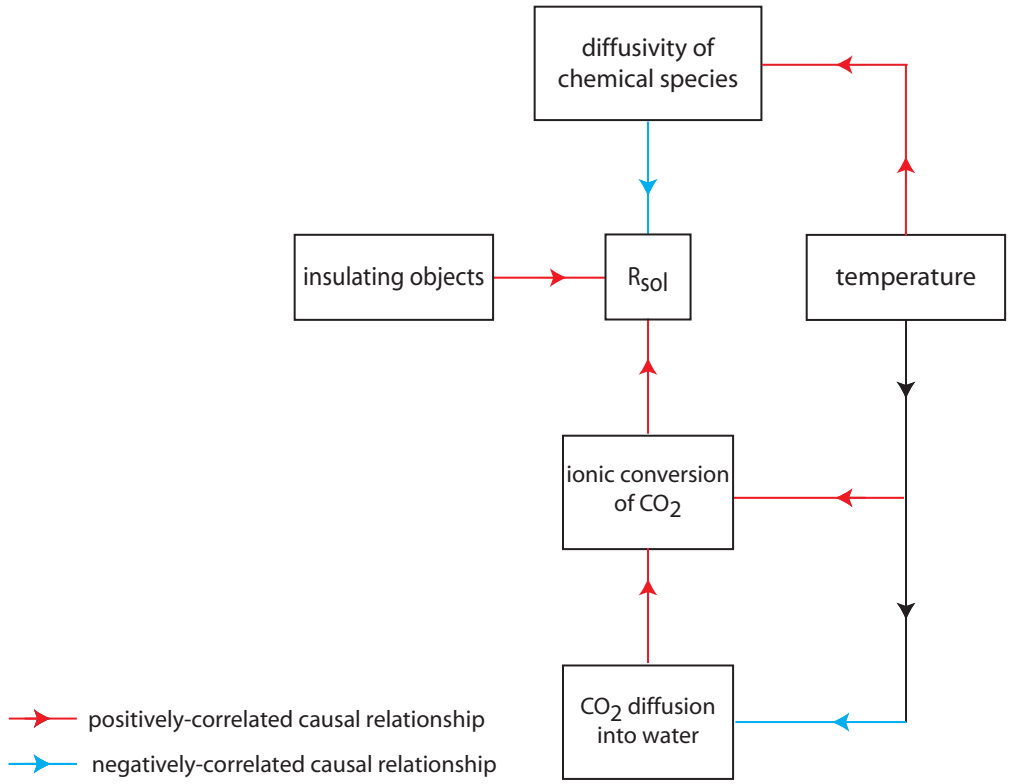

Figure I.7: Organigram illustrating the relationships between R_{sol} and the parameters influencing it.

By definition, R_{sol} depends upon the amount of ions present in solution. But other parameters such as CO_2 diffusion, temperature and the amount of insulating objects influence R_{sol} (Figure I.7). CO_2 reacts with water to form H_2CO_3, a weak acid, which partially dissociates into H^+ and HCO_3^-, which in turn partly decomposes into H^+ and CO_3^{2-}. Accordingly, CO_2 diffusion into water augments R_{sol} until reaching a plateau.

Temperature usually affects equilibria of chemical reactions ($\Delta G = -RT \ln K$), the diffusivity of chemical species in water and the solubility of gas in aqueous solution. A temperature rise decreases the amount of CO_2 dissolved into water, increases the proportion of CO_2 in solution that reacts with water to form H_2CO_3, as well as the relative amount of those, which undergoes subsequent decompositions into ions. An augmentation of the temperature raises the diffusivity of the chemical species, which in turn increases the conductivity of the solution and diminishes R_{sol}. Hence, it appears somewhat difficult to qualitatively predict the thermal effect on R_{sol}. The insulating objects modify the geometry of the IDEs and distort the electric-field lines on the transducer, augmenting the cell constant and thus R_{sol}. For example, de la Rica Roberto, Fernández-Sánchez César and Baldi Antonio have applied positive dielectrophoresis to trap latex beads and have actually shown that ΔR_{sol} (temperature-drift and CO_2-diffusion rid R_{sol}) increases with their amount.[36] To remove the effect of temperature drift and CO_2 diffusion on the R_{sol}, they used two pairs of IDEs to simultaneously measure the impedances of the glycine-buffer (as a control) and glycine-buffer/latex beads systems and substracted their corresponding R_{sol} values obtained by fitting:

$$\Delta R_{sol} = R_{sol}(\text{IDEs/latex beads/glycine buffer}) - R_{sol}(\text{IDEs/glycine buffer})$$

Therefore, monitoring the presence of insulating objects in real time requires impedimetric measurements in parallel of the control and the sample at ν_{rt}, either utilizing two identical IDEs or the same IDEs (one measurement for the control and the sample at a time), each method presenting disadvantage and plot $\Delta Z'$ against the time. $\Delta Z'$ obeys the following equations:

$\Delta Z' = Z'(\text{sample}) - Z'(\text{control})$

$\Delta Z' = Z'$(insulating objects/aqueous solution) – Z'(aqueous solution)

Simultaneously measuring the impedance of the control and the sample with two identical IDEs permits to subject them to the same experimental conditions (temperature, CO_2 concentration), conversely to using the same IDEs for both measurements, one at a time. However, two identical IDEs are indistinguishable up to a given extent: they probably do no exhibit the exact same cell constant.

I.3. Peptide-nanotube biochips for label-free detection of multiple pathogens.[34] (project led by Dr. de la Rica, Appendix 2)

Nowadays, worldwide flows of populations and goods reach such a scale that they promote epidemic outbreaks, even pandemic one such as the one related to the H1N1 virus. Consequently, a lot of efforts are invested in the elaboration of sensors able to detect pathogens. Ideally, those sensors must be sensitive to the presence of a handful of pathogens, specific to a given kind of harmful microorganisms; fast-performing and multiplex-analyses oriented in order to quickly identify the type of pathogenic threat and to implement measures to avoid their growth and spread. Moreover, those sensors must be portable to be brought in the field and lower the risk of contamination. They must be cost-effective too, focusing on their reusability.

To fulfill all of those requirements, de la Rica Roberto, Pejoux Christophe, Fernández-Sánchez César, Baldi Antonio and Matsui Hiroshi devised a detection scheme involving an array of $(IDEs)_1$ and peptide nanotubes targeting common pathogenic

bacteria, *Escherichia coli* and *Salmonella typhi*. The detection scheme concentrates on two aspects, the multiplex analyses thanks to the array of $(IDEs)_1$ (the variation of the cell constants was less than 5%) and their reusability by physically separating the biorecognition event from the impedance measurement. The detection scheme works as follows. Antibody-labeled BSA-coated peptide nanotubes are incubated with bacteria for an hour. Provided that the antibody-labeled peptide nanotubes target the introduced bacteria, the higher the bacteria concentration is, the more decorated and the heavier the nanotubes are. A drop of mixture is deposited on the $(IDEs)_1$. Due to gravity, the most loaded nanotubes settle down the first on the $(IDEs)_1$ surface. When entering the probed area, the bacteria bound to the peptide nanotubes distort the AC electric-field lines generated by the $(IDEs)_1$, whereas peptide nanotubes are electric-field transparent. Those perturbations can be monitored in real time through the Z' values acquired at ν_{rt} (i.e. 316 kHz). The control experiment used was rabbit IgG-labeled peptide nanotubes (they do not target *E. coli* or *S. typhi*) incubated with various concentration of bacteria (0, 10^2 ,10^3, 10^4 cells) to remove the thermal drift, parasitic components of the equivalent circuit, CO_2 diffusion and non-specific adsorption of bacteria on the nanotubes. As expected, de la Rica Roberto, Pejoux Christophe, Fernández-Sánchez César, Baldi Antonio and Matsui Hiroshi were able to observe that $\Delta Z'$ (collected in fifteen-second measurements) is positive and grows faster as the number of bacteria increases and that the dynamic range of the system is comprised between 10^2 and 10^4 cells, which is far lower than the minimum infective value (Figure I.8). They also remarked that after a ten-second deionised-water rinsing in between measurements, $\Delta Z'$ for a given bacteria concentration varied less than 5% for 20 measurements, pointing out the efficiency of the easy cleaning

process and the subsequent reusability of the $(IDEs)_1$. They, in addition, proposed to convert the ΔZ' signal into a color code much easier to comprehend by common people (Figure I.8.b).

Figure I.8: Refer to figure 3. of the bibliographic reference [34].
a. Curve representing ΔZ' against the time for 0, 10, 10^2 & 10^3 E. coli cells.
b. Conversion of %(ΔZ'(15s)) values into a color brightness.

$$\%(\Delta Z'(15s)) = \frac{\Delta Z'(15s)}{(\Delta Z'(15s))_{max}} \times 100$$

I.4. Label-free cancer cell detection with impedimetric transducers.

Much of de la Rica and colleagues' work was devoted to the $(IDEs)_2$-based detection of cells through the determination of R_{sol} [25, 33, 34](or C_{sol}[30]). There are different ways to monitor the presence of given cells via monitoring R_{sol}. Given that R_{sol} depends on the amount of ions nearby the IDEs, the first one consists in utilizing urease-labeled antibodies to target given cells (physisorbed on the IDEs) and reveal their presence through the addition of its specific substrate urea to generate ammonia and CO_2, which both partially react with water to form ions.[25] The second one relies on the distortion of the electric-fields lines (generated by the IDEs) exerted by the cells, when they behave as insulating objects. Besides the example mentioned in the previous section [34], de la Rica Roberto, Thompson Sebastian, Baldi Antonio, Fernández-Sánchez César, Drain Charles Michael and Matsui Hiroshi designed an ingenious scheme to detect cancer cells diluted in a plethora of normal cells.[33] Cells subjected to hyposmotic stress tend to swell by absorbing water and to "burst" after a given time. However, cancer cells can accommodate a larger size increase than normal cells do, before their membranes rupture. Provided that $(IDEs)_2$ are able to detect cells when they act as insulating objects, de la Rica and colleagues monitored the size change of normal and corresponding cancer cells dipped in deionised water by performing real-time optical and impedimetric measurements (Appendixes 4 and 5).

The surface of $(IDEs)_2$ was incubated for 30 minutes with polylysine to promote the cell adhesion, then rinsed with deionised water and dried with nitrogen gas. Next, a drop of 5µl of medium was cast on the $(IDEs)_2$. After 20 minutes of incubation, the $(IDEs)_2$ were dipped in three consecutive deionised-water baths to remove any traces

of medium and 100µl deionised-water drop was spotted on the electrodes. The real-time impedance of the control experiment was recorded at 20kHz (ν_{rt} of $(IDEs)_2$). After rinsing and drying the electrodes, 5µl of medium containing a certain amount of cells were left in contact with the $(IDEs)_2$ for half-an-hour. Following the 3 deionised-water rinsings, the real-time impedimetric measurement of the sample was run.

Using the protocol mentioned above, de la Rica and colleagues studied the behavior of three pairs of cancer cells / normal cells: K:Molv NIH 3T3 cells / NIH 3T3 cells, 786-O human kidney carcinoma cells / HEK 293 cells and MPSC-1 ovarian cancer cells / OSE cells. They demonstrated that the curve representing $\Delta Z'(t)$ related to cancer cells raises much higher than the one of normal cells. They also showed that the values of $\Delta Z'$(2min.) depicting a given number (10, 10^2, 10^3) of cancer cells in presence of 10^3 normal cells, increases with the number of cancer cells. The slopes of the curve representing $\Delta Z'$(2min.) vs. log(cancer cells) for each cell type were 1215, 705 and 398Ω, respectively. Being able to detect 10 cancer cells among 10^3 normal cells is extremely interesting when it comes to analyze biopsied tumors, which may contain normal cells too.

Our aim was to determine whether the larger impedance increase observed for the three types of cancer cells (mentioned earlier and subjected to hyposmotic stress) compared to their corresponding non-cancer cells is common to any other cancer cell/normal cell pairs. We decided to study the impedimetric behavior of the human PC3 carcinoma prostate cells/immortalized normal human PNT1A prostate cells pair (Appendix 3). For men, prostate cancer is actually the second most common cancer after skin cancer. According to the statistical analyses conducted by the National Cancer

Institute in 2010, 217,730 new cases of prostate cancer were detected in USA and 32,050 men died of it.[37] Prostate-cancer diagnostics heavily rely on prostate biopsy procedures (more than 600,000 per year [38]), inherently dangerous since they could promote metastasis by releasing cancer cells in the blood stream. Fujita Kazutoshi, Pavlovich Christian P., Netto George J., Konishi Yuko, Isaacs William B., Ali Syed, De Marzo Angelo and Meeker Alan K. chose to take a safer path to diagnose patients affected by prostate cancer, namely urine cytology (coupled to fluorescence microscopy), however challenging due to the scarcity of prostate cells present in urine.[38] They overcame this obstacle via physical manipulations applied on the patient prostates prior to the urine collection, which is known to boost the amount of prostate cells shed in urine.[38] Their subsequent multiplex immunofluorescence-microscopy method successfully labeled 9 patients as being affected by cancer out of the 25 biopsy-proven ones and "cleared" the 15 ones who were not.[38] Our ultimate goal is to couple urine cytology with impedimetric measurements following the method of de la Rica and colleagues to diagnose prostate cancer. Before achieving it, we had to demonstrate that PC3 cells spiked or not into urine could be detected via impedimetric measurements.

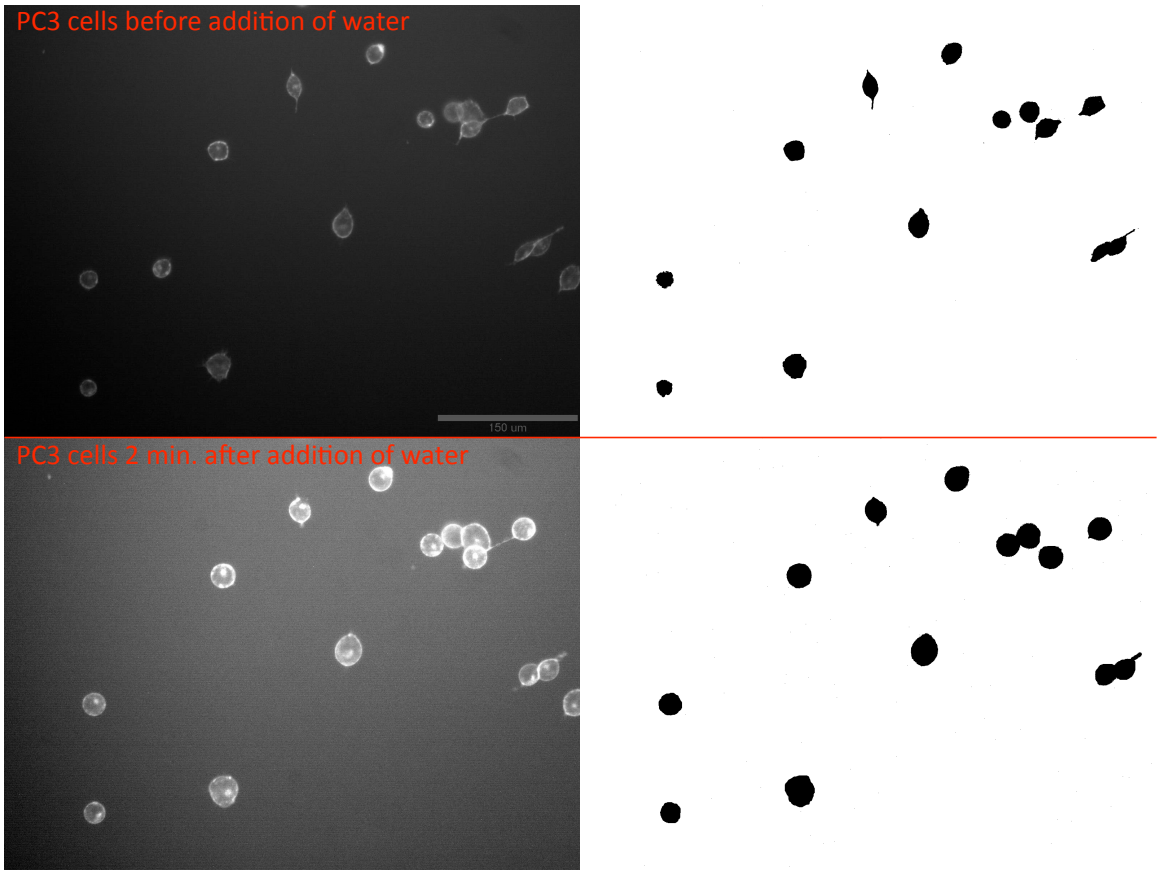

Figure I.9: Images representing PC3 cells before and 2 minutes after being subjected to hyposmotic stress. The pictures located on the left side are acquired by fluorescence microscopy, whereas the ones on the right side are their corresponding "binarized" images obtained after processing using the freeware ImageJ (Appendix 4).

image J

file	name	magnification	# cells	area (um^2)	swelling (um^2)	swelling(%)
72010	PC3_agg_5_r_1pp	X20	10	4619.46		
72010	PC3_agg_5_r_60spp	X20	10	5175.05	555.59	12.03
72010	PC3_agg_5_r_2minpp	X20	10	6238.03	1618.57	25.95
72010	PC3_agg_6_r_2pp	X20	9	4095.54		
72010	PC3_agg_6_r_2minpp	X20	9	5556.28	1460.75	35.67
73010-2	PC3_agg_1_1p	X20	11	4260.28		
73010-2	PC3_agg_1_2minp	X20	11	6241.37	1981.09	46.50
73010-2	PC3_agg_2_1p	X20	13	4778.82		
73010-2	PC3_agg_2_2minp	X20	13	7107.31	2328.48	48.73
73010-2	PC3_agg_3_1p	X20	11	3578.73		
73010-2	PC3_agg_3_2minp	X20	11	5812.29	2233.56	62.41
		total	54	**average**	1924.49	45.11

scale bar for X20	**pixel**	**um**	**pixels/um**
	387.67	150	2.584

Table I.1: Table containing the data provided by ImageJ (Appendix 4).

Given that the behavior of cells is type-dependent, we had to check first that PC3 cells swell when immersed into deionised water. To do so, PC3 cells stained with fluorescein-conjugated germ agglutinin were imaged through fluorescence microscopy (Figure I.9) and their footprints were measured via image processing realized by the freeware ImageJ (Appendix 4). This image analysis probed 54 PC3 cells and revealed that after 2 minutes exposed to deionised water, their size grew of 45.1%. (Table 1) The next step was to determine if the enlargement of the PC3 cells could be monitored through impedimetric measurements. The graphs related to three data sets (Table 2) are displayed on the six following pages.

	Time of incubation of the cells with the IDEs (min.)	**Amount of cells**
Set 1 (3 experimental repeats)	20	460
Set 2 (3 experimental repeats)	60	700
Set 3	60	3000

Table I.2: Information related to the sets 1, 2 and 3.

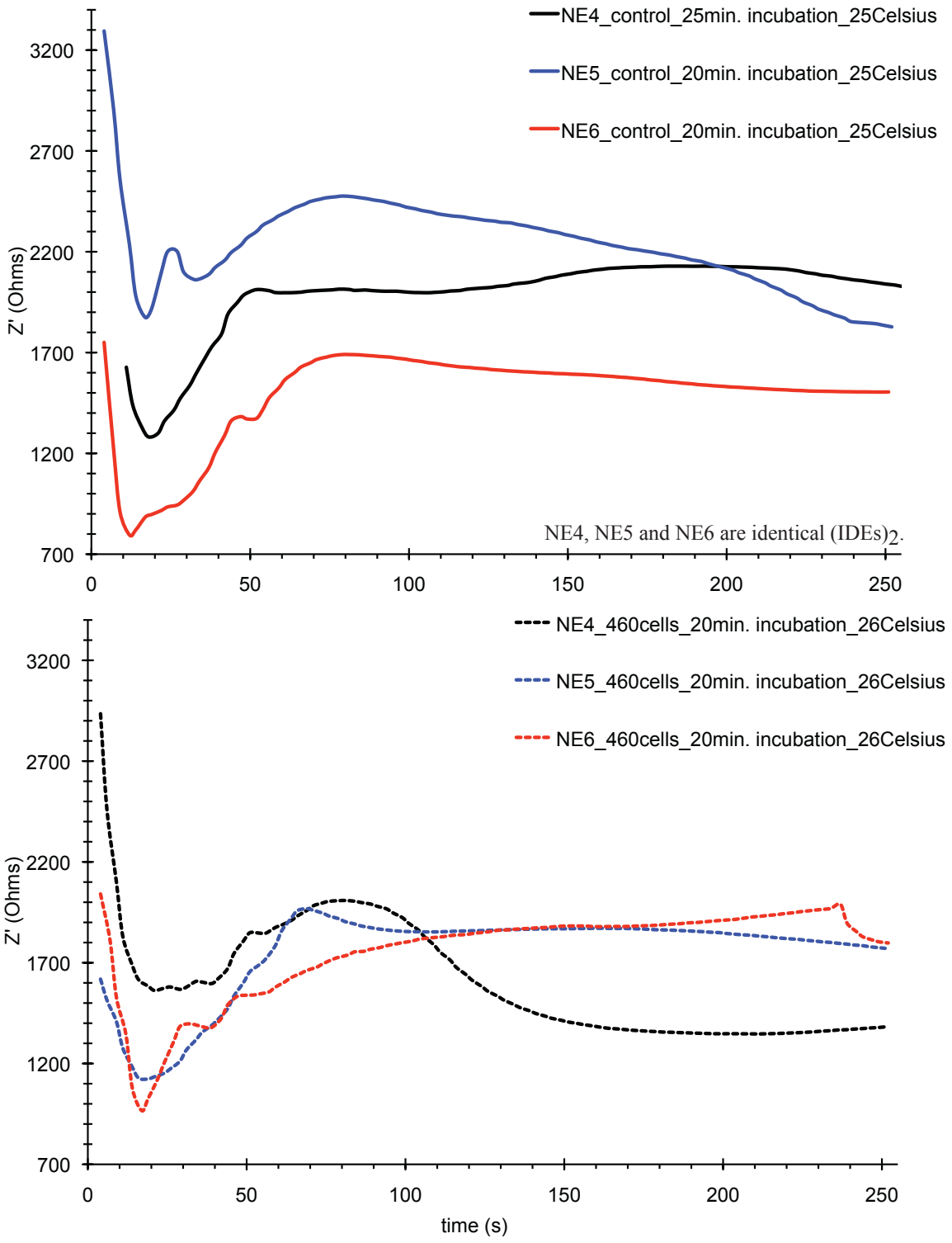

Figure I.10:
Graph 3: time-dependent evolution of Z' related to the control experiments of set 1.
Graph 4: time-dependent evolution of Z' related to the samples of set 1.

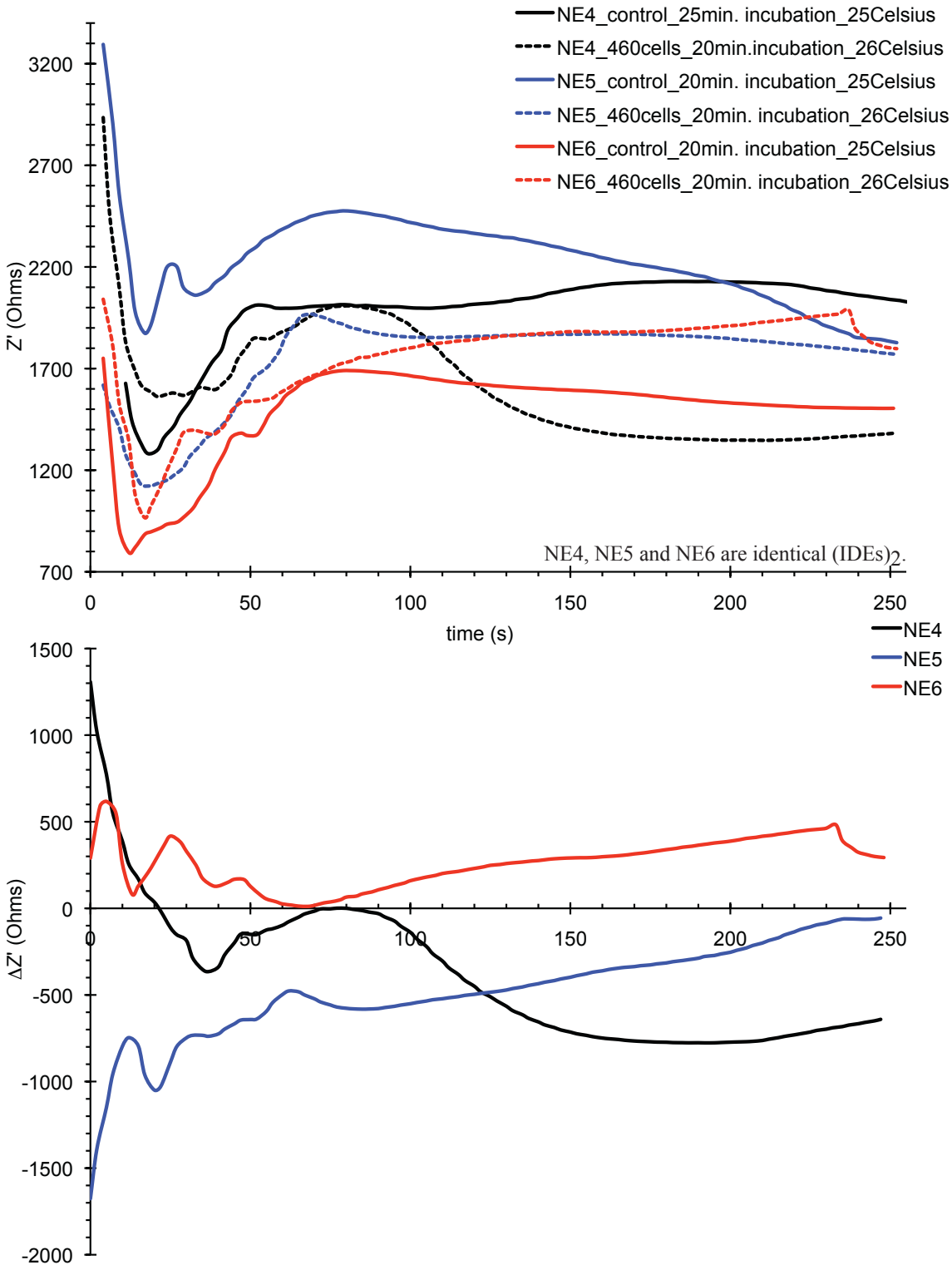

Figure I.11:
Graph 5: merged version of graphs 3 & 4.
Graph 6: time-dependent evolution of ΔZ'of set 1.

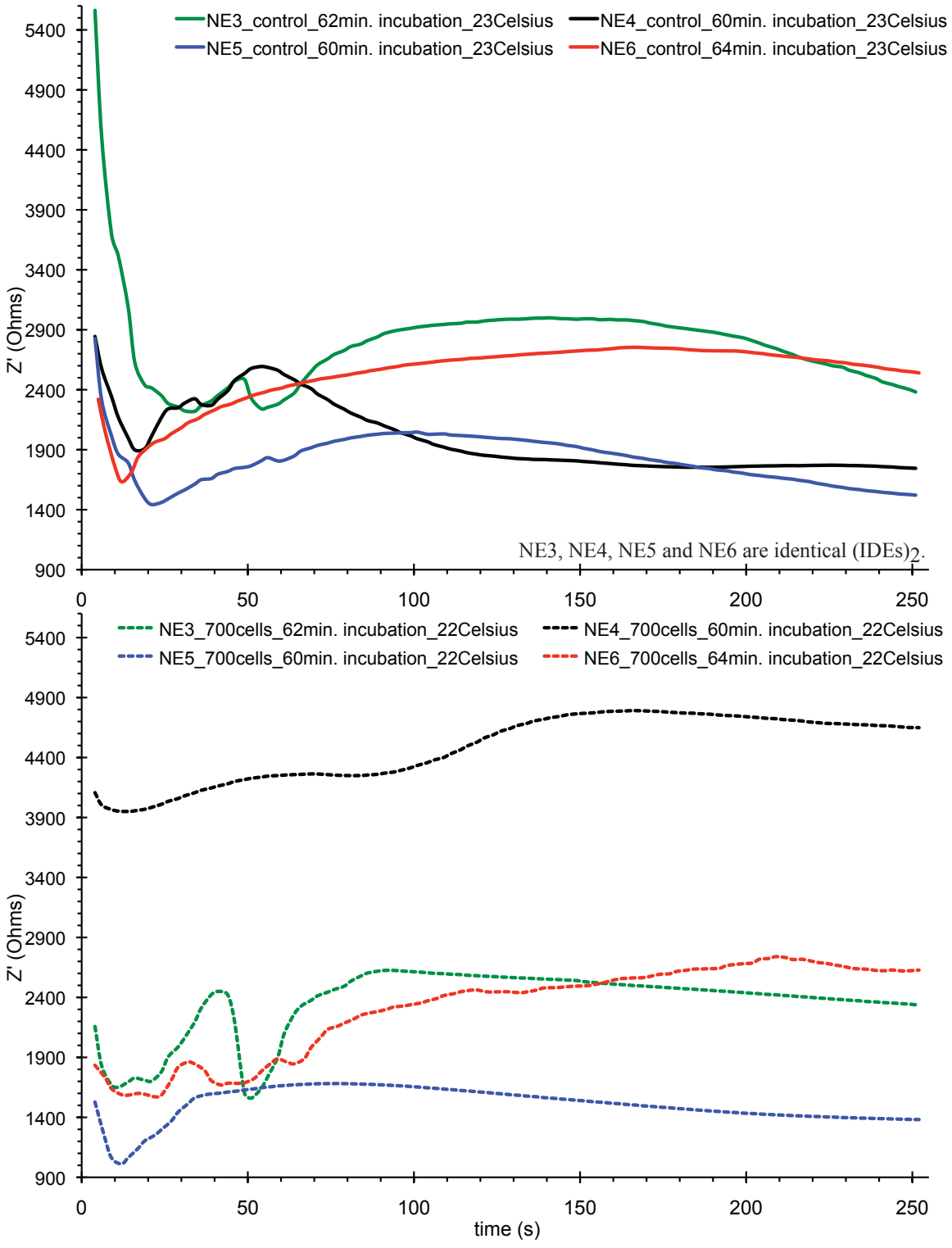

Figure I.12:
Graph 7: time-dependent evolution of Z' related to the control experiments of set 2.
Graph 8: time-dependent evolution of Z' related to the samples of set 2.

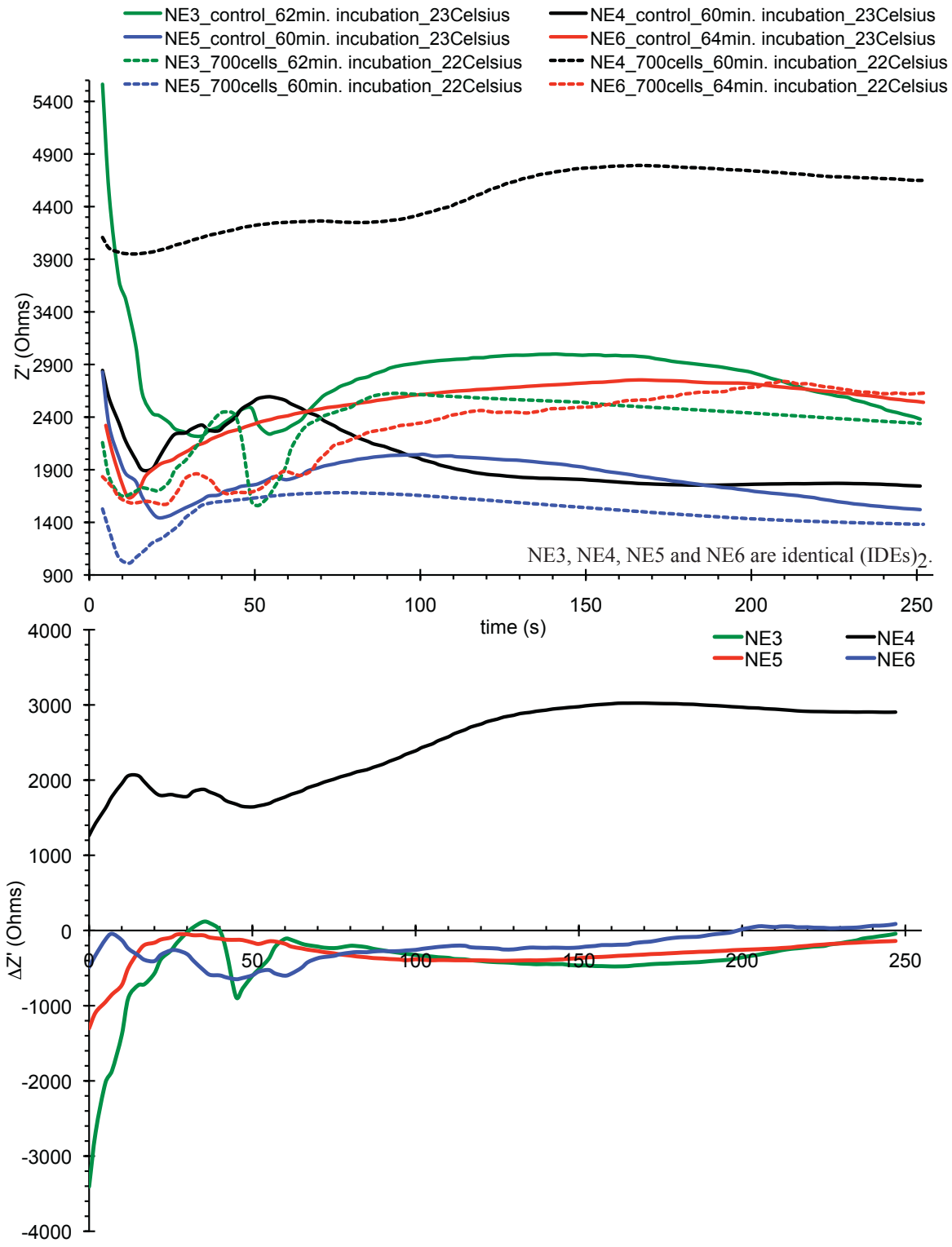

Figure I.13:
Graph 9: merged version of graphs 7 & 8.
Graph 10: time-dependent evolution of ΔZ'of set 2.

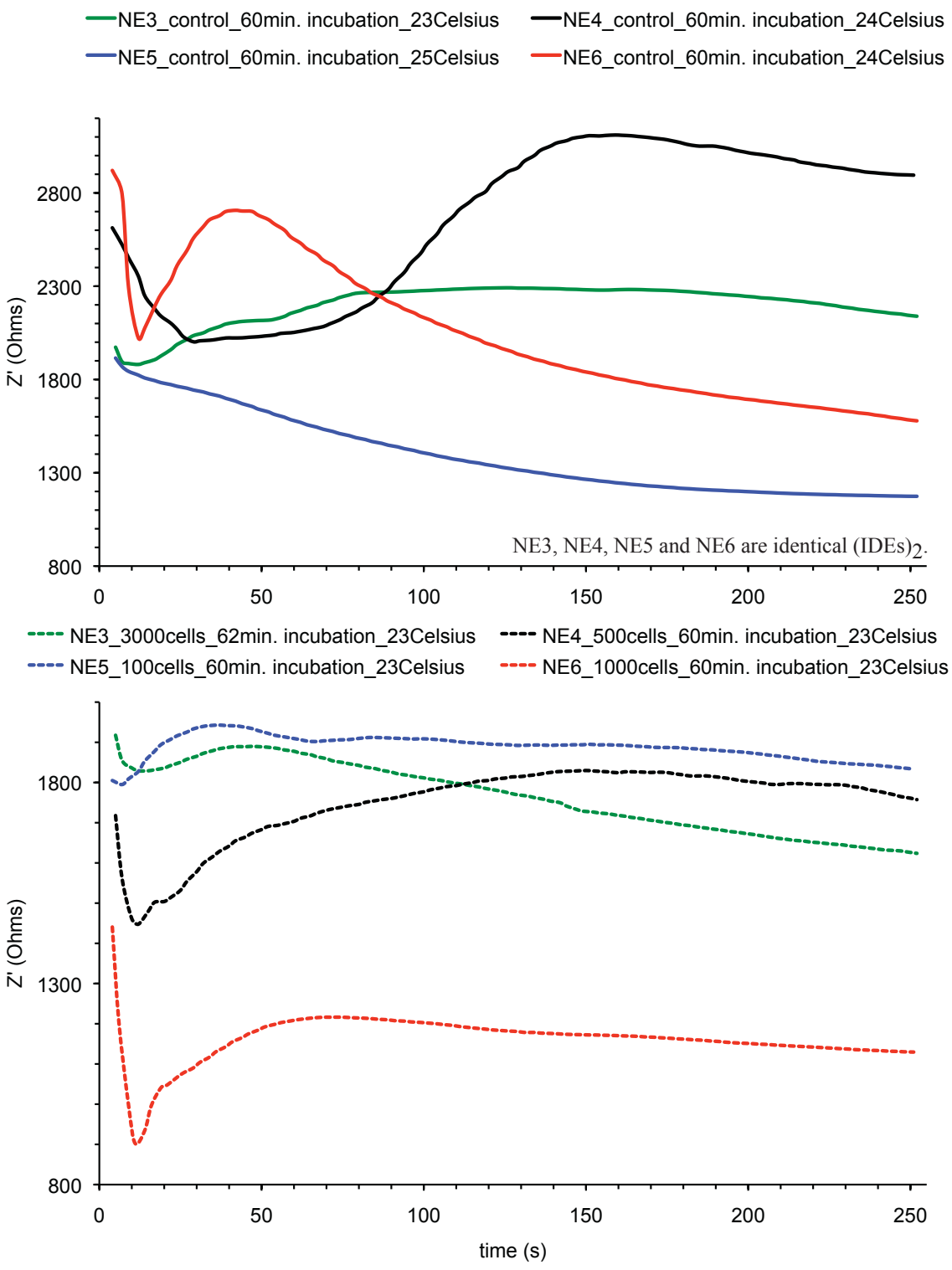

Figure I.14:
Graph 11: time-dependent evolution of Z' related to the control experiments of set 3.
Graph 12: time-dependent evolution of Z' related to the test samples of set 3.

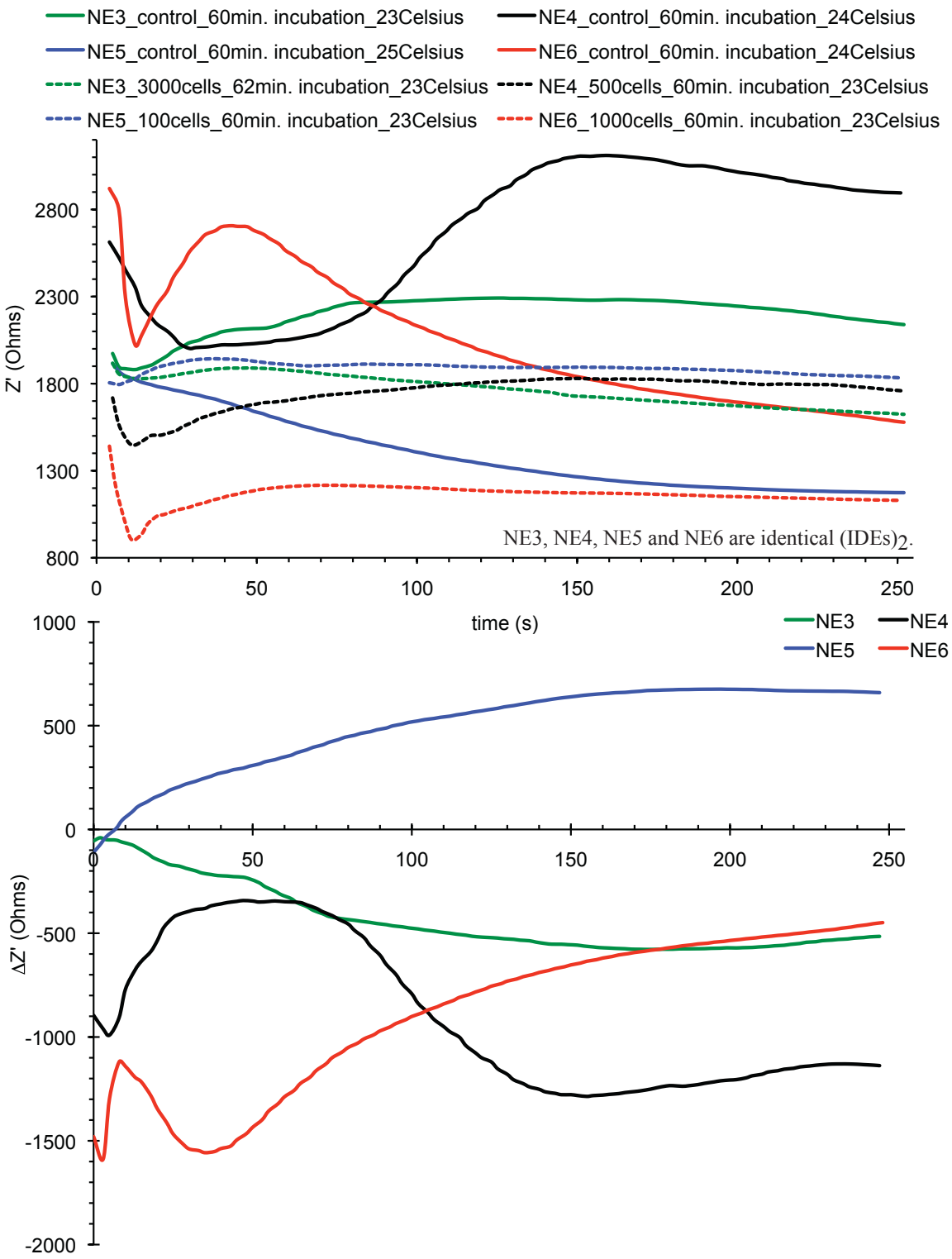

Figure I.15:
Graph 13: merged version of graphs 11 & 12.
Graph 14: time-dependent evolution of ΔZ'of set 3.

Sets 1 and 2 (both of which deal with a definite amount of cells) clearly show that the measurements corresponding to the control experiments and the samples are not reproducible at all and that the curves do not follow any given pattern (Figures I.10-I.13). In addition, set 3 unexpectedly reveals that the amount of cells incubated with $(IDEs)_2$ does not determine the relative positions of the curves (Figures I.14 and I.15): the lowest amount of cells exhibit the highest ΔZ'. (The higher the amount of cells attached on the IDEs is, the larger Z' and ΔZ' are.) Irreproducibility and the non-attachment of the cells on the IDEs could be at the origin of the misplacement of the curves.

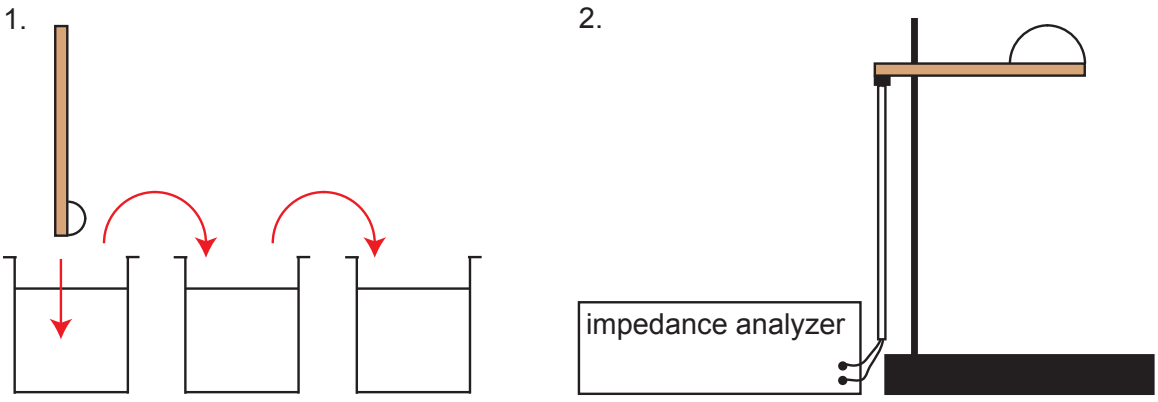

Figure I.16:
1.Schema representing the washing of the IDEs.
2.Schema illustrating the position of the IDEs during the measurement.

The irreproducibility of our measurements, especially visible in the ones related to the control experiments, derives from the uncontrolled dilution of the medium during the "dipping" of the IDEs into the three deionised-water bathes and the subsequent addition of 100µl of deionised water on the IDEs (Figure I.16.), as well as from the CO_2 diffusion. The function of the bathes and of the 100µl is to get rid of the medium and to surround the cells with enough water to trigger their swelling, respectively. All of those

operations are executed by a human being, which inherently introduces irreproducibility. The medium used to feed PC3 cells contains glucose, penicillin/streptomycin, vitamins, red phenol (pH indicator), salts like sodium bicarbonate (to buffer the medium), amino-acids such as L-glutamine, glutathione and fetal bovine serum which includes lot of proteins. This medium is very conductive (low Z') as it can be seen on figure I.17. The Z' value (i.e. 650Ω) of medium diluted 1000 times is lower than the ones related to the control experiments (comprised between 700 and 5,400Ω), in other words, the dippings and the water addition dilute the medium more than 1000 times (Figure I.17). At this stage, we do not know if this dilution level may or may not be too low to induce the cells to swell. Another source of irreproducibility is from CO_2 diffusion. When deionised water is "impedimetrically" monitored in real time, the standard deviation related to ten measurements of Z' is huge (Figure I.22). Each time the drop of deionised water lands on the IDEs, its shape varies in an uncontrollable manner. The shape of the water drop, more precisely its surface area might control the CO_2 diffusion. The effect of CO_2 diffusion on Z' is more apparent as the medium is diluted. That is the reason why, the Z' values corresponding to the medium diluted 10,000 and 100,000 times decrease with time (Figure I.17). It is important to note that CO_2 is vital for the cells: their metabolism tends to make the pH of the surrounding solution to surge, and ambient CO_2 is directly involved in the buffer system to keep the pH to physiological standard. And only live cells can swell under hyposmotic stress. To alleviate those problems of irreproducibility, we must reduce as much as possible the extent of the manual tasks. For example, we could run the impedimetric measurements right after having vertically positioned the IDEs in a large beaker full of deionised water at a defined depth to diminish the influence

of the human operator and CO_2 diffusion. This supposes that the cells firmly "stick" on the vertically-positioned IDEs.

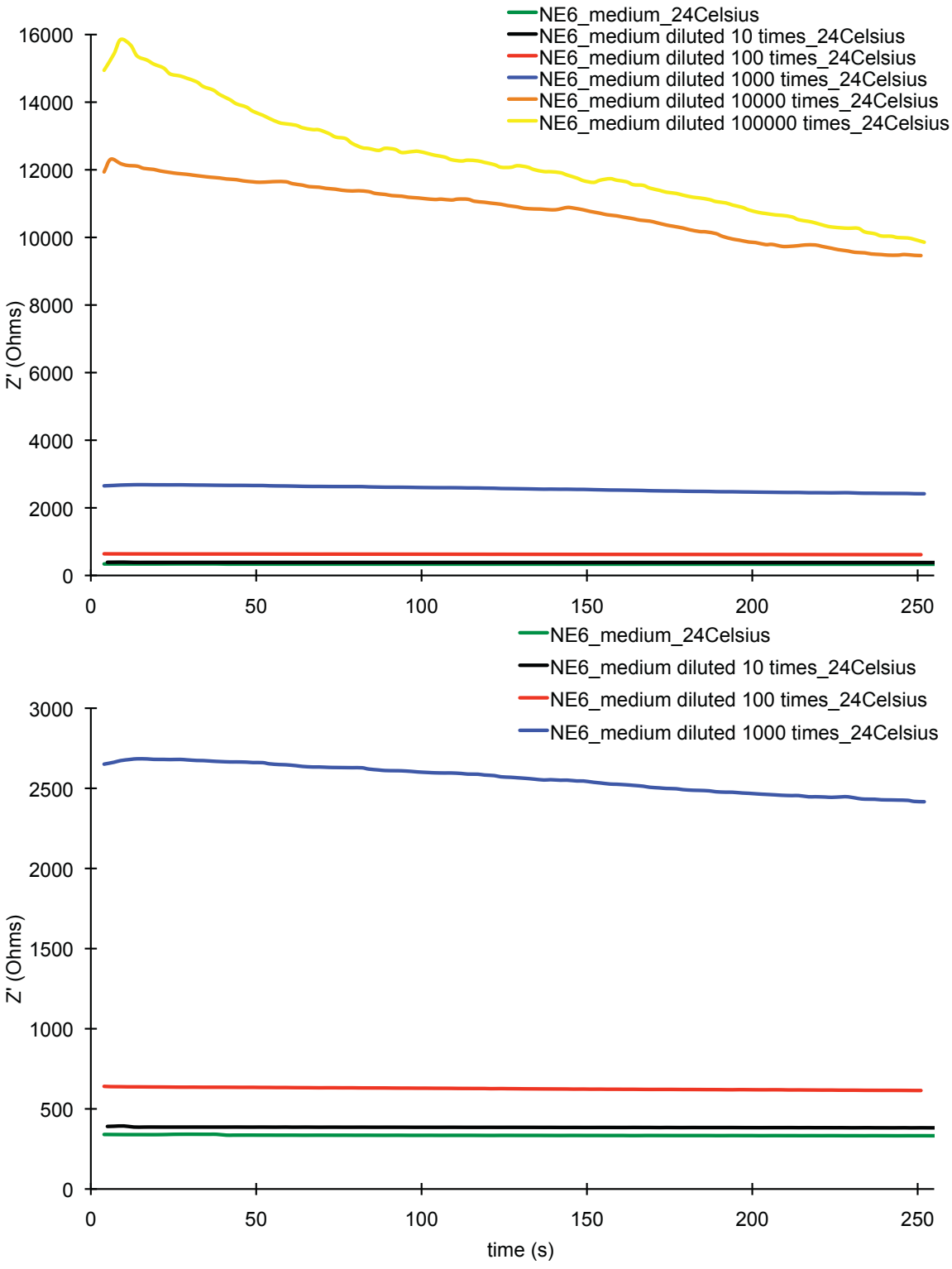

Figure I.17:
Graph 15: time-dependent evolution of Z' of medium and diluted mediums.
Graph 16: magnification of some curves of graph 15.

The flasks in which we culture PC3 cells are coated with polylysine to promote the cell adhesion by coulombic attraction: at physiological pH, cell surface exhibits a net negative charge due to the presence of carboxylates and phosphates [39], whereas polylysine is positively charged. The flasks are placed in an incubator maintaining the temperature at 37.5°C, the CO_2 percentage of the atmosphere at 5% and a given humidity rate (a recipient full of water is placed within the incubator). In those conditions, cells adhere on the surface of the flask in less than half-an-hour, which is easily visible through optical microscopy. In our experiments, the medium/cell drop is deposited on the polylysine-coated IDEs and left for 20 to 60 minutes at room temperature in open atmosphere, at lower CO_2 and humidity rates, conditions that may not favor the attachment of the PC3 cells on the IDEs. The augmentation of the incubation time of the PC3 cells on the IDEs to 60 minutes did not change the random character of the impedimetric spectra. Our IDEs are not transparent like culture flasks and the state of their surface (Figure I.18) as well as the micropost connector does not facilitate the observation of cells on the IDEs. Because of the micropost connector, the IDEs have to be tilted below the objective to get an image of poor quality. Only its middle part is in focus due to the micropost connector and reveals bands, which are actually the interdigitated electrode fingers. The small black spots cannot be clearly identified as cells (Figure I.18).

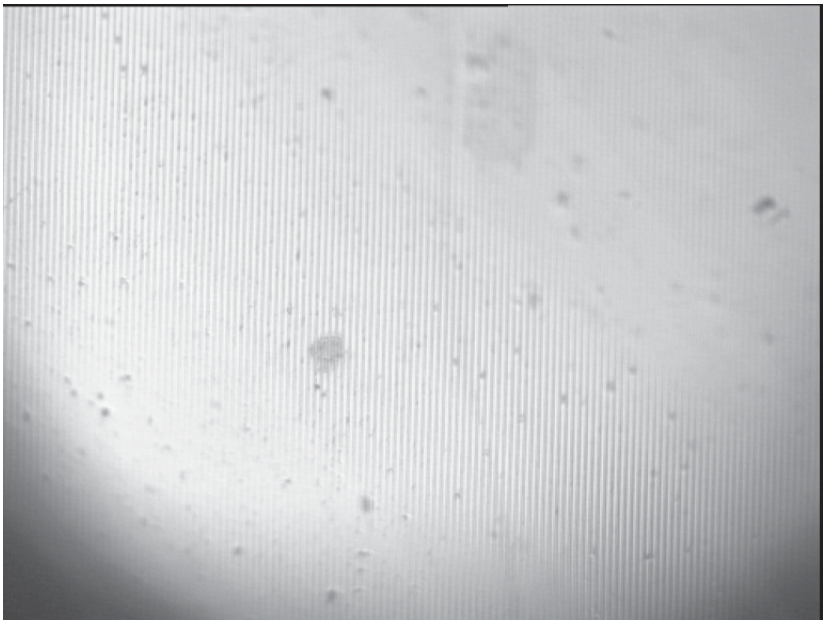

Figure I.18: Picture of $(IDEs)_2$ surface after cell incubation and washing in deionised-water baths.

It appears crucial to determine at first the parameters favoring the binding of PC3 cells on the IDEs and then perform the impedimetric measurements. Quartz Crystal Microbalances (QCM) have been known to quantitatively assess the cell adhesion on quartz substrates.[40] An oscillating voltage applied on the piezoelectric crystal makes it mechanically oscillate around its steady-state position. This mechanical-oscillation frequency is highly sensitive to any adsorption event occurring at the crystal surface, such as cell adhesion. Today, various materials such as SiO_2 cover the piezoelectric crystals, allowing to mimic the surface of the $(IDEs)_2$. The discrimination between weakly-bound and firmly-attached cells is accomplished by a stream of buffer solutions. QCM analyses will allow us to quantify the cell adhesion while subjecting the cells to different conditions (temperature, CO_2 percentage, humidity rate, incubation time, coating of proteins promoting cell adhesion). One important aspect of cell adhesion is based on the protein coating whose function is to assist the cell attachment. Poly-D-lysine is commonly employed for this purpose. Nevertheless, it was proven to be dose-dependent cytotoxic for some cell types (i.e. HeLa cells): it is supposed to perturb the membrane structure leading to cell lysis.[41] In our experiment, we incubated the IDEs with a 100µl drop of poly-D-lysine solution (1mg/ml) for 20 minutes (this drop covers far more than the IDEs area). We also tried smaller volumes and lower incubation times, however no change in the impedimetric spectra was recorded (data not shown). There are potent candidates such as fibronectin to substitute for polylysine. Fibronectin mediates the cell attachment via receptor-ligand interaction [42], which should be stronger than coulombic attraction. In the future, an extensive QCM-based study will have to be conducted on the attachment of PC3 and PNT1A cells exposed to various conditions. QCM also offers the

possibility to directly investigate the swelling of attached cells since the composition of the liquid stream used to rinse off the weakly-bound cells can be tuned. By flowing pure deionised water, attached cells swell and their mass change should induce a mechanical-oscillation frequency shift. This method might appear adequate to detect cancer cells among a plethora of normal cells and will be tried in parallel with the impedimetric measurements.

Dr. Antonio Baldi and his team are designing new $(IDEs)_2$ (Figure I.19) to culture cells *in situ* by having the IDEs at the bottom of a well and to integrate microfluidics, more precisely a removable PDMS chamber possessing a central channel. The well and the CO_2-permeable PDMS chamber will permit us to incubate the cells with the IDEs under the optimum conditions of the incubator. The PDMS chamber will reduce the CO_2 diffusion into the nitrogen-bubbled deionised water flowing through the channel and more importantly might fix it to a constant value, improving the reproducibility of the impedimetric measurements. (The thickness of the PDMS-chamber walls commands the CO_2 diffusion.)

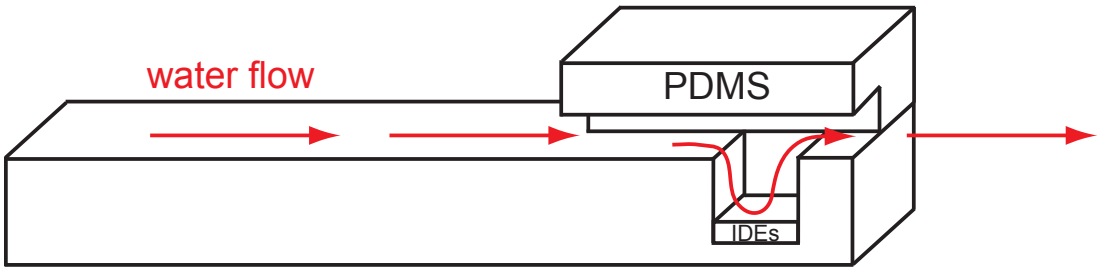

Figure I.19: Schema depicting a longitudinal section of the new $(IDEs)_2$.

I.5. Hydrogel beads.

de la Rica Roberto, Thompson Sebastian, Baldi Antonio, Fernández-Sánchez César, Drain Charles Michael and Matsui Hiroshi were able to monitor the size change of cells using impedimetric measurements.[33] Following the same idea, we intended to visualize the size change of hydrogel beads exposed to external stimulus through impedance. As said earlier, hydrogel beads hold great promises for drug delivery. Being able to "impedimetrically" keep track of hydrogel-bead size variations could help us to follow the release of ionic drugs via impedance measurements. Two types of hydrogel beads were investigated.

I.5.1. Photosensitive and thermoresponsive hydrogel beads.

These hydrogel beads are a generous gift from Dr. Svetlana Suskivishli's laboratory (Stevens Institute of Technology, New Jersey, USA). They are composed of 100nm gold cores onto which PDMA/PNIPAM copolymer chains (Figure I.20) are grafted. The interest of synthesizing PDMA/PNIPAM copolymer chains is to combine the hydrophilicity of PDMA to the thermoresponsive trait of PNIPAM, a less hydrophilic polymer, in order to improve the stability of the hydrogel beads within aqueous solutions. PNIPAM is a thermoresponsive polymer (Figure I.21): below and beyond the lower critical solution temperature (LCST=30-35°C [12]), PNIPAM adopts a hydrophilic conformation and a hydrophobic one, respectively.[12] The temperature-dependent conformation switch is explained by the following equation:

$$\Delta G_{mixing} = \Delta H - T\Delta S$$

ΔG_{mixing}, ΔH, T and ΔS stand for the free energy of PNIPAM chains/water molecules mixing, the enthalpy of formation of hydrogen bonds established between the polymer polar groups and water molecules, the temperature of the system and the entropy of mixing.[12] Water molecules rearrange around apolar regions of the polymer chains, being unable to hydrogen bond to them, resulting in the decrease of the entropy of mixing ($\Delta S < 0$). The hydrogen bonding between the polar groups and water molecules is exothermic ($\Delta H < 0$). At the LCST, ΔG_{mixing} becomes positive, resulting in the phase separation. The point of having gold cores is to render the hydrogel beads photosensitive (plasmon absorption ~550nm) and to directly convert the light absorption into heat to induce the conformation switch of the copolymer chains. Their size can reversibly be changed by cooling them. The size of those hydrogel beads depends upon the temperature and the pH. At pH 5.5, their size is comprised between 480 and 200 nm and their LCST reaches 35°C (unpublished data).

PNIPAM
Poly(N-isopropylacrylamide)

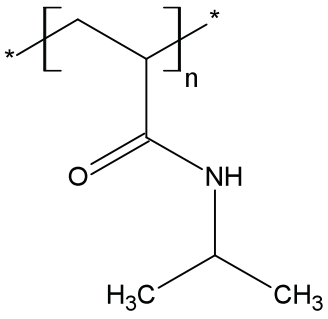

PDMA
Poly(N,N-dimethylacrylamide)

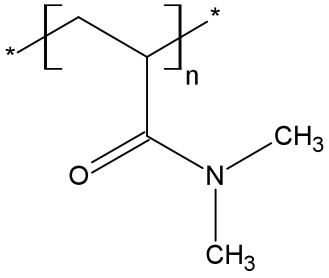

Figure I.20: Chemical formulas of PNIPAM and PDMA.
PDMA develops a positive charge on the nitrogen atom bound to two methyl groups via its protonation.

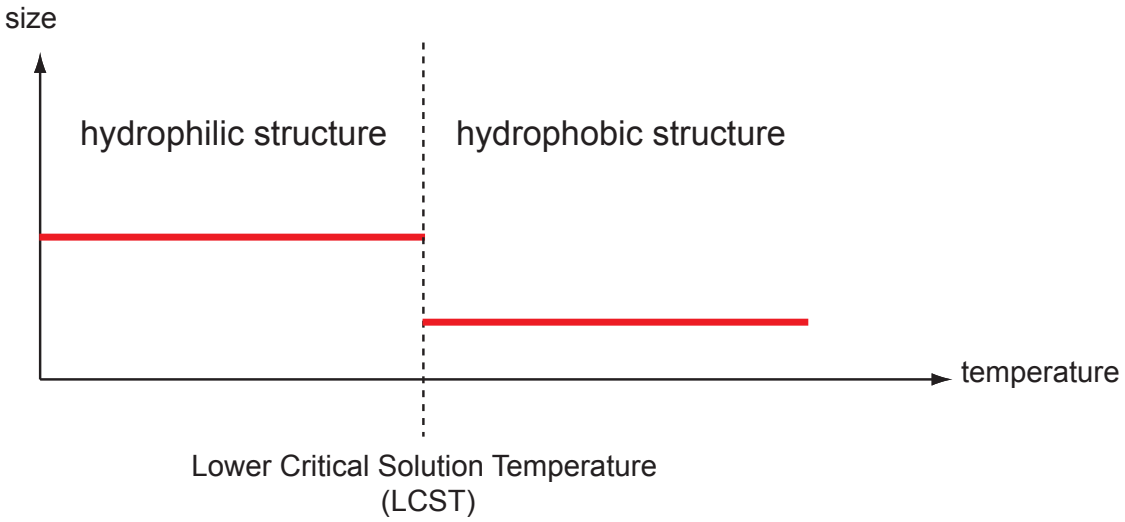

Figure I.21: Schema representing the temperature-dependent evolution of the hydrogel-bead size.

The beads are washed once with deionised water through centrifugation/decantation/deionised-water addition/vortex/centrifugation/decantation. Then, they are dispersed into a diluted aqueous HCl solution (pH = 5.5). Since our goal was to monitor the size change of the hydrogel beads, simple physisorption was preferred over covalent attachment. A 10µl drop of the hydrogel-bead solution were spotted on the IDEs and left for an hour, then rinsed with deionised water and dried with nitrogen gas. Then, a given volume of deionised water was placed on the IDEs and real-time impedimetric measurements were run at 20kHz, while a green laser whose emission is centered around 532nm was alternatively turned on and off or a hot mantle filled of water at 45°C was "encapsulating" the IDEs in an on and off manner for given time periods. After each measurement, the IDEs are dried with nitrogen gas. The control experiment consists of a 10µl deionised-water drop deposited on the IDEs.

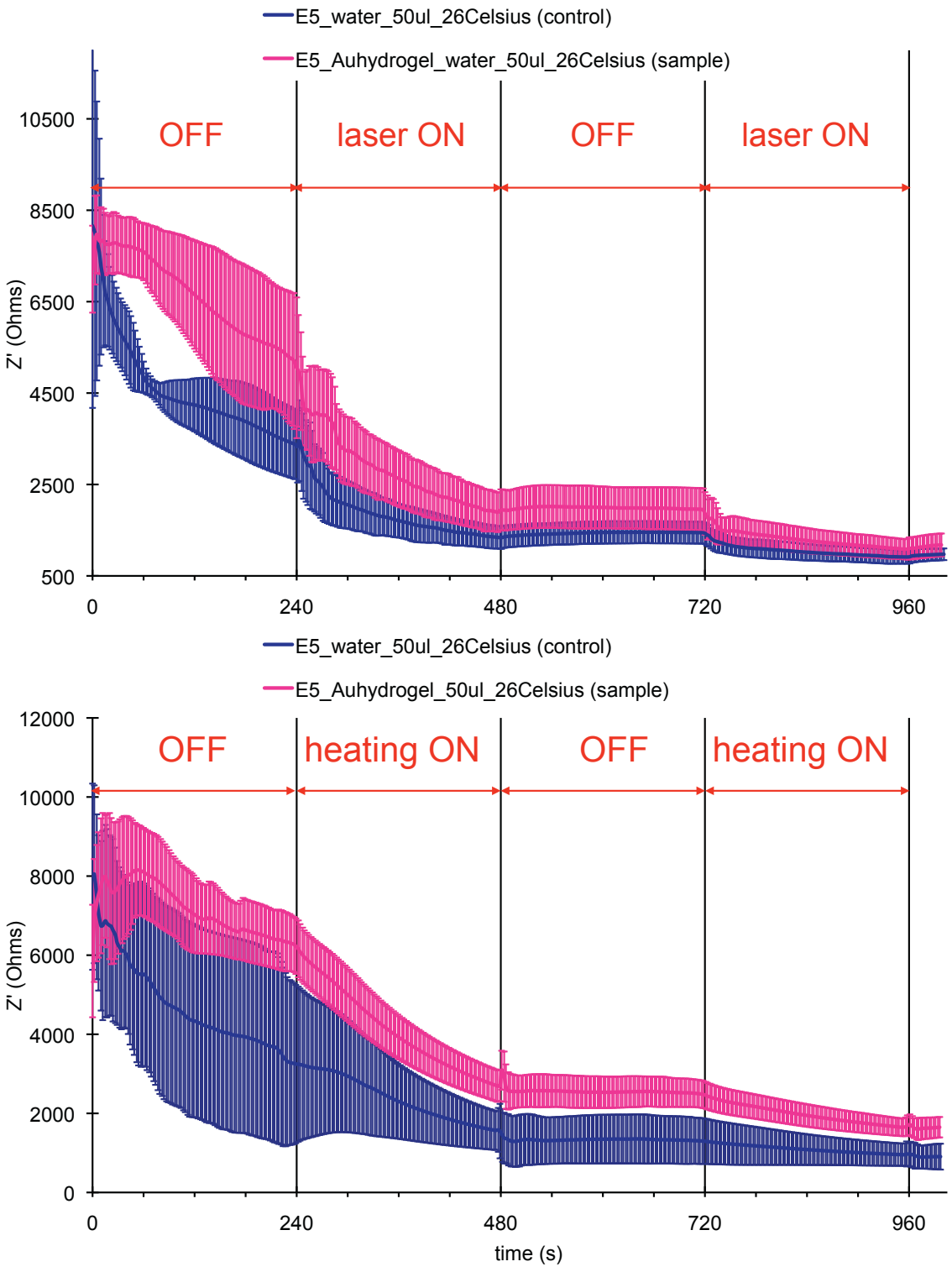

Figure I.22:
Graph 17: time-dependent evolution of Z' related to set 4.
Graph 18: time-dependent evolution of Z' related to set 5.
(Error bars are calculated from ten measurements.)

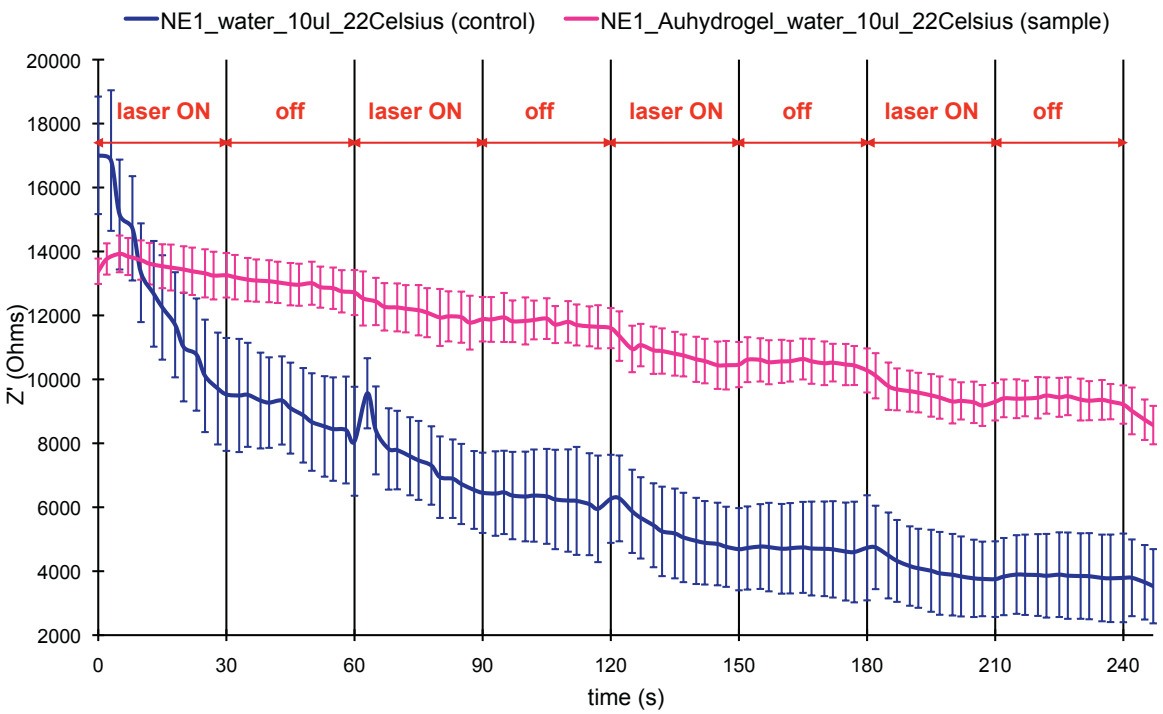

Figure I.23: Graph 19: time-dependent evolution of Z' related to set 6.
(Error bars are calculated from five measurements)

	Experimental conditions	Graphs
Set 4	Succession of four-minute periods during which the laser is either on or off.	Graph 17
Set 5	Succession of four-minute periods during which a hot mantle is either surrounding the IDEs or removed.	Graph 18
Set 6	Succession of thirty-seconds during which the laser is either on or off.	Graph 19

Table I.3: Information related to the sets 4, 5 and 6.

Here are the observations derived from figures I.22 and I.23. The curves representing Z'(gold hydrogel beads_water) and Z'(water) against time are somewhat

parallel and decay with time due to CO_2 diffusion into water. The laser makes them decrease faster as the hot mantle. The temperature rise caused by the laser or the hot mantle increases the diffusivity of CO_2 into water for both cases and reduces the size of the hydrogel beads. This last effect offers more space in the probed area to accommodate more CO_2 molecules and supposedly decreases the distortion of the electric-field lines exerted by the hydrogel beads (Z' increases with the size of the insulating objects), which should result in a higher decrease of Z'. Nevertheless, the size effect on Z' is, if present, so negligible that it could not be visualized by impedimetric measurements since the curves representing Z'(gold hydrogel beads_water) and Z'(water) against time are somewhat parallel. The decrease of laser exposure time to 30 seconds does not make the hydrogel-bead size change visible.

Z'(gold hydrogel beads_water) > Z'(water), in other words gold hydrogel beads behave like insulating objects. This remark is not always valid at the measurement onset. This discrepancy of behavior might be explained by assuming that deionised water freshly drawn from the deionised water dispenser may be less conductive than the hydrogel beads. With time, CO_2 diffuses for both cases. However, despite the CO_2 diffusion, hydrogel beads physisorbed at the IDEs surface are detected through impedimetric measurements.

To confirm that the hydrogel beads behave as insulating objects, we made the decision to determine the cell constant of the system comprising the IDEs and the hydrogel beads using KCl (Figure I.24). For graph 20, the impedimetric measurements were performed from the highest KCl concentration to the lowest one, while for the graph 21, they were done in the reverse order. Surprisingly, the hydrogel beads diminish the

cell constant of the bare IDEs, which contradicts the insulating behavior observed in figures 22 and 23. Nevertheless, KCl was not used during the impedimetric measurements displayed in figures 22 and 23 and salts are known to reduce the LCST by interacting with PNIPAM [12]. KCl might be at the origin of the decrease of the cell constant resulting from the diminution of R_{sol} whose values were obtained by fitting. We could imagine that hydrogel beads pull a large amount of ions in the area probed by the IDEs in such a way that their insulating comportment is completely masked.

To conclude, the presence of those hydrogel beads can be detected through impedimetric measurements but their size variation cannot. Visualizing it might require to get rid of CO_2 by integrating some CO_2-proof microfluidics. However, the size span of these hydrogel beads is probably too small to be noticed by impedance measurements. That is the reason why we tried to analyze larger hydrogel beads.

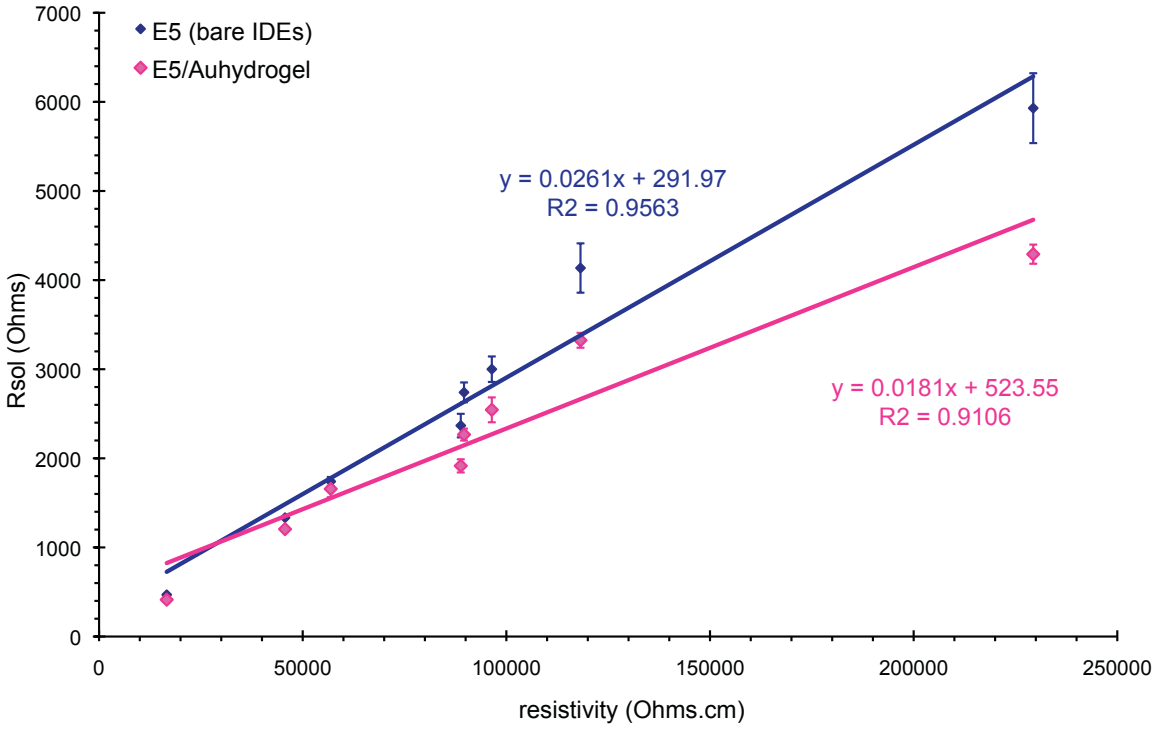

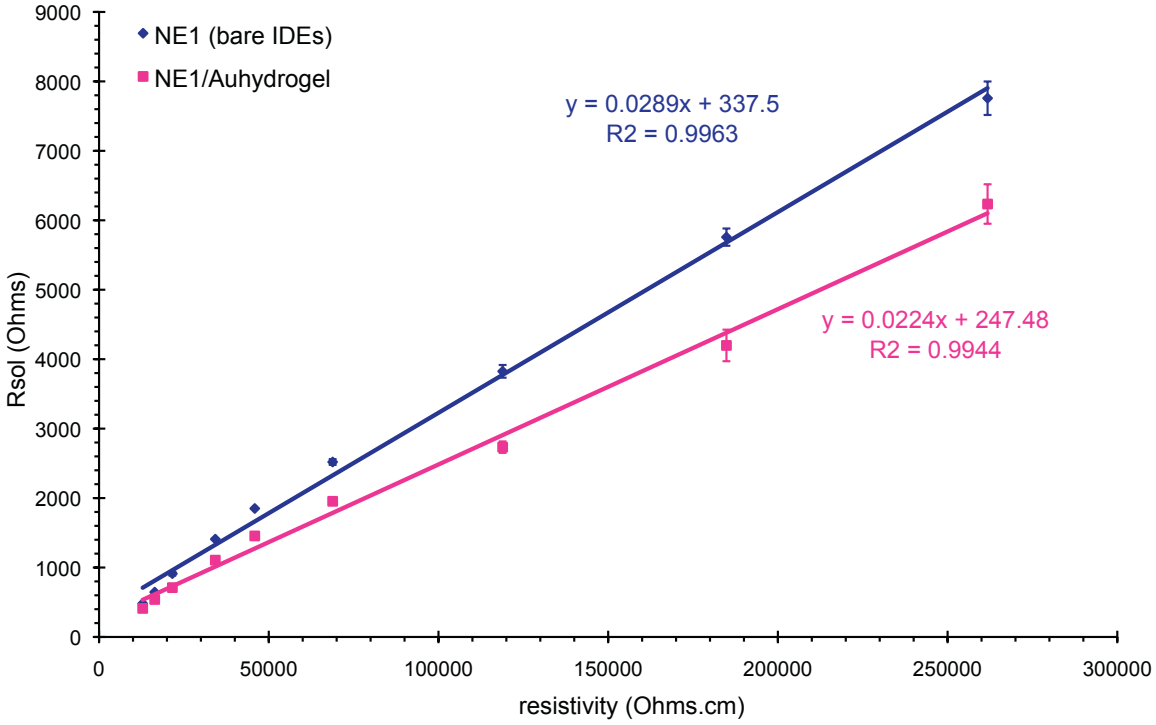

Figure I.24:
Graph 20: Cell-constant determination in absence and presence of gold hydrogel beads.
Graph 21: Cell-constant determination in absence and presence of gold hydrogel beads.
(Error bars are calculated from five measurements)

I.5.2. Enzyme-responsive hydrogel beads.

Those hydrogel particles (Figure I.25) are graciously offered by Dr. Rein Ulijn's laboratory (University of Strathclyde, Glasgow, UK). They are made of 150-300µm $PEGA_{800}$[20] spheres functionalized with Arg-Ala~Ala-Asp-Fmoc[21] peptides: the terminal carboxylic group of the Arg amino-acid is anchored to the $PEGA_{800}$.[13] At basic pH, the side chains of the arginine and aspartic acid are positively and negatively charged, respectively. Proteases such as elastase cleave this peptide between the alanine residues in such a way that a positive charge is left on the terminal amine of the alanine (connected to the arginine) and a negative one on the terminal carboxylic group of the other alanine (connected to the aspartic acid). Therefore, two negative charges remain on each leaving peptide part (Ala-Asp-Fmoc) and two positive charges on each grafted peptide part (Arg-Ala). The proximity of the positive charges bore by the grafted peptide parts trigger the enlargement of the hydrogel beads due to coulombic repulsions. The swelling of those particles is irreversible.

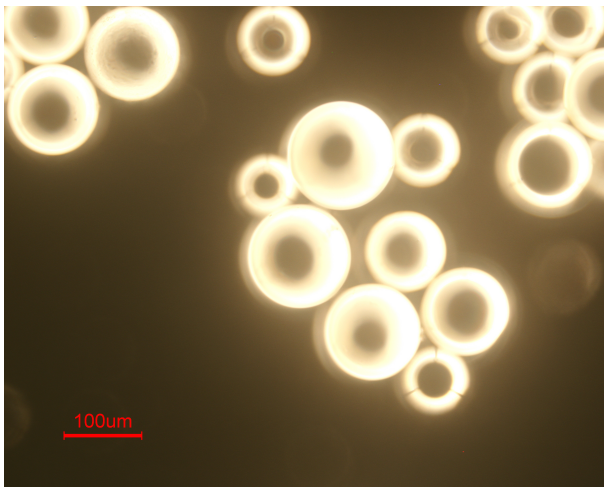

Figure I.25: Picture depicting enzyme-responsive hydrogel particles.

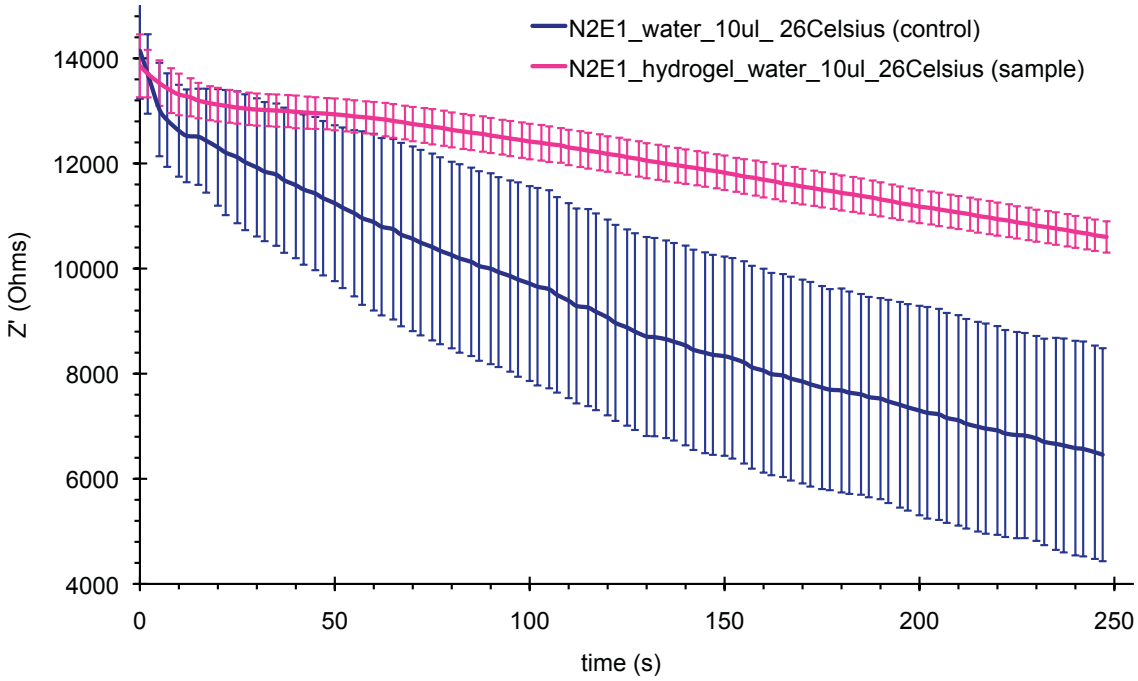

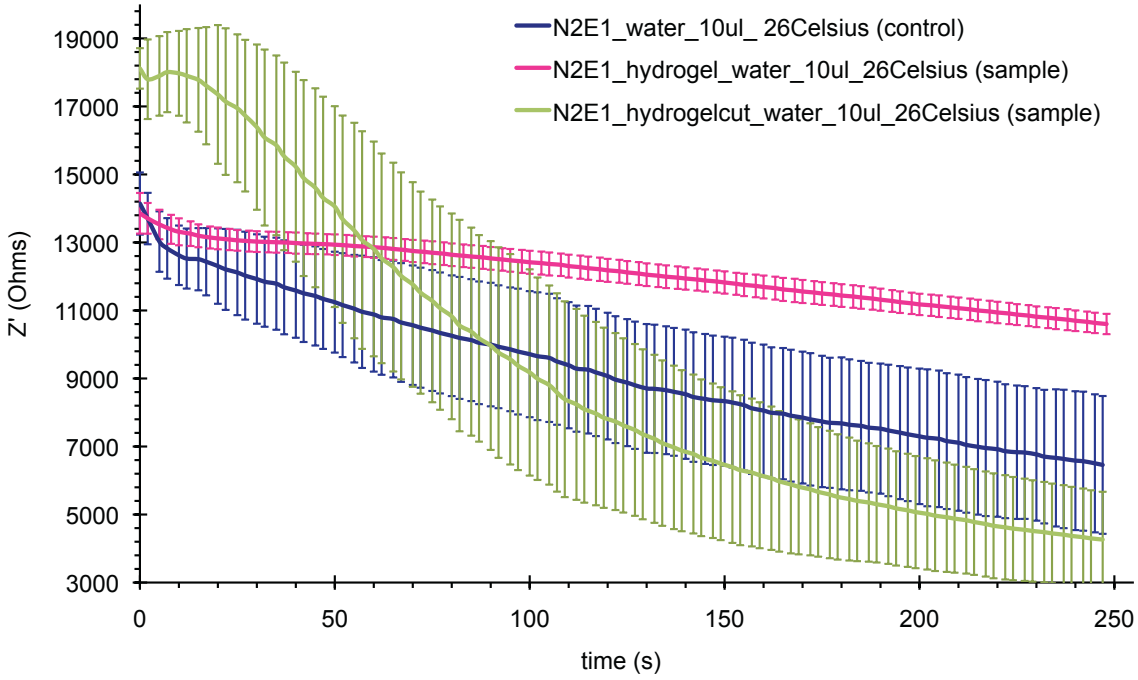

Figure I.26:
Graph 22: Z'(t) in absence and presence of hydrogel particles.
Graph 23: Z'(t) related to cleaved hydrogel beads was added to Graph 22.
(Error bars are calculated from 10 measurements)

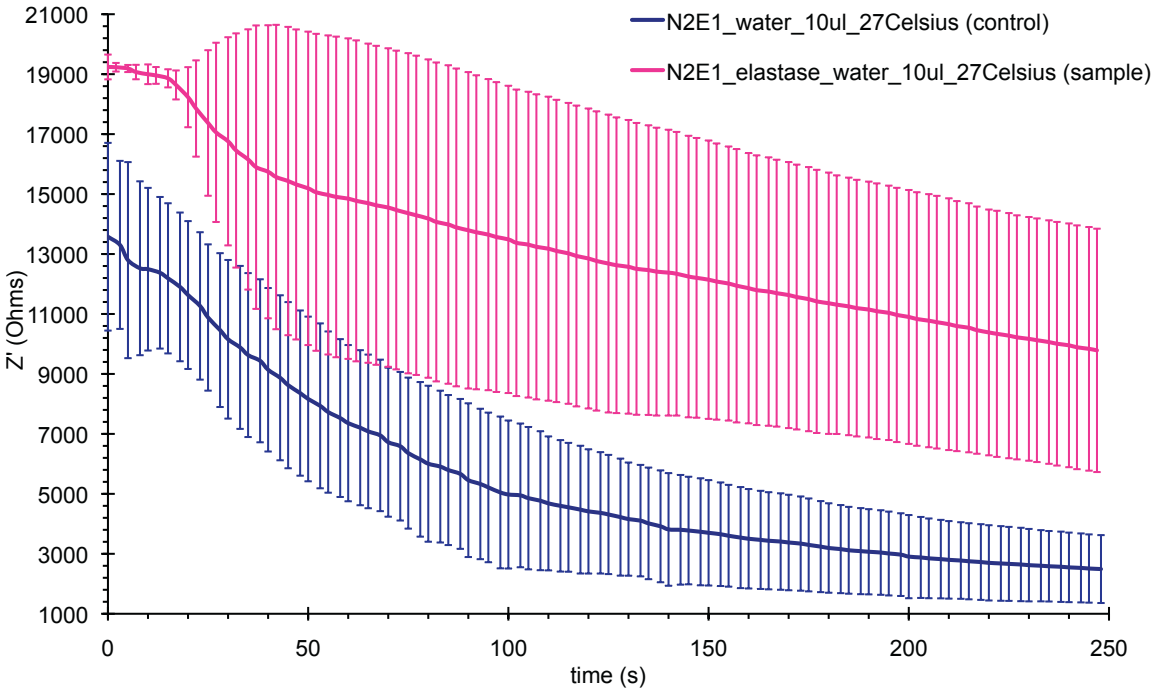

Figure I.27: Graph 24: Time-dependent evolution of Z' in absence and presence of elastase. (Error bars are calculated from 10 measurements)

The hydrogel particles were redispersed into water. The IDEs were incubated with 10µl of the hydrogel-particle solution for one hour, rinsed with deionised water and dried with nitrogen gas. A 10µl drop of deionised water was deposited on the IDEs followed by real-time impedimetric measurements performed at 20 kHz. After rinsing and drying, a 10µl drop of elastase-saturated solution[22] was placed on the IDEs and left for 30 minutes. After rinsing, drying and the addition of 10µl of deionised water, real-time impedimetric measurements were run. After each measurement, the IDEs are dried with nitrogen gas. The control experiment consists of a 10µl deionised-water drop deposited on the IDEs.

The remarks regarding the previous type of hydrogel beads are also valid for this one: Z'(hydrogel_water) > Z'(water) and they decay with time due to CO_2

diffusion. However, these hydrogel beads present some particularities. The standard deviation related to the untreated hydrogel beads is extremely small (Figure I.26), which means that the impact of the untreated hydrogel beads on Z' is reproducible and much larger than the one of CO_2 diffusion. After each rinsing, the hydrogel beads remain at their place and occupy the majority of the area probed by the IDEs. CO_2 diffusion is actually not detrimental to the detection of the hydrogel particles since with time, it amplifies the difference between the control and the unaltered hydrogel beads (Figure I.26).

When the IDEs are incubated only with elastase solution for 30 minutes, the curve representing Z'(elastase_water) is above the one describing Z'(water) and its corresponding standard deviation is even larger than the one associated with CO_2 diffusion except at the beginning of the measurements (Figure I.27). The first fact implies that elastase adsorb on the IDEs and form a film thick enough to influence Z' (thus R_{sol}). The second observation could be explained by the following scenario. At the beginning of the measurement, a homogeneous dry film of elastase covers the IDEs. With time, elastase becomes hydrated and adsorption/desorption events occur in an irreproducible manner, leaving a heterogeneous film still able to affect Z'. When hydrogel beads are exposed to elastase, they expand. This size increase should translate as a higher Z' than the one of the untreated hydrogel particles. It is actually the case only during the first minute of the measurement (Figure I.26, Graph 23): Z'("hydrogelcut"_water) > Z'(hydrogel_water). After the first minute, the reverse is observed. The standard deviation associated to elastase-exposed hydrogel beads is larger than the one of the control. Elastase completely modifies the impedimetric behavior of the hydrogel beads.

After the elastase incubation and the subsequent water rinsing, only remain the positively-charged hydrogel beads and the elastase proteins adsorbed on the IDEs. Since the elastase-exposed hydrogel beads have a larger size than the untreated ones (150-300μm), the IDEs area occupied by adsorbed elastases should be extremely small and should have a negligible effect on Z'. The elastase-exposed hydrogel beads should be far more porous than the unaffected ones and are accordingly more CO_2 permeable. Their CO_2 permeability and their positive charges could explain the drastic decline of Z' and the high standard deviation.

Enzyme-responsive hydrogel beads can be detected through real-time impedimetric measurements and their signal is strengthened by CO_2 diffusion. Elastase entirely changes their impedimetric comportment by doubling the positive charges present within and on the hydrogel beads and by increasing their porosity and thus their CO_2 permeability. Accordingly, the size variation of these hydrogel beads or more precisely their structure modification can be qualitatively visualized through impedance measurements.

Chapter II.

Fabricating an inorganic analogue of the Horse Radish Peroxidase (HRP) for Enzyme-Linked ImmunoSorbent Assays (ELISA).

II.1. Introduction.

HRP is an enzyme, which catalyzes the oxidation of a chromogenic substrate by H_2O_2 into a dye molecule. Conjugated to an antibody, it becomes sensitive to the presence of given antigens (molecules, proteins, cells, microorganisms or materials) in a sample. Consequently, HRP-labeled antibodies establish a correlation between the amount of targeted antigens present in a sample and the quantity of dyes produced during the color development. The latter one is assessed by measuring the absorption of the formed dye at a given wavelength. The HRP-labeled antibody is thus the key component on which are based ELISA (Figure II.1).

While HRP is commonly employed in ELISA, it presents three shortcomings. Its extraction relies on costly and time-consuming traditional methods of protein purification resulting in low specific activities, yields and fold purification.[43] The stability of its enzymatic activity drastically decreases from 4 years in a lyophilized form to at least 2 weeks when dissolved into 0.1 M phosphate buffer at pH 6.0, and kept at room temperature.[44] Its enzyme activity is further reduced by the utilization of sodium azide

(being a HRP inhibitor) usually employed to extend the shelf life of antibodies.[44] The only way to prevent the oxidation reaction from occurring is by denaturing the enzyme (pH change, temperature) or starving the enzyme by removing its specific substrate, namely H_2O_2. Fabricating a biocompatible, stable-over-time, easy-to-make, low-cost and easily on-and-off turned inorganic alternative to HRP would be appealing for the large community performing daily ELISA.

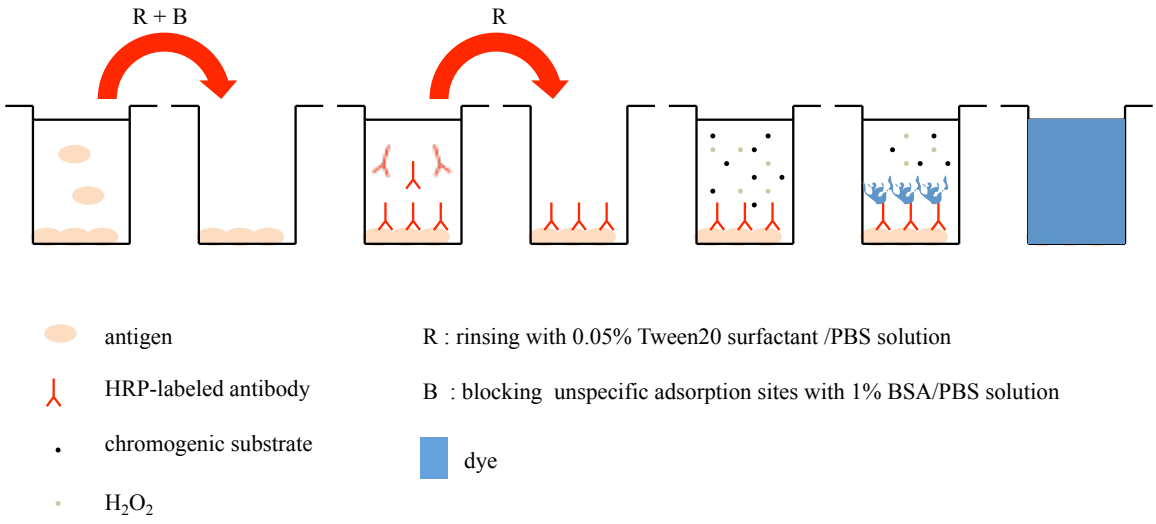

Figure II.1: Schema depicting ELISA.

TiO_2 is chemically inert as reflected by the high value of its band gap (3.23eV for bulk anatase and 3.06eV for bulk rutile [45]), supposedly weakly-toxic to humans and animals, timewise unalterable, easily-synthesized, inexpensive as well, justifying its widespread use into paints, sunscreens, toothpastes, food and medicine.[46] Subjected to UV exposure, TiO_2 nanoparticles photogenerate electron/hole pairs whose charged components exhibit short lifetimes and are accordingly engaged in redox reactions with adsorbed species.[47] Electrons or holes photogenerated by TiO_2 nanoparticles might convert a chromogenic substrate into a dye.

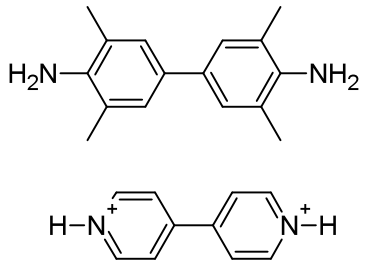

Figure II.2: 3, 3', 5, 5'-tetramethylbenzidine (TMB)
1, 1'-dimethyl-4, 4'-dipyridinium dication (MV^{2+})

3, 3', 5, 5'-tetramethylbenzidine also named TMB is a very popular chromogenic substrate for ELISA. HRP catalyzes its oxidation by H_2O_2 into a blue dye absorbing at 370 and 655 nm. The reaction is generally stopped after 10 minutes by adding 2M sulfuric acid to enhance 2-4 folds the sensitivity and the absorption is monitored at 450 nm.[48] Sadly, it is UV-sensitive which forbids its use with TiO_2 nanoparticles[48]: UV light oxidizes TMB into the corresponding blue dye. Methylviologen dichloride (also called paraquat) presents a very similar chemical structure to TMB (Figure II.2). It is one of the most used non-selective herbicide in the world. Its herbicidal activity relies on its ability to disrupt the intracellular electron-transfer involved in photosystem I of plants. Photoelectrons derived from Photosystem I reduce MV^{2+} ions into MV^{+} radicals, which in turn react with O_2 molecules to form Reactive Oxygen Species (ROS), which readily oxidize the unsaturated lipids of the membranes, resulting in cell death.[49] Besides being an excellent electron relay, methylviologen exhibits an oxidation state-dependent color: MV^{2+} ions are colorless while $MV^{\bullet+}$ radicals are blue. The concentration of the latter ones could be monitored at 395 and 605 nm.[50] Its electron-relay property and its color change have made it the candidate of choice for decades to study electron transfers from photoexcited TiO_2.[51]

To be able to mimic HRP-labeled antibody, the covalent attachment of antibodies on TiO_2 nanoparticles has to be addressed. TiO_2 nanoparticles have been known to photodegrade organic molecules [52, 53], proteins [54], viruses [55], bacteria [56], yeasts [56] and cancer cells [5, 45] by promoting the formation of reactive oxygen species (ROS) [5, 45, 53, 55]. Those, unfortunately, exhibit very short half-times.[54] For instance, the lifetime of singlet oxygen in water equals to 4.10^{-6}s corresponding to a diffusion distance of 220 nm.[57] Therefore, ROS have to be photogenerated in close proximity to the species they are supposed to decompose. Immobilizing antibodies on TiO_2 nanoparticles was naturally the next step to bring targeted killings into reality thanks to their high affinity and specificity to given antigens. Accordingly, TiO_2 nanoparticle-labeled antibodies were successfully manufactured to photodegrade cancer cells [5, 45] and hormones polluting fresh-water resources [54] and as expected, display a higher degradation efficiency than TiO_2 nanoparticles alone.

Our goal was to prove the versatility of TiO_2-labeled antibodies by assessing their ability to detect antigens in ELISA (Figure II.3). The first step consisted in demonstrating that at a fixed time of UV-light exposure, the amount of TiO_2 determines the amount of $MV^{\bullet+}$ photogenerated and the corresponding absorption at 605nm. The second step was to covalently attach antibodies on the TiO_2 nanoparticles and to quantitatively appreciate their efficiency in ELISA.

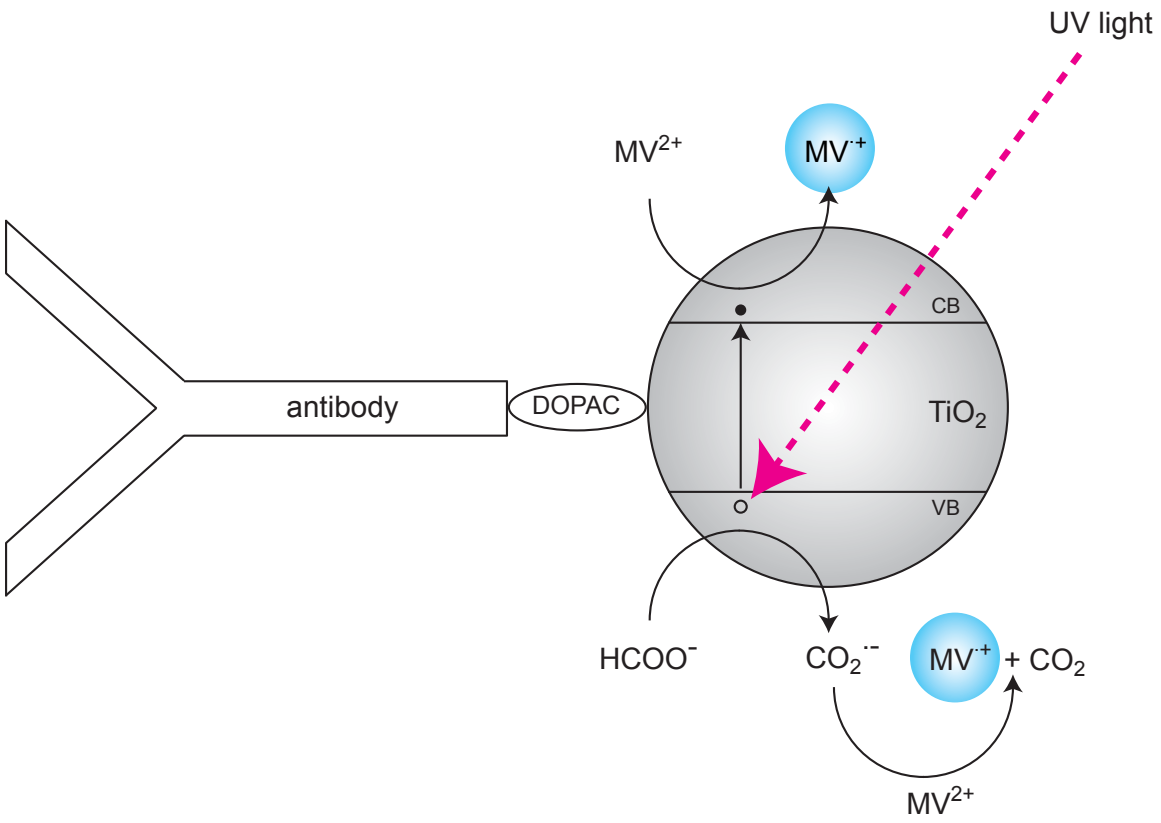

Figure II.3: Schema depicting the formation of the blue color by a TiO_2-labeled antibody exposed to UV light.

II.2. Correlation between the amount of TiO_2 nanoparticles and the absorbance of $MV^{\bullet+}$ radicals at 605nm.

Our strategy relied on the utilization of TiO_2 nanoparticles (Appendix 6) subjected to UV exposure to sustain the "color development" (Appendix 7), of methylviologen dichloride as our chromogenic substrate and sodium formate as a hole scavenger and a color amplifier [58, 59] (Figure II.3). Electrons promoted to the conduction band (CB) by the UV exposure reduce adsorbed MV^{2+} ions into $MV^{\bullet+}$ radicals. The holes left in the valence band (VB) are scavenged by $HCOO^-$ ions, bringing

about the formation of $CO_2^{\bullet-}$ radicals, which spontaneously decompose into CO_2 molecules and electrons able to reduce MV^{2+} ions into $MV^{\bullet+}$ radicals.[58] Here are the reactions describing our developing system UV light/TiO_2/MV^{2+}/HCOONa:

$TiO_2 + h\nu \leftrightarrow (e^-)_{CB} + (h^+)_{VB}$ (1)

$(MV^{\bullet+})_{ads} \leftrightarrow (MV^{\bullet+})_{free}$ (2)

$(e^-)_{CB} + (MV^{2+})_{ads} \rightarrow (MV^{\bullet+})_{ads}$ **(3)**

$(HCOO^-)_{ads} + (h^+)_{VB} \rightarrow (CO_2^{\bullet-})_{ads} + H^+$ **(4)**

$(CO_2^{\bullet-})_{ads} \rightarrow (CO_2)_{ads} + (e^-)_{CB}$ (5)

$(CO_2^{\bullet-})_{ads} \leftrightarrow (CO_2^{\bullet-})_{free}$ (6)

$(CO_2^{\bullet-})_{free} + (MV^{2+})_{free} \rightarrow (CO_2)_{free} + (MV^{\bullet+})_{free}$ **(7)**

$(MV^{\bullet+})_{free} + O_2 \rightarrow (MV^{2+})_{free} + O_2^-$ **(8)**

The pH of our developing solution ($MVCl_2$, HCOONa, water) has to be basic to promote the reaction (3). When pH increases, the TiO_2 conduction-band energy level decreases, whereas the redox potential of $MV^{2+}/MV^{\bullet+}$ remains at its position (since it is pH independent), which narrows the energy gap keeping them apart.[60] Therefore, a pH increase favors the reduction of MV^{2+} ions into $MV^{\bullet+}$ ions. The other reason stems from the fact that at acidic pH, the TiO_2 surface is positively charged due to the adsorption of H^+ ions, which prevents the one of MV^{2+} ions.[58] The pH of our developing solution should not be too basic to avoid TiO_2 surface to exhibit a too large

negative charge detrimental to the occurrence of the reaction (4). Sodium carbonate buffer solution (pH ~ 11) was selected.

Our system still presents some serious challenges. $MV^{\bullet+}$ ions get oxidized by O_2 molecules (reaction (8)). In 1977, Jones and Garland devised an anaerobic methylviologen-based assay to assess the activity of nitrate reductases.[61] MV^{2+} ions were reduced into $MV^{\bullet+}$ ions by sodium dithionite. Their subsequent oxidation by NO_3^- ions catalyzed by nitrate reductases was monitored via spectrophotometry (~ 600nm). To insure anaerobic conditions, a sealed cuvette completely filled with nitrogen-saturated solutions was employed. This method is not convenient at all since it requires large quantity of samples and does not offer the opportunity to realize multiplex analyses. Ridley Helen, Watts Carys A., Richardson David J. and Butler Clive S. improved this assay by integrating microplates and an absorbance-based microplate reader (BMG Labtech FLUOstar OPTIMA) possessing a venting gas system to control the composition of the atmosphere.[62] This microplate reader might spread the utilization of our developing system (TiO_2-labeled antibodies/UV light/$MVCl_2$/HCOONa) among the ELISA community if its efficiency appears to be similar to the traditional one (HRP-labeled antibodies/H_2O_2/TMB) and if the microplate can be properly sealed. Unfortunately, we did not have access to this microplate reader, so we had to resort to utilize air-tight UV-transparent plastic cuvettes.

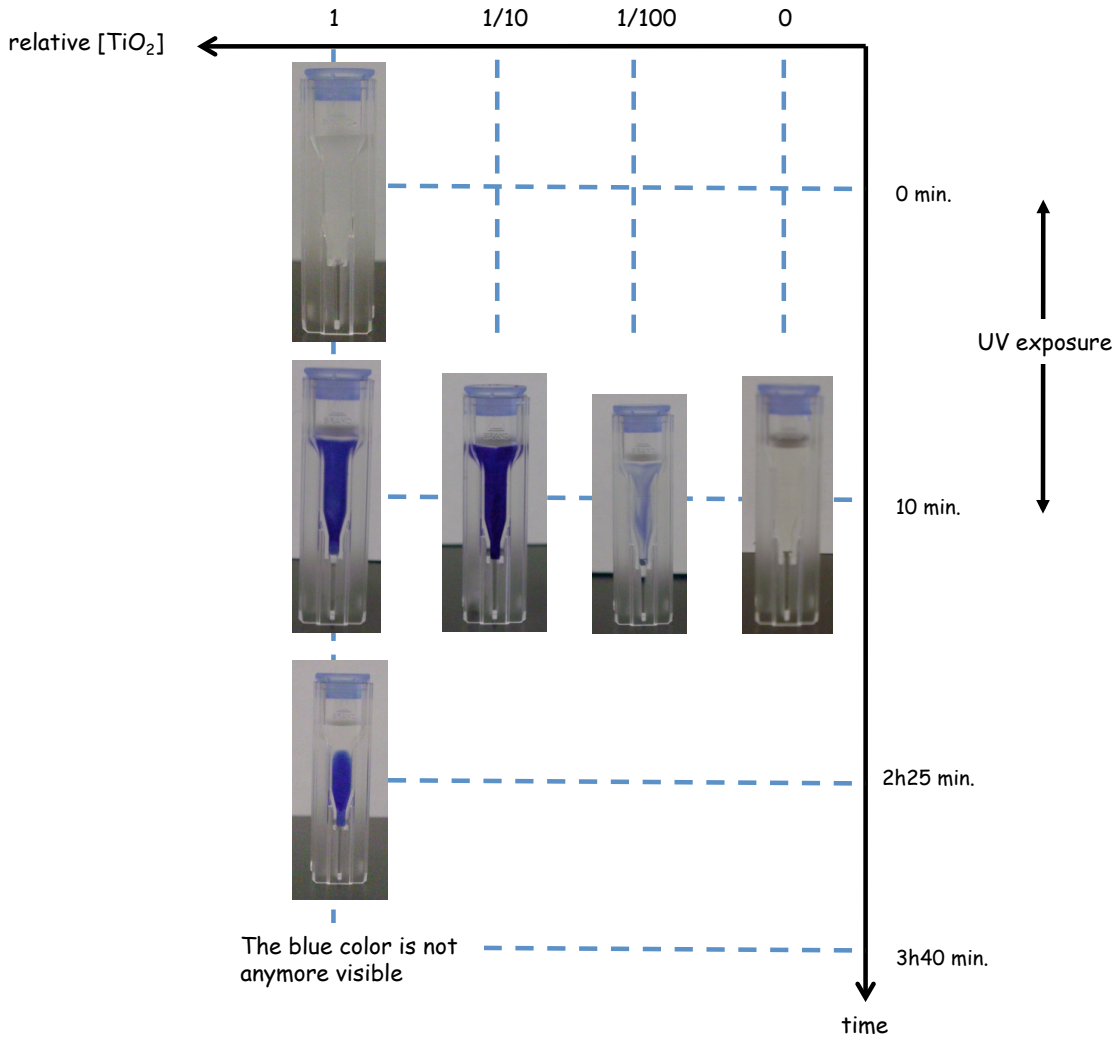

Figure II.4: Relationship between the TiO_2-nanoparticle concentration and the blue-coloration persistence.

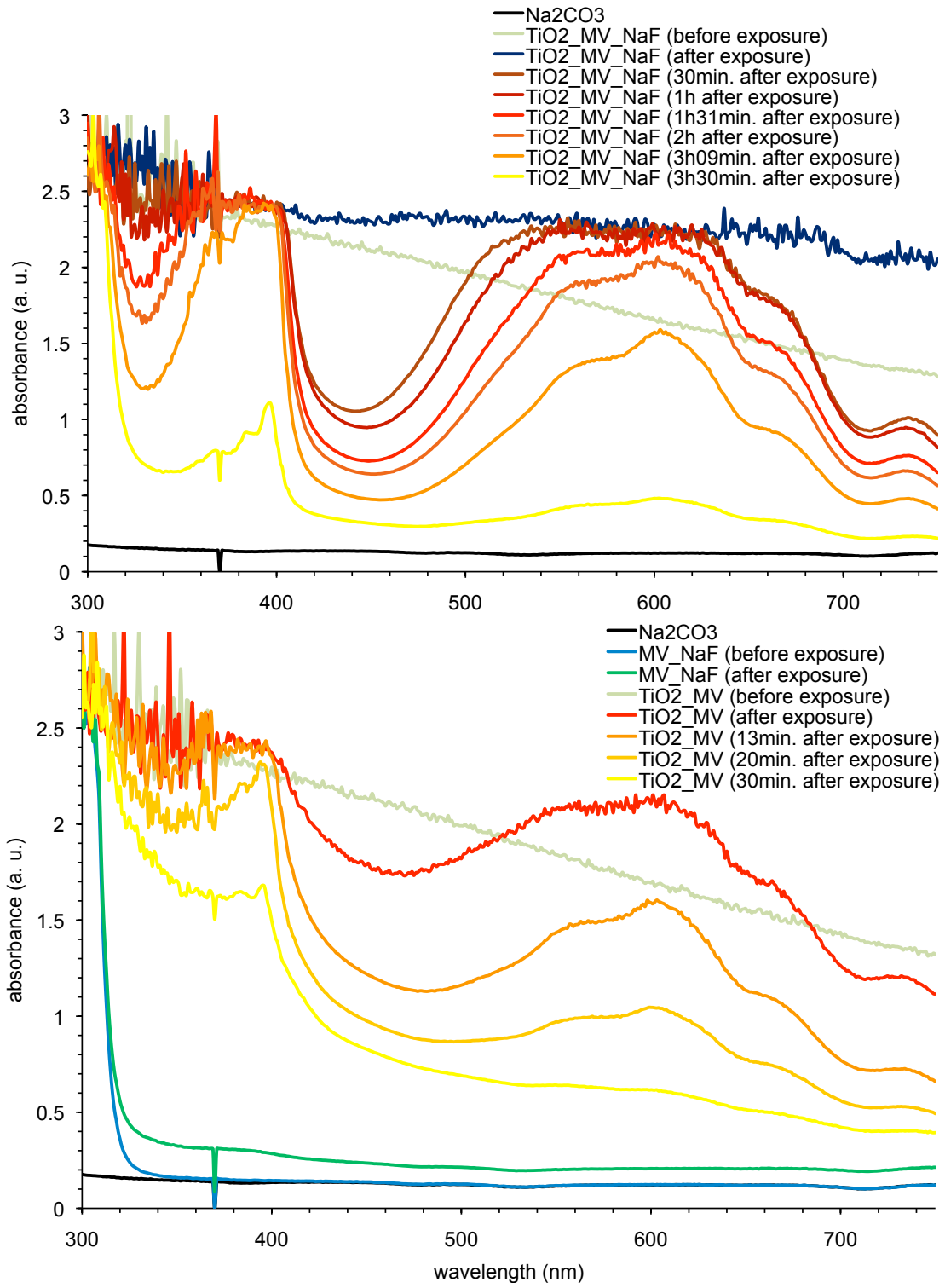

Figure II.5: Effect of sodium formate (NaF) on the blue-coloration persistence.

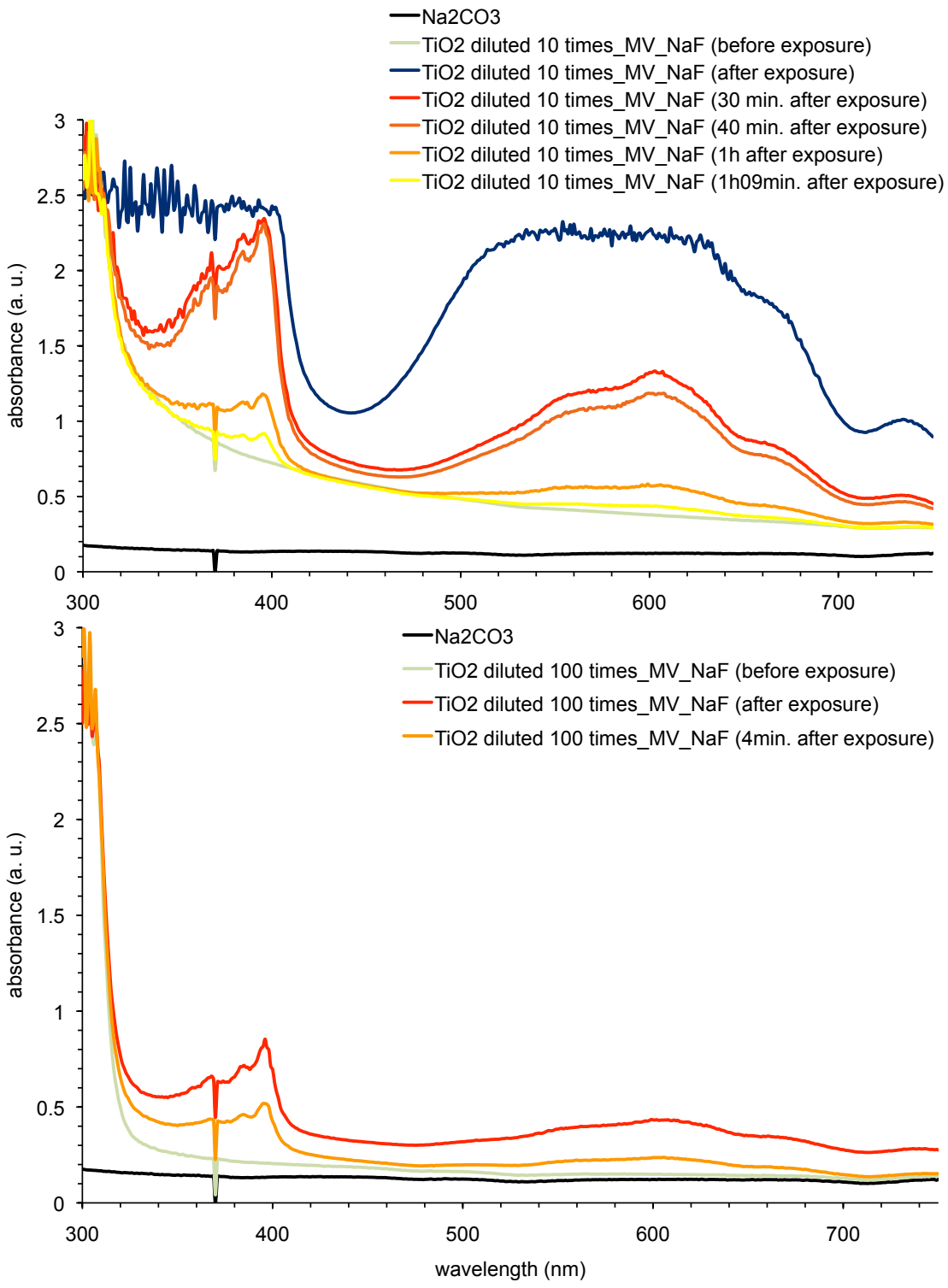

Figure II.6: Relationship between the TiO_2-nanoparticle concentration and the blue-coloration persistence.

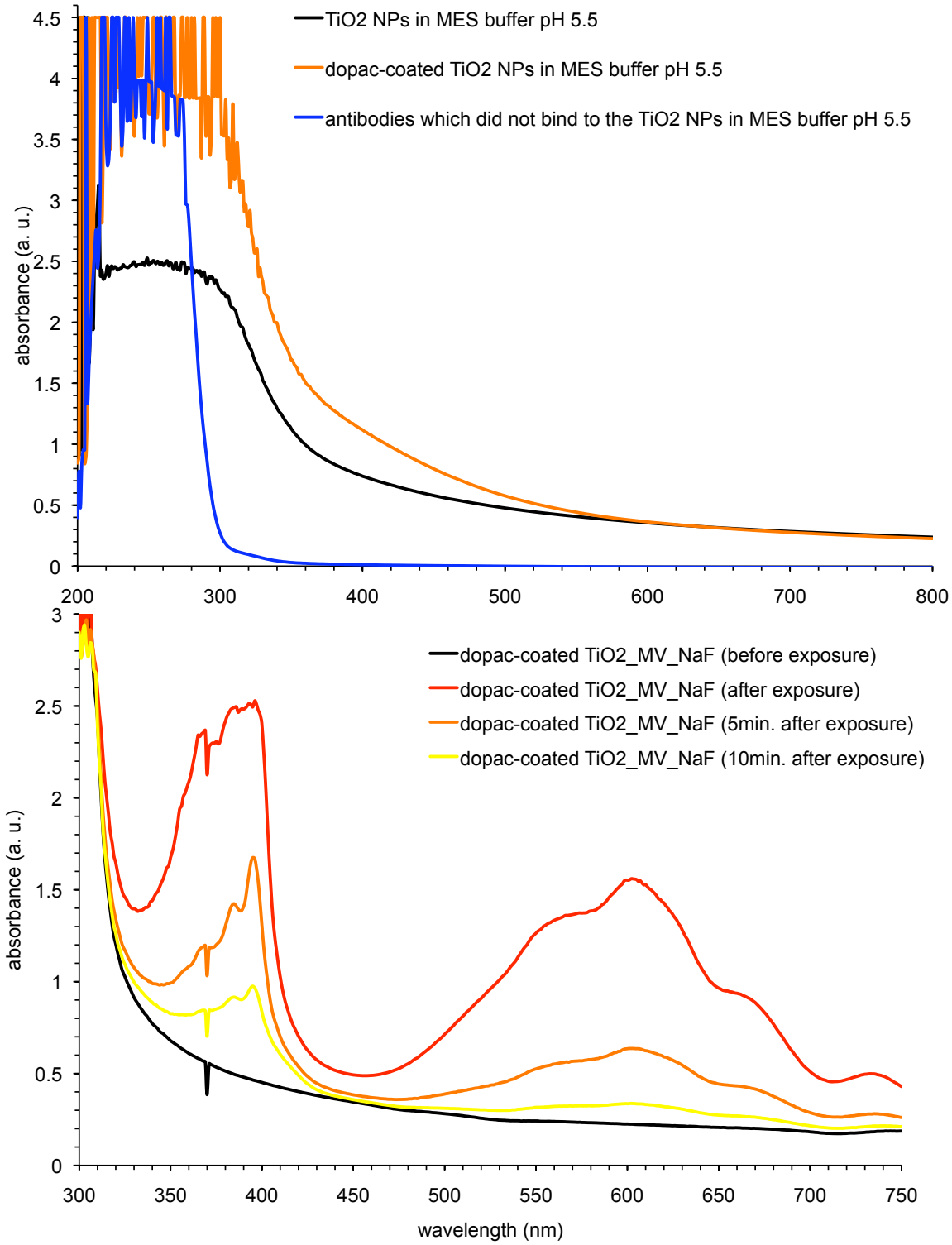

Figure II.7: Relationship between the DOPAC-coated TiO_2-nanoparticle concentration and the blue-coloration persistence.

Figures II.3, II.4 and II.5 show that the absorption at 605nm depends upon the amount of TiO_2 nanoparticles present in solution. Figure II.4 demonstrates that sodium formate increases the amount of $MV^{\bullet+}$ radicals formed as it was expected. Figures II.4, II.5, II.6 and II.7 demonstrated that O_2 molecules penetrate into the capped cuvette and oxidize blue $MV^{\bullet+}$ radicals into colorless MV^{2+} ions (Figure II.8). With the initial presence of 1.4ml of air in the cuvette (the volume of the developing solution amounts for 1ml), which in turn is prone to air diffusion, our sample containing 5mg of TiO_2 nanoparticles have still exhibited some blue color for three hours and half. The decrease of the mass of TiO_2 nanoparticles to 50μg permits the blue color to persist for 5 minutes, a small time however far larger than the one required to record the absorbance at a given wavelength. Our developing system allows to discriminate samples according to the amount of TiO_2 nanoparticles they hold (Table II.1). However, two samples having a relative TiO_2 concentration of 1 and 0.1 display a very similar absorbance right after the exposure, meaning that ~2.3 represents the absorbance-saturation level. Recording their absorption at a given time after their exposure circumvents this discrimination issue. Varying the UV-lamp intensity, or the distance UV-lamps/sample should also modulate the sample absorbance. Sealing the cuvette and removing the initial volume of air should lead to a reduction of the exposure time.

Figure II.8: O_2 diffusion into the cuvette.
(The TiO_2 nanoparticles settled down.)

	relative [TiO_2]			
	uncoated TiO_2 NPs			DOPAC-coated TiO_2 NPs
time after exposure (min.)	1	1/10	1/100	1
0	2.28	2.25	0.43	1.56
30	2.24	1.32		

Table II.1: Absorbance of developed samples recorded at different times after their exposure to UV light.

II.3. Covalent attachment of antibodies on TiO_2 nanoparticles (Appendix 8) and optimization of the TiO_2-labeled antibody concentration (Appendix 9).

DOPAC is known to strongly bind to TiO_2-nanoparticle surface. Its catechol group chelates one Ti(IV) atom [51] and the corresponding ligand-to-particle charge transfer band is visible at 420nm (Figure II.7) [5]. As soon as DOPAC is added to TiO_2 nanoparticles "dissolved" into a MES buffer pH~5.5, the mixture becomes orange. Then, after some time, an orange precipitate floats "in between two waters" leaving the rest of the solution colorless. DOPAC-coated TiO_2 nanoparticles are orange and thus absorb in the visible. DOPAC makes the TiO_2 nanoparticles sensitive to the visible spectrum.[5] In the future, we might excite the DOPAC-coated TiO_2 nanoparticles at 420nm to produce the blue $MV^{\cdot+}$ radicals in order to reduce as much as possible the competition between these two species for the absorption of the incident light. The absorbance of photoproduced $MV^{\cdot+}$ radicals is indeed at its lowest level in the wavelength range comprised between 410 an 460nm (Figure II.5).

Our DOPAC-coated TiO_2 nanoparticles subjected to our development system display a lower absorbance than the one of the corresponding bare TiO_2 nanoparticles. (Figures II.4 and II.7 and Table II.1) Catechols have been shown to promote the electron transfer from TiO_2 to MV^{2+} ions (in anaerobic conditions, at acidic pHs, in presence of poly(vinyl alcohol) on the TiO_2-nanoparticle surface) by shifting the TiO_2 surface states into its conduction band.[51] DOPAC should not impede the adsorption of MV^{2+} ions on the TiO_2-nanoparticle surface and the subsequent electron transfer resulting in their reduction into $MV^{\cdot+}$ radicals. Nevertheless, the TiO_2-nanoparticle surface should be saturated since the same amount of moles of DOPAC as of Ti atoms present in our TiO_2 nanoparticles was added. The saturated TiO_2-nanoparticle surface may hinder MV^{2+} ions and formate anions to interact with it, decreasing the amount of $MV^{\cdot+}$ radicals formed during the development.

The point of coating our TiO_2 nanoparticles with DOPAC is to have them display carboxylic groups able to react with the amine groups of antibodies through the EDC/NHS protocol [63] in order to covalently attach them.[5] (Appendix 6) Consequently, the amount of DOPAC added to the TiO_2 nanoparticles has to be as low as possible to accommodate at most one antibody in the ideal case and to avoid perturbing the redox reactions at the TiO_2-nanoparticle surface. As a first trial to graft antibodies on the TiO_2, we saturated the TiO_2-nanoparticle surface with DOPAC and followed the protocol mentioned in Appendix 6. Before being able to perform ELISA, we had to assess the optimum concentration of TiO_2-labeled antibody able to discriminate between a small amount of antigens (0μg) and a large one (20μg) applying our developing system. (Figure II.9). Figure II.9 reveals that whatever the amount of antigens, the quantity of

TiO_2-labeled antibodies and the UV-light exposure time, the absorbance remains the same as the one of the developing solution. Here are the potential origins of this detection failure:

- the antibodies were not anchored on the TiO_2-nanoparticle surface or a small amount of TiO_2-labeled antibodies was synthesized compared to the quantity of TiO_2 nanoparticles available. The method used to conjugate antibodies onto the DOPAC-coated TiO_2 nanoparticles is not very different from the one established by Rozhkova Elena A., Ulasov Ilya, Lai Barry, Dimitrijevic Nada M., Lesniak Maciej S. and Rajh Tijana, which did appear successful.[5] Those assumptions might accordingly be not valid.

- TiO_2 nanoparticles aggregate in MES buffer pH ~5.5 and in PBS buffer (Table II.2), which leads to the attachment of antibodies on a small amount of TiO_2 nanoparticles and the reduction of TiO_2-labeled antibodies/antigens interactions due to steric hindrance and probable antibody denaturation.

- the antibodies were anchored on the TiO_2-nanoparticle surface but were denatured and could not recognize the antigens.

- the antigens did not physisorb on the plastic cuvette during the overnight incubation.

- the antigens and/or TiO_2-labeled antibodies were removed during the rinsing steps.

- the amount of TiO_2-labeled antibodies bound to the antigens was too small to trigger a detectable blue coloration.

- there was far too much air in the cuvette (2.3ml of air vs. 0.1ml of developing solution to mimic the volume used in ELISA) preventing the blue color from appearing. (reaction (8)). This hypothesis seems the most plausible.

	deionised water	TiO_2 in deionised	PBS buffer pH 7.4	DOPAC-coated TiO_2/antibody in PBS
1st trial	3.40	49.00	1396.00	2460.00
2nd trial	1.93	50.80	2420.00	2360.00
3rd trial	6.56	47.60	1018.00	2440.00
4th trial	0.93	52.00	1824.00	2340.00
5th trial	3.96	47.80	2720.00	2360.00
average	3.36	49.44	1875.60	2392.00
stdev	**2.15**	**1.92**	**703.13**	**54.04**
stdev (%)	**64.17**	**3.87**	**37.49**	**2.26**

	MES buffer pH 5.5	TiO_2 NPs in MES buffer	Polyacrylic acid-coated TiO_2 NPs in MES buffer
1st trial	2980.00	1060.00	214.00
2nd trial	3340.00	1278.00	250.00
3rd trial	330.00	1226.00	258.00
4th trial	2300.00	1010.00	244.00
5th trial		1204.00	230.00
average	2237.50	1155.60	239.20
stdev	**1342.79**	**114.69**	**17.41**
stdev (%)	**60.01**	**9.93**	**7.28**

Table II.2: Average diameters obtained by DLS measurements.
(The values are expressed in nanometers.)

To supplant the traditional ELISA implementation, the problems listed earlier have to be addressed. A single DOPAC molecule is necessary to graft a single antibody on a single TiO_2 nanoparticle via the EDC/NHS process. Part of its unoccupied surface could accommodate some molecules able to insure the colloidal stability of the TiO_2 nanoparticles subjected to buffer solutions of different natures, pHs and ionic strengths such as MES buffer pH~5.5 and PBS buffer pH 7.4. Each of these buffers is used for a given purpose. Provided that the half-life stability of EDC in slightly acidic

MES buffer and in PBS buffer equal to 20h and 0.4h, respectively [63], MES buffer appears to be the most suited medium to promote the covalent attachment of antibodies on TiO_2-nanoparticle surface. PBS buffer guarantees the optimum level of antibody/antigen interactions. The stabilizing molecules cannot mediate the colloidal stability through electrical charges since salts could screen them. Those molecules have to sterically hinder the nanoparticles aggregation. Phosphonate-terminated PEG [64] oligomers might be the solution since phosphonate groups strongly anchor to the TiO_2-nanoparticle surface [65]. Dilute solutions of phosphonate-terminated PEG oligomers and of DOPAC should be used to partially cover the TiO_2-nanoparticle surface. The phosphonate-terminated PEG and DOPAC-functionalized TiO_2 nanoparticles should be dispersed into the buffer solutions to check their colloidal stability via spectrophotometry and DLS. Their color-developing ability should also be assessed. If those nanoparticles pass those two tests, we could proceed to the next step, the covalent attachment of the antibody. The phosphonate-terminated PEG and antibody-labeled TiO_2 nanoparticles should be purified via HPLC or gel chromatography. The recognition ability of those hybrids should be monitored in PBS buffer by a quartz-crystal microbalance functionalized with the antigens. Regarding the O_2 diffusion, we could add glucose oxidase and β-D-glucose in the developing solution to consume O_2 (reaction (12)). Given that Ghica Mariana Emiliana Brett and Christopher M. A. fabricated an amperometric biosensor made of a carbon electrode covered by a BSA/glutaraldehyde/glucose oxidase/Nafion polymer/methylviologen dichloride film to detect glucose [66] (reactions (9), (10), (11) and (12)), there should not be any interactions between glucose oxidase, glucose and MV^{2+} ions.

$MV^{2+} + e^-$ (from carbon electrode) → $MV^{\cdot+}$ (9)

$MV^{\bullet+} + O_2 \rightarrow MV^{2+} + O_2^-$ (10)

$2O_2^- + 2H+ \rightarrow O_2 + H_2O_2$ (11)

β-D-glucose + O_2 + H_2O → D-glucono-δ-lactone + H_2O_2 (12)

Nevertheless, the color-development ability of our new developing solution (made of methylviologen dichloride, sodium formate, sodium carbonate buffer pH ~ 11, glucose oxidase and glucose) will have to be assessed. pH will likely have to be decreased to permit glucose oxidase to properly function. The effect of the UV light and sodium formate on glucose oxidase will have to be determined too. We could pour this new developing solution into a microplate. After sealing it well and exposing it to UV light, it will be inserted into a traditional microplate reader to measure their absorbance.

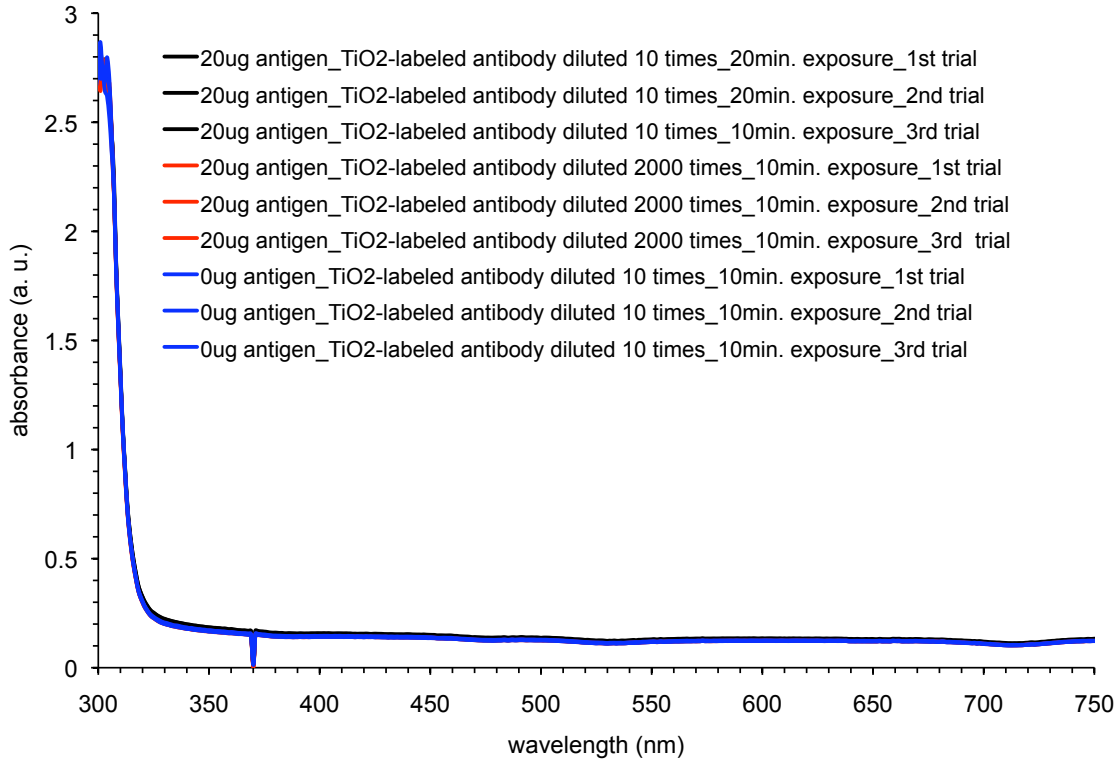

Figure II.9: Attempts to optimize the TiO_2-labeled antibody concentration. All the lines are superimposed.

Chapter III.

Biomimetic crystallization of sulfide semiconductor nanoparticles in aqueous solution.[67]

Pejoux Christophe, Roberto de la Rica and Hiroshi Matsui.

Conclusions.

So far, our method was unable to detect PC3 cancer cells. Nevertheless, there is room for improvement. It appears vital to determine at first if the experimental conditions (room temperature, uncontrolled CO_2 and humidity contents, cell-incubation time equal to 20 or 60min., polylysine incubated with the bare IDEs for one hour) imposed on PC3 cells allow their attachment on the IDEs by employing a SiO_2-coated Quartz Crystal Microbalance. If it is not the case, experimental conditions (temperature, CO_2 and humidity contents, cell-incubation time, type of cell adhesion-promoting proteins (polylysine, fibronectin, etc…) and their incubation time) will have to be optimized to promote the adhesion of cells on the IDEs. In addition, the protocol related to the impedimetric measurements will have to be modified to reduce as much as possible the human intervention, source of irreproducibility. To do so, after having attached the cells on the IDEs and vertically positioned the IDEs at a fixed depth in a beaker filled with deionised water (the given volume of deionised water should be much larger than the one of the cell solution), the impedimetric measurement is run (two of the dippings into a water bath and the subsequent addition of water are removed from the protocol). In this configuration, CO_2 diffusion should be similar whatever the measurement since the water/air interface remains the same (better reproducibility).

Moreover, the Quartz Crystal Microbalance could offer the opportunity to detect the cell swelling since it quantitatively assesses the cell attachment and controls in real time the composition of the liquid stream in contact with the cells (the dilution of the

medium is performed by the device, improving the measurement reproducibility). However, the Quartz Crystal Microbalance must still sense the increase of the cell mass induced by the migration of water molecules within them to make the cell-swelling detection a reality.

Regarding the new IDEs, they will permit to culture cells in the incubator thanks to the presence of a trough whose bottom is made of the IDEs. The removable PDMS chamber on the IDEs displays a central channel into which a water stream flows. Its function is to decrease and fix the CO_2 diffusion to a given level for a better measurement reproducibility and to dilute the medium in a more reproducible manner compared to the manual dippings and water addition (although the water flow is controlled by a syringe operated by a human being).

IDEs can detect the presence of hydrogel beads and CO_2 diffusion emphasizes it for the case of the enzyme-responsive ones. Nevertheless, IDEs were powerless to quantitatively monitor the size change of the hydrogel beads exposed to an external stimulus. At most, for the case of the enzyme-responsive hydrogel beads, IDEs were able to sense a change of impedimetric behavior between the untreated and treated ones.

Our developing system (UV exposure, methylviologen dichloride and sodium formate dissolved in sodium carbonate buffer pH~11) could discriminate between different amounts of TiO_2: the larger the amount of TiO_2, the longer the blue-color persistence. And sodium formate does increase the blue-color persistence too (Figure II.5). TiO_2 and sodium formate promote the formation of $MV^{\cdot+}$ ions during the UV-light

exposure (reactions (3) and (4) and (7), respectively). The blue color of the highest relative concentration of TiO_2 and the 10-times diluted one (both in presence of sodium formate) persists for 3.5h and 1.5h, respectively. After the UV-light exposure, could the blue-color persistence stem also from the formation of formate/$MV^{\cdot+}$ complexes, delaying their oxidation into MV^{2+} ions by O_2 (reaction (8))? The discoloration occurs at the air/solution interface and proceeds downward, which shows the O_2 diffusion within the cuvette (Figure II.8): the cap does not properly seal the cuvette.

The absorbance at 605nm saturates around 2.3 for the highest relative concentration of TiO_2 and the 10-times diluted one (both in presence of sodium formate) and the highest relative concentration of TiO_2 (in absence of sodium formate). What is the origin of this absorbance saturation? The molar-extinction coefficient of $MV^{\cdot+}$ ions equals to 13,700 $M^{-1}.cm^{-1}$ [68]: a change in the concentration of $MV^{\cdot+}$ ions induce a far much smaller variation in the absorbance ($\Delta C = \Delta A/\varepsilon$). Beyond an absorbance of 2.3, the concentration of $MV^{\cdot+}$ ions may not affect anymore the absorbance measured, which is probably due to the spectrophotometer itself (Table C).

	relative [TiO_2]			
	uncoated TiO_2 NPs			DOPAC-coated TiO_2 NPs
time after exposure (min.)	**1**	**1/10**	**1/100**	**1**
0	< 2.2785	< 2.2472	0.43	1.56
30	< 2.2373	1.32		

Table C: Table II.1 slightly modified: Absorbance of developed samples recorded at different times after their exposure to UV light.

In the future, TiO_2-labeled antibodies will have to be thoroughly characterized and their efficiency for ELISA will have to be assessed and compared to HRP-labeled antibodies.

Appendix 1.

Information on the $(IDEs)_2$.

A.1.1. Conductivity measurements.

1. Abundantly rinse the electrode of the conductivity meter (Seven Easy, Mettler-Toledo) with deionised water (Arium® 611DI, Sartorius) and wipe it with Kimwipes. Repeat those operations after each measurement.

2. To calibrate the conductivity meter, dip the electrode in a standard KCl solution (1413µS/cm) and stir it to release any air bubbles trapped. Measure the conductivity and check that the conductivity read and the expected one match each other.

3. To prepare a KCl stock solution, place the content of a spatula of KCl in a 50ml Falcon tube and add 20ml of deionised water. Vortex it well and measure its corresponding conductivity.

4. To prepare diluted KCl solutions, add a given volume of stock solution (100µl for instance) in a 50ml Falcon tube containing 20ml of water. Vortex it well and measure its corresponding conductivity. Repeat the same operations mentioned right before while decreasing the volume of KCl stock solution added. The lower the conductivity of the diluted solutions is, the longer it will take for the conductivity meter to read it.

5. The conductivity values are finally converted into resistivity values by using the following formula: $\rho(\Omega.cm) = \frac{10^6}{\sigma(\mu S.cm^{-1})}$

The conductivity of the deionised water indicated by the deionised-water dispenser is 18.2MΩ.cm, i.e. $\frac{1}{18.2}\mu S.cm^{-1} \approx 0.055\,\mu S.cm^{-1}$. But when measured with the conductivity meter, it is much higher (of the order $\mu S.cm^{-1}$) due to the ambient-CO_2 diffusion through water, resulting in the formation of HCO_3^- and CO_3^{2-} ions.

A.1.2. Cleaning of the $(IDEs)_2$ and their normal impedimetric behavior.

1. IDEs are washed in an aqueous HF (5% v.) solution during 10s, then heavily rinsed with deionised water and dried with N_2. This operation is repeated twice.

2. They are left (undisturbed) in contact with the air for an hour to make sure that a silicon-oxide layer grows on top of them, though the oxidation process spontaneously occurs.[35]

3. Each time the IDEs are washed with HF, the polysilicon fingers are etched. After a certain amount of HF washings, there will be no more polysilicon left, rendering the IDEs useless. Hence, it is necessary to check the IDEs' state. To do so, impedimetric measurements are performed in air and in water, sweeping the frequency from 1 MHz to 10Hz. The ideal impedimetric behaviors of the IDEs in water (10μl water drop) and in air are indicated in figure A.1.1, whereas their normal behaviors are shown in figure A.1.2. Globally, the impedimetric medium-dependent behavior of the IDEs slightly deviates from the ideal one. For instance, in the 1MHz-100Hz range, the theoretical and the experimental curves are very similar. If the IDEs do not behave normally, they are thrown.

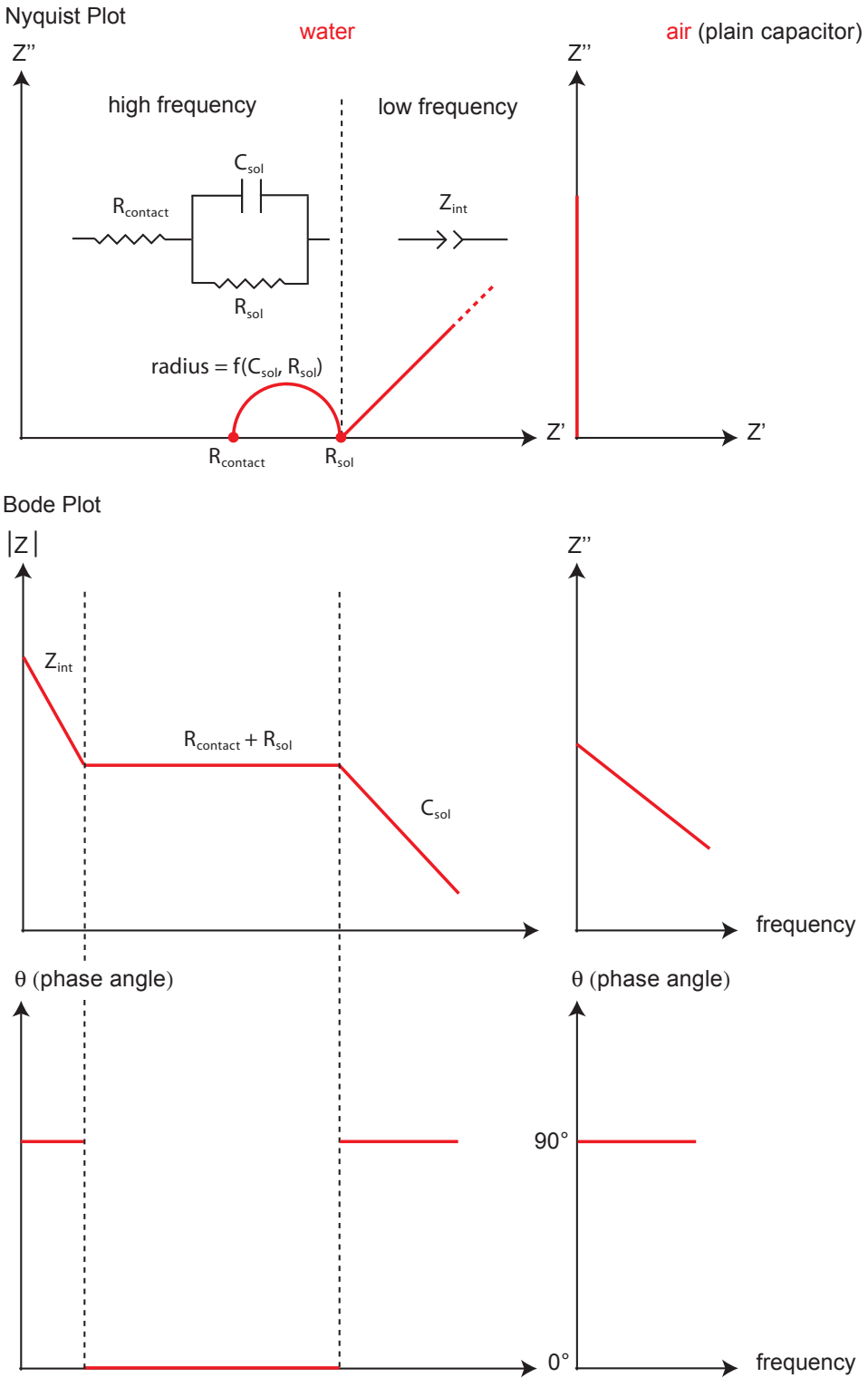

Figure A.1.1: Ideal impedimetric behaviors of IDEs in water and in air.

.

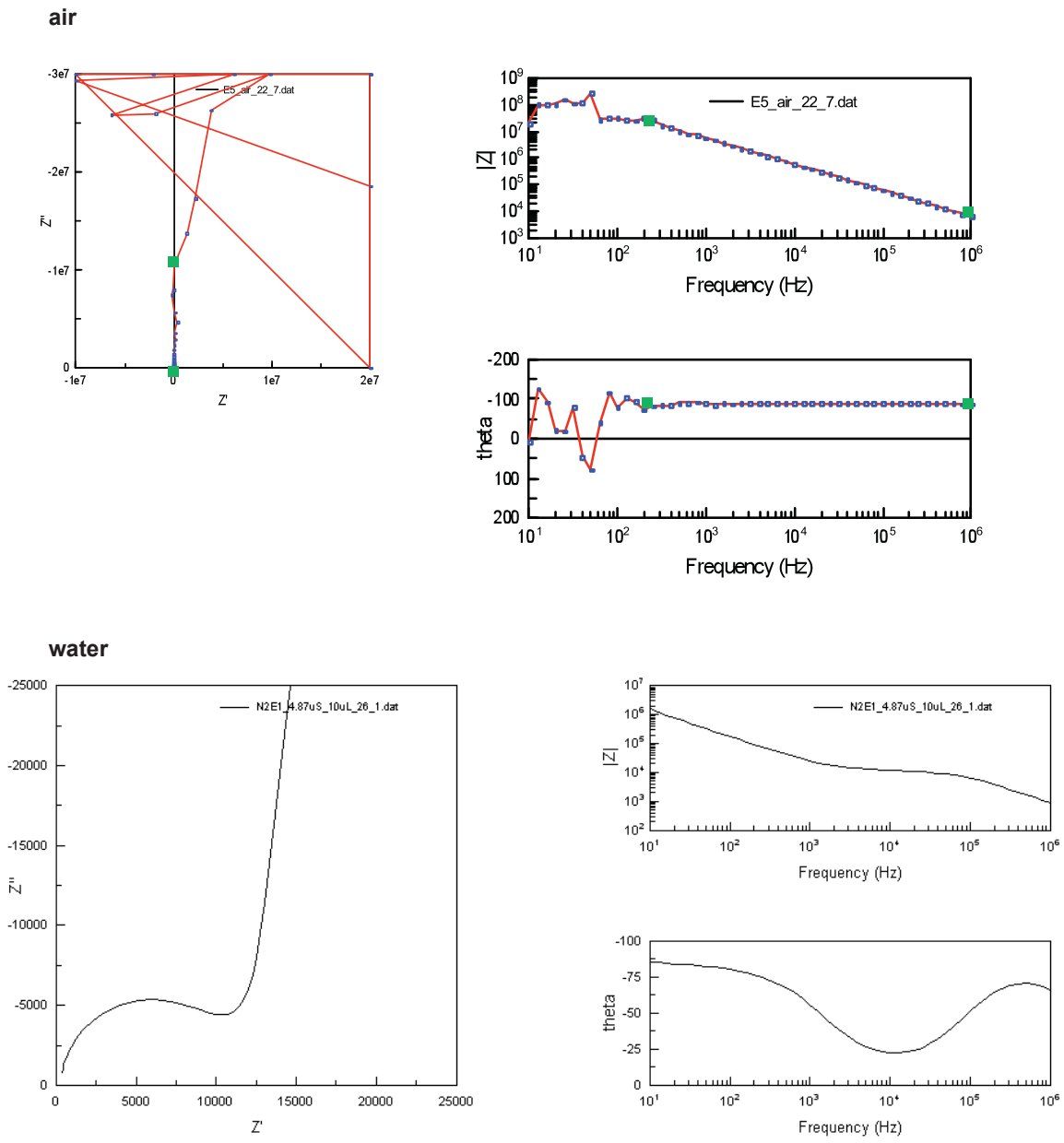

Figure A.1.2: Nyquist plots, Bode plots and phase-angle vs. frequency plots corresponding to the IDEs placed in air or in deionised water.

A.1.3. Nyquist plots observed for aqueous KCl solutions.

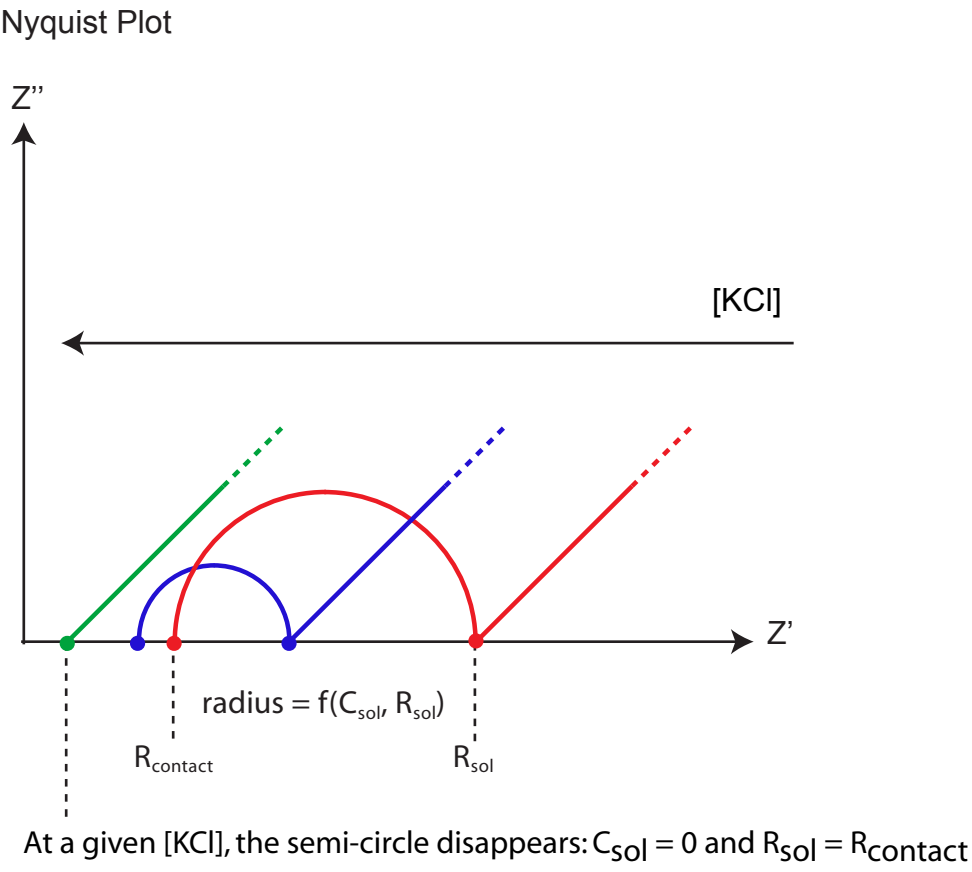

Figure A.1.3: Schematic Nyquist plots for aqueous KCl solutions.

The limits of the semi-circle represent the resistance of contact $R_{contact}$ and the resistance of the solution, R_{sol}, while its diameter is related to R_{sol} and the capacitance of the solution, C_{sol}. The lower the KCl concentration of the solutions (in other words, the lower their conductivity), the higher the semi-circle radius. From a certain KCl concentration, the semi-circle disappears, leaving only the linear part. The higher the concentration of KCl is, the smaller the influence of CO_2 diffusion on the impedance and the more reproducible the impedimetric measurements. That is the reason why the standard deviation of R_{sol} decreases when the concentration of KCl augments (Figure I.24).

A.1.4. SMaRT software. -Solartron-

The SMaRT software controls the impedance analyzer -model 1260A, Solartron-. Two programs were used during our impedimetric measurements: Program #1 and Program #2 collect the impedance over a frequency domain and over a time range at fixed frequency (real-time impedimetric measurement), respectively (Figure A.1.4).

Program #1 related to the determination of the cell constant.

1. Click on the icon entitled Experiment Editor.

2. Set the AC voltage to 10mV (to avoid any redox reaction).

3. Adjust the frequency limits to 1MHz and 10Hz and the amount of points per decade to

10. Check the box related logarithmic scale.

4. Set the integration time to 1s.

Program #1 allows to get a set of data (frequency, Z') for each resistivity corresponding to a definite KCl concentration. By plotting Z' against the resistivity for a given frequency, it is possible to determine the frequency ν_{rt} at which its slope equals the cell constant, i.e. $Z' = R_{sol}$.

Program #2 related to real-time impedimetric measurements.

1. Click on the icon entitled Experiment Editor.

2. Set the AC voltage to 10mV (to avoid any redox reaction).

3. Set the frequency at which $Z' = R_{sol}$.

4. Uncheck the box related to the logarithmic scale and set the number of points to 100 (measurement time ~ 4min.12s).

5. Set the integration time to 1s.

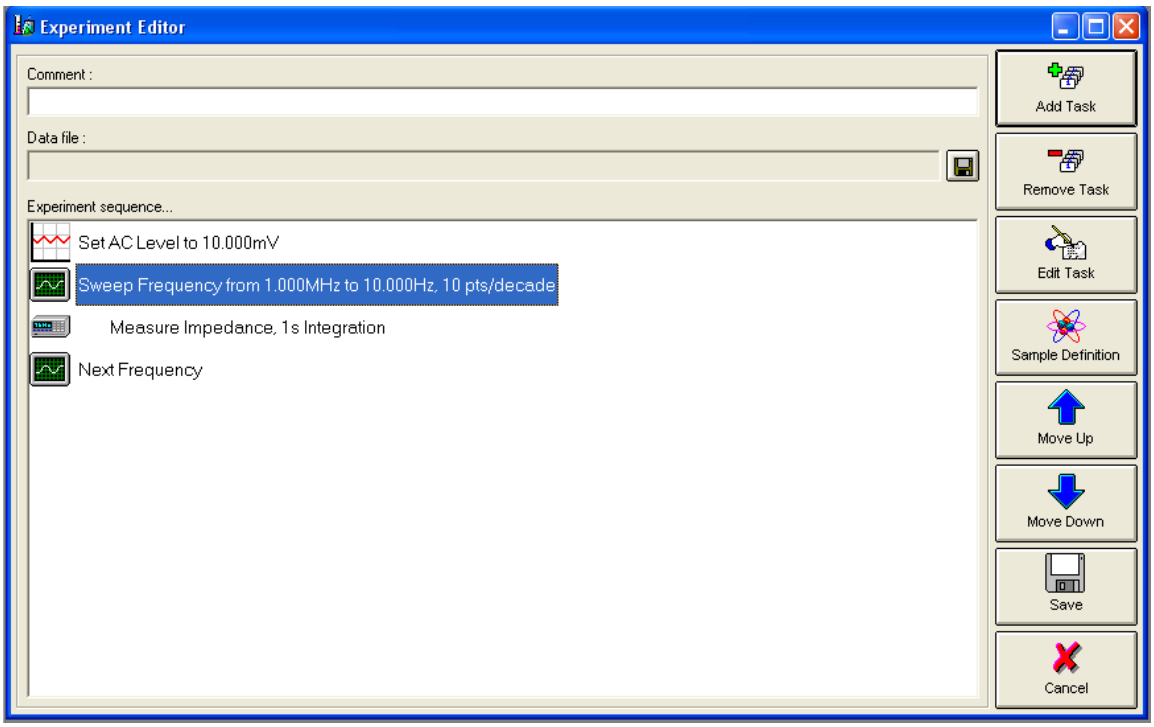

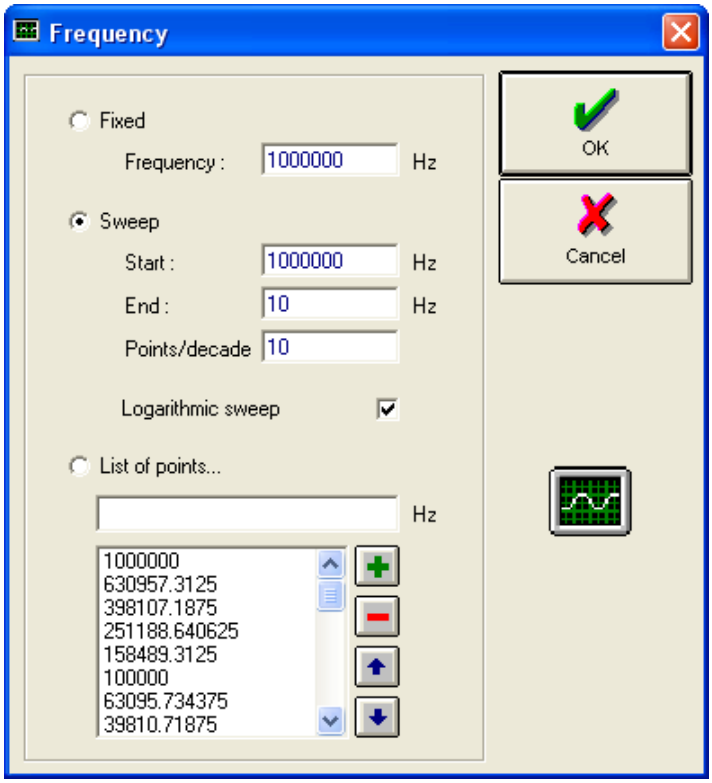

Figure A.1.4: Windows of the Smart software.

A.1.5. Fitting impedimetric measurements to determine R_{sol} through the Zview software. -Scribner Associates-

Regarding the $(IDEs)_2$, there are six parameters to determine C_{sol}, C_{sub}, R_{pSi}, R_{Si}, R_{sol}, and Z_{int} exploiting the impedimetric measurements performed in the air and in aqueous KCl solutions of various concentrations. (five measurements per case)

C_{sub} and R_{Si} are assessed by fitting the impedance measurements run in the air. In this case, R_{sol}, C_{sol} and Z_{int} equal to zero and R_{pSi} is negligible compared to R_{Si}. The "R_S C instant fit" (Figure A.1.5) is applied on the vertical part of the Nyquist plot (Figure A.1.2) to finds out the initial values of C_{sub} and R_{Si}. These ones are then injected into the "equivalent-circuit fit", which in turn delivers intermediate values of C_{sub} and R_{Si}. The five impedance measurements in the air provide five data couples (C_{sub}; R_{Si}). The average of the five values are considered as being the final values of C_{sub} and R_{Si}. Those final values will be valid for any impedimetric measurements performed in aqueous KCl solutions.

There are still R_{sol}, C_{sol}, Z_{int} and R_{pSi} left to be assessed. Two assumptions are made:

1/ The stray capacitance is negligible compared to the capacitance of the solution.

2/ At high frequency, C_{sol} and R_{sol} dominate the impedance of the equivalent circuit, while at low frequency, Z_{int} does.

The "R_s (C-R_p) instant fit" (Figure A.1.5) is thus applied on the frequency range where the capacitor character is the most pronounced (namely at high frequency where the phase is not far from 90° in the phase angle vs. frequency plot or where the semi-circle is

visible in the Nyquist plot) in order to get the initial values of C_{sol} and R_{sol}. The linear part of the Nyquist plot is subjected to the "R_s CPE instant fit" (Figure A.1.6) to get the initial values of Z_{int}. The initial values of C_{sol}, R_{sol} and Z_{int} and the final values of C_{sub} and R_{Si} are entered in the "equivalent circuit fit", which is then triggered (Figure A.1.7). It can be retriggered to make R_{pSi} negligible compared to R_{Si}. The fit is visualized on the three plots (Nyquist, Bode and phase angle vs. frequency plots) in order to assess its righteousness. Moreover, χ^2 values should be at least below 0.0001 to consider the fit as a good one. If it is not the case, you have to select a smaller frequency range on which to apply the "equivalent circuit fit".

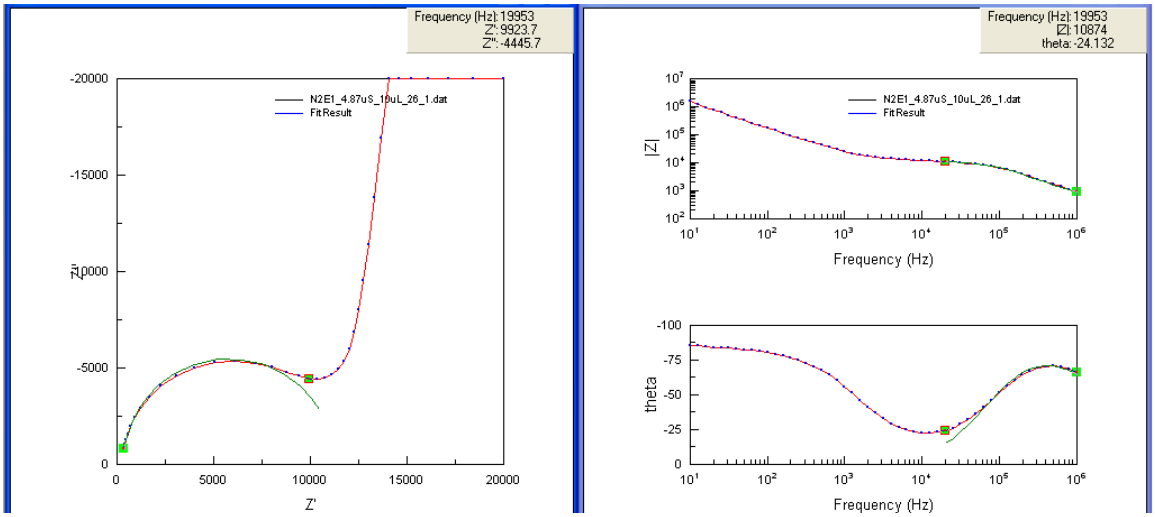

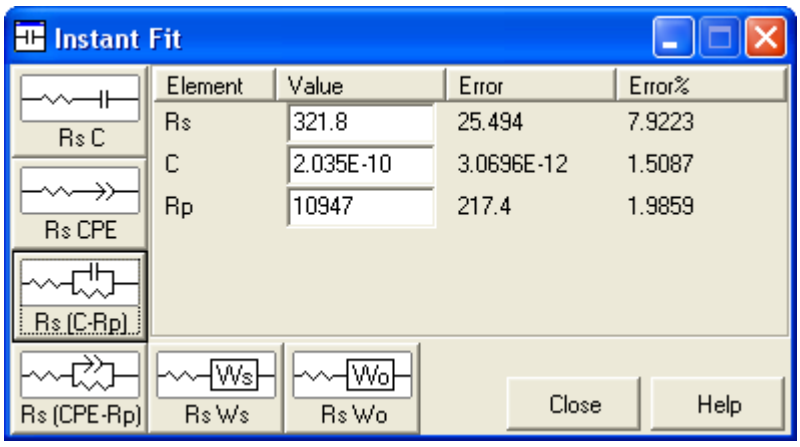

Figure A.1.5: "R_s (C-R_p) instant fit".

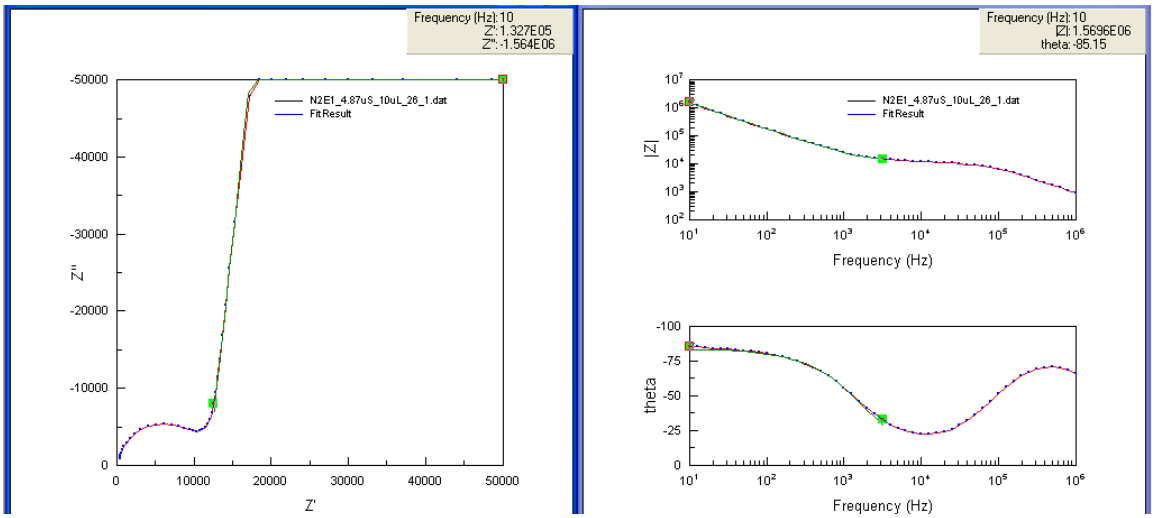

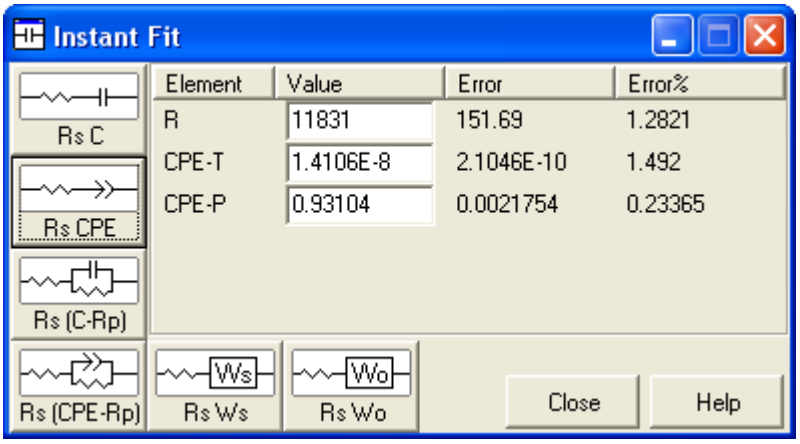

Figure A.1.6: "R_s CPE instant fit".

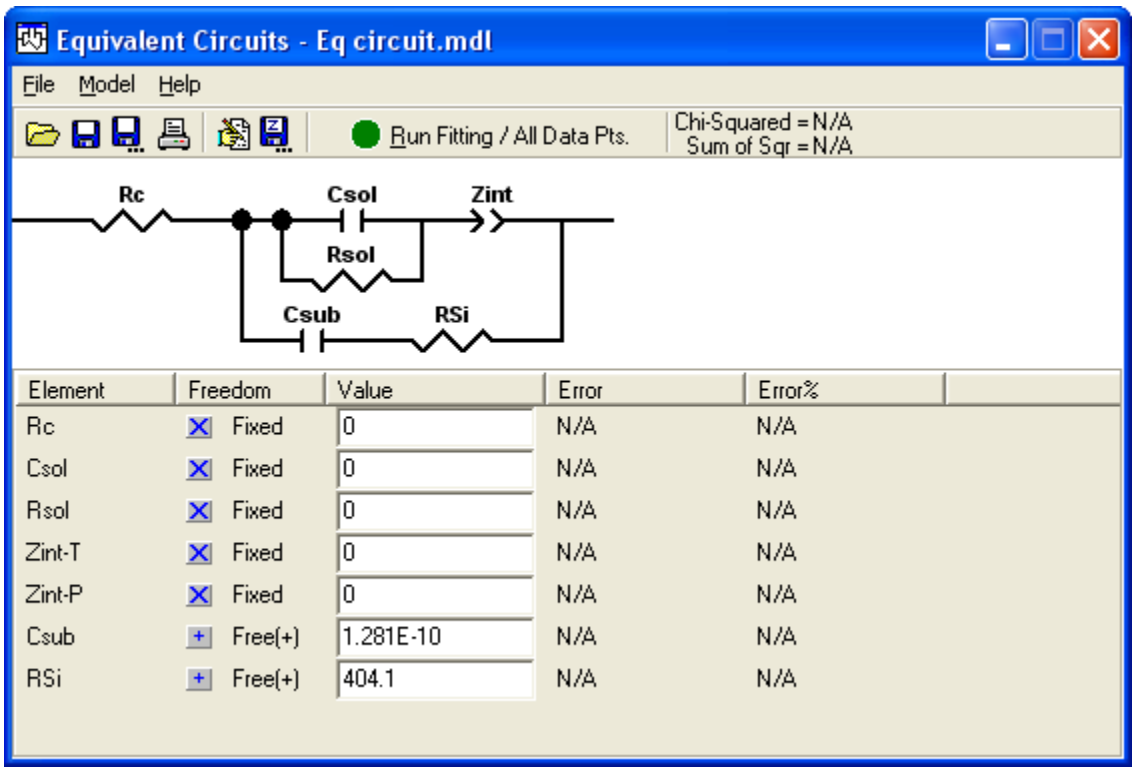

Figure A.1.7: "equivalent circuit fit".

Appendix 2.

Peptide-nanotube biochips for label-free detection of multiple pathogens.[34]

Roberto de la Rica, Christophe Pejoux, César Fernández-Sánchez, Antonio Baldi and Hiroshi Matsui.

Appendix 3.

Cell culture.

A.3.1. Protocol to culture PC3 cells and PNT1A cells.

A.3.1.1. Information related to the chemicals and equipment needed.

Chemicals & equipment	Companies	Catalog numbers
penicillin/streptomycin (P/S)	Invitrogen	15140-122
trypsin solution	Invitrogen	25300-054 (100ml) 25300-062 (500ml)
fetal Bovine Serum (FBS)	Invitrogen	10437-028
medium RPMI 1640	Invitrogen	21870-076
L-glutamine	Invitrogen	25030-081
culture flask (75cm^2)	Fisher Scientific	10-126-37
pipets (5ml)	Fisher Scientific BD Falcon	13-675-22 357543
pipets (10ml)	Fisher Scientific BD Falcon	13-675-20 357551
pipets (25ml)	Fisher Scientific BD Falcon	13-668-2 357525
Petri dishes	Fisher Scientific	S33580
Pipetus (pipet aid)	Spectrum Chemicals	231-30399
Falcon tubes (50ml)	Fisher Scientific BD Falcon	14-432-24 352074

Table A.3.1: Information related to chemicals and equipment used to culture PC3 cells.

• Store RPMI 1640 at 4°C.

• Store FBS at -20°C. Make aliquots of 50ml after having thawed and heated it.

• Store P/S at -20°C. Make aliquots of 5ml.

• Store L-Glutamine at -20°C. Make aliquots of 5ml.

• Store Trypsin solution (0.1% Trypsin, 0.02% EDTA in Hanks' Balance Salt Solutions (HBSS) without Ca and Mg ions) at -20°C. You can store it at 4°C after thawing it.

• Store Phosphate Buffer Saline at 4°C.

• ethanol /water solution (75%/25%)

•Culture flasks (150, 75 and 25cm^2)

T150: 25-30ml of medium solution and 10ml trypsin solution.

T75: 10-15ml of medium solution and 5ml of trypsin solution.

T25: 5ml of medium solution and 3ml of trypsin.

A.3.1.2. Preparation of the medium solution.

1. Thaw the FBS until it becomes liquid.

2. Heat the FBS at 56°C during 30min. to inactivate complement, which is harmful to cancer cells. The heating process has to be done only once. Store at -20°C. It should last for years.

3. Mix 500ml of medium RPMI 1640 + 50ml of FBS + 5ml P/S + 5ml of L-glutamine. Store at 4°C. It should last a couple of months. (no need to filtrate)

A.3.1.3. Passage protocol. (1st method)

(laboratory of M.D./Dr. Neil Bander, Cornell University, New York, USA)

Goal: avoiding the lethal overcrowding of the cancer cells over the culture flask.

When the culture flask is fully covered by cells, you need to collect the living cells and relocate them in another culture flask. (The floating cells are actually dead.) This step is called passage and should be made once a week. However, if the cells are covering the whole surface of the flask, a passage must be performed.

1. Place the medium solution, the PBS solution and the trypsin solution in a water bath whose temperature is set at 37°C for 30-40 minutes.

2. Turn off the UV light of the culture hood and turn on the light and the recirculating air flow.

3. Place a waste beaker in the culture hood on which cotton gauzes are deposited to avoid any back splash while emptying the culture bottle.

4. When the temperature of the solutions is 37°C, remove the bottles from the water bath.

5. Clean the outside of the bottles by spraying ethanol/water solution and wiping them before putting them in the culture hood.

6. Clean your hands too with the ethanol/water solution.

7. Bring the pipet tips inside the culture hood. The pipet tips should never touch anything but the solution you want to pipet. Otherwise, throw it to avoid any contamination.

8. Open the culture flask and place the external face of the caps on the bench of the culture hood. Pour the medium liquid of the culture flask in the waste beaker using the pipet aid.

9. Add 25-30 or 10-15 or 5ml of PBS (depending upon the size of the flask) to remove FBS.

10. Pour 10 or 5 or 3ml of trypsin solution (depending upon the size of the flask) on the side containing the cells.

11. Watch the cells on the optical microscope: as soon as most of them are round (meaning that they are floating), shake off the flask to detach the cells. Keep in mind that trypsin is harmful to cells (need to minimize the contact with trypsin).

12. Add 15 or 8 or 5ml of medium solution (depending upon the size of the flask) in the flask, then mix thoroughly with the pipet.

13. Transfer the solution in a Falcon tube. Centrifuge at 1,000 rpm during 5 min.

14. Decant the solution with a pipet leaving the cell pellet in the Falcon tube. Any leftover of trypsin is inactivated by FBS contained in the medium.

15. Add 5 to 10ml of medium solution in the Falcon tube and mix thoroughly with the pipet. This solution can be divided into 5 or 10 flasks (dilution 1/5 or 1/10).

16. Add 25-30 or 10-15 or 5ml of medium solution (depending upon the size of the flask) in a new culture flask.

17. Transfer a part of the content of the Falcon tube in the new culture flask following the dilution you want to perform. Put back the stopper and tighten it.

18. Write the information (name, date, cell line and # passage).on the culture flask.

19. Have a look on the microscope to make sure that there are some cells within the culture flask.

20. Place rapidly the culture flask in the incubator to keep the concentration of CO_2 and O_2 gases (5% and 95 %, respectively) and the temperature constant (37°C). Don't forget to loosen the cap in order for the CO_2 and O_2 gases to fill the culture flask while placed in the incubator.

A.3.1.4. Passage protocol. (2nd method, the one we used)

(laboratory of Dr. Charles Michael Drain, Hunter College, New York, USA)

1. Place the medium solution in a water bath whose temperature is set at 37°C and let the trypsin solution outside at room temperature.

2. Turn off the UV light of the culture hood, spray some ethanol/water and wipe it.

3. Put the pipet aid within the culture hood, close the culture hood and turn on the UV light to sterilize it.

4. After 10 minutes, open the culture hood and the gas valve and ignite the bunsen burner. Keep the hood window high enough to feel at ease when manipulating and low enough to avoid contamination.

5. Spray your hands with some ethanol/water.

6. Wipe the bottom of the medium and trypsin-solution bottles, abundantly spray them with some ethanol/water and bring them into the hood (not too close to the flame).

7. Close the window and wait until the outside of the bottles is dried.

8. Bring the culture flask into the hood and flame the cap. Open it and flame the inside of the cap as well as the bottle neck. And put back the cap on it. Do the exact same thing when you have to open the medium and trypsin-solution bottles.

9. Remove the medium from the culture flask and pour it to the waste beaker using the pipet aid. Flame the pipet to sterilize it before you dip into solution. Pipets are used once.

10. Slowly add 10ml of trypsin on the surface displaying the cells to rinse any medium leftover. Slowly flush them one more time and remove them from the flask.

11. Add 5ml of trypsin to detach the cells and put the flask in the incubator for 1-2min.

12. Meanwhile, add 15ml of prepared medium to a new culture flask.

13. Take out the culture flask containing the trypsin solution and the cells and keep agitating the flask for a few minutes to break the cells aggregates. You can place the flask in the incubator for a few minutes.

14. When the cells are detached from the surface of the flask, inject a given volume of this cell solution into the new culture flask.

15. Put back the stopper and tighten it.

16. Write the information (name, date, cell line and # passage) on the new culture flask.

17. Have a look on the microscope to make sure that there are some cells within the culture flask.

18. Place rapidly the culture flask in the incubator to keep the concentration of CO_2 and O_2 gases (5% and 95 %, respectively) and the temperature constant (37°C). Don't forget to loosen the cap in order for the CO_2 and O_2 gases to fill the culture flask while placed in the incubator.

A.3.1.5. Feeding protocol.

Feed the cells twice a week (Monday/ Thursday or Tuesday/Friday)

1. Pipet the old medium and pour it in the waste beaker.

2. Add 15 ml of fresh medium.

A.3.2. Protocol to freeze and thaw cells.

(laboratory of M.D./Dr. Neil Bander, Cornell University, New York, USA)

A.3.2.1. Information related to the chemicals and equipment needed.

Chemicals & equipment	Companies	Catalog numbers
prepared medium	see Annex A.3.1.2	
Recovery™ Cell Culture Freezing Medium, liquid	Invitrogen	12648010
cryotubes (1.8 ml)	Fisher Scientific Thermo Scientific	12-565-170N 363401
Pipetus (pipet aid)	Spectrum Chemicals	231-30399
culture flask (25 cm^2)	Fisher Scientific Corning	10-126-28 430639
pipets of 5 ml	Fisher Scientific BD Falcon	13-675-22 357543
pipets of 10 ml	Fisher Scientific BD Falcon	13-675-20 357551
pipets of 25 ml	Fisher Scientific BD Falcon	13-668-2 357525
Falcon tubes (50ml)	Fisher Scientific BD Falcon	14-432-24 352074

Table A.3.2: Information related to chemicals and equipment used to freeze and thaw PC3 cells.

A.3.2.2. Protocol to freeze cells.

There are 3 options regarding the medium to redisperse the cells:

- 90% prepared medium + 10% DMSO (solution1)

- 90% FBS + 10% DMSO (solution2)

- Recovery™ Cell Culture Freezing Medium (solution3). This is the one we used.

1. Prepare solution1 (since it is readily available compared to FBS which is stored in the freezer) and keep it at 4°C.

2. While in the tissue culture hood, pipet the whole content of T-75 culture flask and pour it into a 50ml Falcon tube and closely tighten the cap (to avoid any contamination)

3. Centrifuge it at 1,000 rpm during five minutes.

4. Go back to the tissue culture hood, remove the supernatant and add 3ml of solution1.

5. Mix thoroughly with the pipet aid and deposit 1 ml in each cryotube, which is wiped with a tissue soaked in ethanol/water solution to sterilize it. The content of one T-75 culture flask is going to fill 3 vials of 1ml whereas the content of one T-25 culture flask is going to fill 1 vial of 1ml.

6. Write down its information (name, date, cell line and # passage).

7. Put the cryotubes on ice for an hour.

8. Transfer the cryotubes into the freezer at -20°C for an hour.

9. Finally transfer the cryotubes into the -80°C chamber (lifetime = six months). If you were storing them under liquid nitrogen, the cells could be indefinitively kept.

A.3.2.3. Protocol to thaw cells.

1. In the tissue-culture hood, pipet 9-10ml of medium into a Falcon tube.

2. Hold the tube (containing the frozen cells) into a water bath whose temperature is comprised between 37 and 42°C until complete thawing. Make sure that the bath water is far enough from the cap. The thawing process should last less than a minute (DMSO is harmful to cells).

3. Wipe the tube with some Kimwipes, bring it within the hood and place it on a holder.

4. Wipe the upper side of the tube with a tissue moistened with ethanol. (Do it twice)

5. Pipet the whole content of the tube into a Falcon tube containing 9 ml of prepared medium in order to dilute the DMSO which is harmful to the cells.

6. Thoroughly mix it with the pipet and close the cap of the Falcon tube.

7. Centrifuge at 1,000rpm for five minutes at room temperature. After centrifugation, a pellet should be visible at the bottom of the Falcon tube.

8. When in the hood, remove the supernatant and add 5ml of medium. Thoroughly mix it with the pipet.

9. Inject the 5ml of solution in a small culture flask (T25). The cells need to be in close proximity to live, otherwise their population will never grow, that is the reason why a small flask has to be used.

10. Tightly close the cap and go to the optical microscope. The cells should look round and shiny, visible signs of their viability.

11. Put the flask in the incubator.

12. Two days after having thawed the cells, if the cells attach well on the flask (cells should not appear round), the medium can be changed.

Appendix 4.

Protocol to monitor the swelling of cells subjected to hyposmotic stress via fluorescence microscopy.

A.4.1. Information related to the chemicals and equipment needed.

Chemicals & equipment	Companies	Catalog numbers
tissue culture plates (12 wells, well volume = 6ml)	Fisher Scientific	08-772-29
calcein, AM 1mg/mL solution in anhydrous DMSO (cytoplasm staining)	Invitrogen	C3099
wheat germ agglutinin, fluorescein conjugate (membrane staining)	Invitrogen	W834
pipet tips (5ml)		
sterile graduated transfer pipets	Fisher Scientific	13-711-50
stopwatch	Fisher Scientific	S90861
ImageJ freeware	http://rsbweb.nih.gov/ij/	
prepared medium	see Annex A.3.1.2	
trypsin solution	Invitrogen	25300-054 (100ml) 25300-062 (500ml)
Falcon tubes (50ml)	Fisher Scientific BD Falcon	14-432-24 352074

Table A.4: Information related to chemicals and equipment used to monitor the swelling of PC3 cells via fluorescence microscopy.

A.4.2. Seeding the tissue-culture plate wells.

(laboratory of Dr. Charles Michael Drain, Hunter College, New York, USA)

Each step is performed in the tissue culture hood in the presence of a flame to get a sterile environment.

1. Remove the medium from the culture flask.

2. Slowly add 10ml of trypsin on the surface displaying the cells to rinse any medium leftover. Slowly flush them one more time and remove them from the flask.

3. Add 5ml of trypsin to detach the cells and put the flask in the incubator for 1-2min.

4. Keep agitating the flask for a few minutes to break the cells aggregates.
Assessing the amount of single cells and monitoring their swelling when subjected to hyposmotic stress is more readily done than for cells aggregates. Don't keep the cells too long in the trypsin solution otherwise they would die.

5. When the cells are detached from the surface of the flask, add 15ml of medium to inhibit the trypsin. In half-an-hour or less, cells will attach back on the flask.

6. Flame the tissue-culture plate.

7. Add 2 ml of medium in every well of the tissue culture plates.

8. Add one to two drops of cell solution in each well.

9. Put the plate in the incubator for 2-3.5 hours. This time is suitable for PC3 cells.

After 2 hours, all the cells are round-shaped: they are weakly or not attached. While removing the medium and/or adding the deionized water, cells could be detached from the wells. After 4 hours, most of the cells exhibit an elliptical shape, characteristic of a good attachment. The wells are not used to culture cells in our case, just to attach single living cells. (Those observations are valid for PC3 cells.)

10. Add 2µl of cytoplasm staining agent or 10µl of membrane-staining agent in each well and let the plate sit in the incubator for half-an-hour more.

11. Go to the inverted optical microscope. Don't let your plate exposed too long to day light.

A.4.3. Taking pictures using the inverted optical microscope.

1. Create a folder.

2. Run the program MetaMorph 7. 1. 3. 0

3. Select the X20 magnification (which is a good compromise between image details and amount of cells).

4. Select the brightfield filter, activate the live image and turn on the white lamp.

5. In brightfield, quickly determine a spot where there is a large amount of single cells and focus.

6. Turn off the white lamp, deactivate the live image, select the FITC filter (fluorescence mode), and activate the live camera.

7. While removing the medium by using a transfer pipet (the wastes are poured in a Falcon tube), check that there are still enough visible single cells, otherwise quickly find another area. Make sure that you do not displace the plate while drawing the medium out.

8. Optimize the time of exposure and focus.

9. Take a picture by clicking Acquire.

(the name of this picture will be: cell line_dye_well#_1)

10. Take 4ml of deionised water with the 5ml pipet and zero the stopwatch.

11. Activate the live camera, add right after the deionised water paying attention not to move the tissue-culture plate, and trigger the stopwatch.

12. After 10s, click Acquire. Every 10s during the first minute, you take a picture then every minute during 5 minutes.

13. Save the image only at the end of each well analysis under the following names: cell line_dye_well#_1, cell line_dye_well#_10s and so on, otherwise the temporary name of each picture is going to change.

14. For the cell line_dye_well#_1, select calibrate distances, then X20, then display, calibration bar and stamp. Save it as cell line_dye_well#_1sb

A scale bar is required to determine the area occupied by the cells when they are normal or swollen via the freeware I*mageJ*.

A.4.4. Image analysis with *ImageJ*.

Refer to pages 66-72, 93-96, 126-135 of the *ImageJ* user manual.

The goal is to determine the area increase of the cells due to their absorption of water, by binarizing the pictures: the cells and the background appear as black and white, respectively.

1. Open the image (cell line_dye_well#_1) twice. The former one is the reference and the latter the black-and-white picture (called "binarized" picture).

2. Click on *Adjust* and *threshold* and select *B&W*.

3. "Play" with the scroll bars to make the background white and the cells black, paying attention to faithfully reproduce the size of the cells of the reference image.

i. Underestimate or overestimate the black level in order to define the outline of the cells. You likely have to set up different black-level values to determine the outline of each cell.

ii. Click on the *color picker* icon, and select a black area on the picture to pick the black color.

iii. Color the cells in black by clicking on the *pencil* or *paintbrush tool* icons and delicately move the mouse to define the cells. Don’t hesitate to use the magnifying glass and the reference picture to guide your hands.

4. Check that the "binarized" and reference pictures fit by using the overlay option.

i. Select the "binarized" picture by clicking on *Edit*, *Selection* and *Select All*.

ii. Click on *Image*, *Overlay* and *Add Selection*.

iii. Click on the reference picture and on *Image*, *Overlay* and *Add Image*. Select the "binarized" picture as the *picture to add* and set up the level of *opacity* to see both pictures.

If they do match, *Apply* the Threshold to the "binarized" picture, which results in the creation of 8-bit black and white picture and save it as the initial name of the image to which a p is added. If they don't, go back to steps 2.

5. Set up the scale.

i. Click on the line and the shift key to draw a straight line whose length is equivalent to the scale bar.

ii. Click on *Analyze* and *Set Scale*.

iii. Fill the *known distance* and the *unit of length* boxes.

6. Determination of the area of the cells.

i. Count the cells manually.

ii. Click *Analyze Particles*.

iii. Indicate the range of particle area (um^2) considered. Don't write 0 as the tiny black dots should not be taken into account.

iv. Set the *Show* box to *Outlines.*

v. Check the *Display Results* and *Summarize*, then click *OK*.

7. Create an Excel file and the following table. Then, fill it with the results obtained from *ImageJ*. (Table I.1)

file	name	magnification	# cells	area (um^2)	swelling (um^2)	swelling (%)

Swelling (um^2) = area (t=2 min) – area (t=0 s)

Swelling (%) = [Swelling (um^2) / area (t=0 s)] * 100

Appendix 5.

Cell swelling monitored by real-time impedimetric measurements.

A.5.1. Protocol to prepare the cells to be analyzed through impedimetric measurements.

A.5.1.1. Information related to the chemicals and equipment needed.

Chemicals & equipment	Companies	Catalog numbers
tryptan Blue solution	Sigma	T8154
hemacytometer	Fisher Scientific	02-671-5
Pipetus (pipet aid)	Spectrum Chemicals	231-30399
autoclaved pipet tips		
pipets of 5 ml	Fisher Scientific BD Falcon	13-675-22 357543
pipets of 10 ml	Fisher Scientific BD Falcon	13-675-20 357551
pipets of 25 ml	Fisher Scientific BD Falcon	13-668-2 357525
Falcon tubes (50ml)	Fisher Scientific BD Falcon	14-432-24 352074

Table A.5: Information related to the chemicals and equipment used to monitor the cell swelling via real-time impedimetric measurements.

A.5.1.2. Preparation of the cell solution (within the tissue culture hood).

Before beginning, make sure that the IDEs are cleaned and coated with polylysine and its impedance was measured.

1. Remove the medium from the culture flask.

2. Slowly add 10ml of trypsine on the surface displaying the cells to rinse any medium leftover. Slowly flush them one more time and remove them from the flask.

3. Add 5ml of trypsine to detach the cells and put the flask in the incubator for 1-2min..

4. Keep agitating the flask for a few minutes to break the cells aggregates.

5. Add 15ml of medium to inhibit the trypsin.

6. Use the pipet to stir the cell solution. You can also shake it.

7. Transfer the mixture into Falcon tubes. Centrifuge it during 5min. at 1,000rpm and at 25°C. Remove the supernatant in the culture hood (to avoid contaminations) leaving the cell pellet. The goal is to remove the inhibited trypsin (just in case). Then, pour a given volume of medium (1-2ml) with the pipet aid into the Eppendorf tube and stir it up (using the pipet aid) to homogenize the cell solution.

8. Pipet 50µl of cell solution employing a common pipet and put it in an Eppendorf tube.

A.5.1.3. Counting cells with a hemacytometer.

1. Spray the hemacytometer and the top glass slide with the ethanol/water mixture and wipe them.

2. Mix 50µl of trytan Blue solution and 50µl of cell solution with a pipet in an Eppendorf tube (or 100µl of each solution). Let it incubate for 1-2 min..

The tryptan blue dye stains the dead cells in blue in order to exclude them from the census. "The reactivity of this dye is based on the fact that the chromophore is negatively charged and does not react with the cell unless the membrane is damaged. Live (viable) cells do not take up the dye and dead (non-viable) cells do."[69]

3. Meanwhile, select the 40X-magnification objective and place the hemacytometer on the microscope.

4. Put one drop of the tryptan blue/cell solutions on the hemacytometer notch and place the glass slide on top of it. Make sure that the $9mm^2$ squares are covered by the solution, otherwise add more of it.

5. Count the unstained cells located within the central $1mm^2$ square using the "cell counter". $\#cells.mm^{-3} = \#cells.\mu l^{-1} = \#cells\ counted \times 2 \times 10$

A.5.1.4. Preparing the cell solution.

1. Pipet 10ml of prepared medium using the pipet aid and put them in a sterile Falcon tube.

2. Need to concentrate the cell solution via centrifugation (1,000rpm for 5min.) or dilute it by addition of medium in order to get at most 1000cells/µl to avoid cell/cell interaction (cell aggregates).

3. Take a given volume of cell solution and dilute it five times with some fresh medium, since a 5µl drop of cell solution will be deposited on the IDEs.

A.5.2. Protocol to monitor the swelling of cells subjected to hyposmotic stress via real-time impedimetric measurements.

A.5.2.1. Cleaning of the IDEs.

1. Stir the IDEs in 5% HF solution for 10s.

2. Rinse the IDEs with deionised water for 10s and dry with streaming N_2.

3. Repeat those two operations.

4. Leave the IDEs undisturbed in the air for an hour.

A.5.2.2. Coating the IDEs with polylysine.

1. A 100µl drop of 0.1 $mg.ml^{-1}$ poly-D-lysine hydrobromide solution (Sigma) is deposited on the IDEs and left for 20 min..

2. The IDEs are rinsed with deionized water and dried in streaming N_2.

A.5.2.3. Impedimetric measurement of the control experiment at 20 kHz.

1. Incubate a 5µl drop of medium with the polylysine-coated IDEs for 30 minutes. Put the IDEs in an ajar Petri dish containing some warm water to keep the inside atmosphere humid enough to avoid the drop to dry out.

2. Vertically dip the IDEs into three deionised-water baths and horizontally attach them on a stand. Then, add 100µl of deionised water (freshly poured from the water dispenser) on the IDEs. Washing the IDEs, setting up the IDEs and adding the drop should last less than 10s.

3. Trigger the measurement.

4. Rinse and dry the IDEs.

A.5.2.4. Impedimetric measurement of the sample at 20 kHz.

1. On the very same IDEs, incubate a 5µl drop of cell solution (Appendix A.5.1) with the polylysine-coated IDEs for 30 minutes. Put the IDEs in an ajar Petri dish containing some warm water to keep the inside atmosphere humid enough to avoid the drop to dry out. The cells have to be kept alive and left undisturbed to favor their adhesion on the IDEs.

2. Vertically dip the IDEs into three deionised-water baths and horizontally attach them on a stand. Then, add 100µl of deionised water (freshly poured from the water dispenser) on the IDEs. Washing the IDEs, setting up the IDEs and adding the drop should last less than 10s.

3. Trigger the measurement.

4. Rinse and dry the IDEs.

A.5.2.5. Data processing.

At 20 kHz, Z' equals to R_{sol}, whose value depends upon the amount and the size of the cells attached on the IDEs. The variation of the real part of the impedance, $\Delta Z'$, obeys the following equation: $\Delta Z' = Z'_{sample} - Z'_{control}$

Appendix 6.

TiO_2 nanoparticles.

A.6.1. Synthesis of TiO_2 nanoparticles.

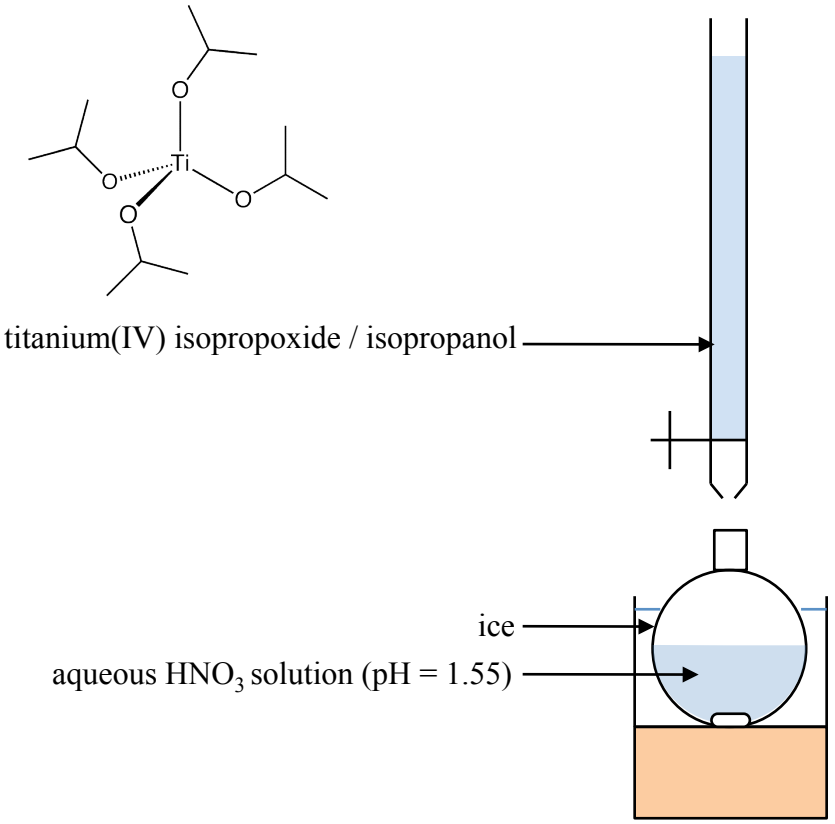

Figure A.6.1: Schema describing the experimental setup used to produce TiO_2 nanoparticles.

We followed the synthesis of TiO_2 nanoparticles invented by Ma Linglan, Liu Jie, Li Na, Wang Jue, Duan Yanmei, Yan Jinying, Liu Huiting, Wang Han and Hong Fashui [70] employing a different titanium precursor, namely titanium(IV) isopropoxide (TIP) (Figure A.6.1). 1ml of TIP was dissolved into 20ml of isopropanol. The mixture is

then added dropwise to a flask containing 50ml of a cold aqueous HNO_3 solution (pH = 1.55) agitated by a magnetic stirrer. These are the reactions describing the results of the operations mentioned right before [71]:

$Ti(OR)_4 + 4\ H_2O \rightarrow Ti(OH)_4 + 4\ ROH$ (hydrolysis)

$Ti(OH)_4 \rightarrow TiO_2x(H_2O) + (2\text{-}x)\ H_2O$ (condensation)

The dilution of TIP in isopropanol, its subsequent dropwise addition and the low temperature aim at forming a large amount of minute TiO_2 nuclei. The nitric acid provides H^+ ions able to adsorb at the surface of the TiO_2 nuclei, which makes their surface positively charged and allows their stabilization (Figure A.6.2).

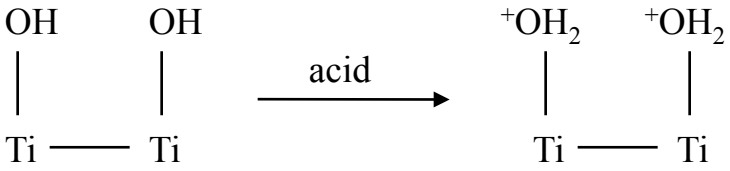

Figure A.6.2: Schema describing the adsorption of H^+ ions on TiO_2-nanoparticle surface.

Next, the mixture is stirred and maintained at 55°C by a heating mantle during 6 hours to promote the crystallization of TiO_2 nanoparticles.

$$[TIP] = \frac{d_{TIP}}{M_{TIP}}$$

$$[TiO_2] = \frac{m_{TiO_2}}{V_{TIP+H_2O}} = [TIP] \times V_{TIP} \times M_{TiO_2} = 5.34\, mg.ml^{-1}$$

A.6.2. Colloidal stability of the TiO_2 nanoparticles. (Table II.2)

After centrifugation at 14,000rpm for five minutes (Figure A.6.3), the deposit of TiO_2 nanoparticles at the bottom of the Eppendorf tube is transparent. Only the interface solution/TiO_2 nanoparticles is actually visible (white thin band). Consequently, those TiO_2 nanoparticles do not scatter the visible light, which implies that their size is smaller than 100nm.

Figure A.6.3: Solution centrifuged right after the synthesis.

After removal of the supernatant, the TiO_2 nanoparticles are redispersed in other solvents (deionised water, MES buffer pH~5.5, sodium carbonate buffer pH~11) using ultrasounds. Redispersed in deionised water, the TiO_2 nanoparticles are very stable. After 4 days, the solution is still whitish, although a small white pellet is visible at the bottom of the Eppendorf tube. Redispersed in MES buffer or sodium carbonate buffer, the TiO_2 nanoparticles tend to form aggregates, which float "between two waters" (Table II.2). pH

and ionic strength determine the electrical charge exhibited at the TiO_2-nanoparticle surface and accordingly their colloidal stability.

A.6.3. TEM pictures and SAED patterns and crystalline structure.

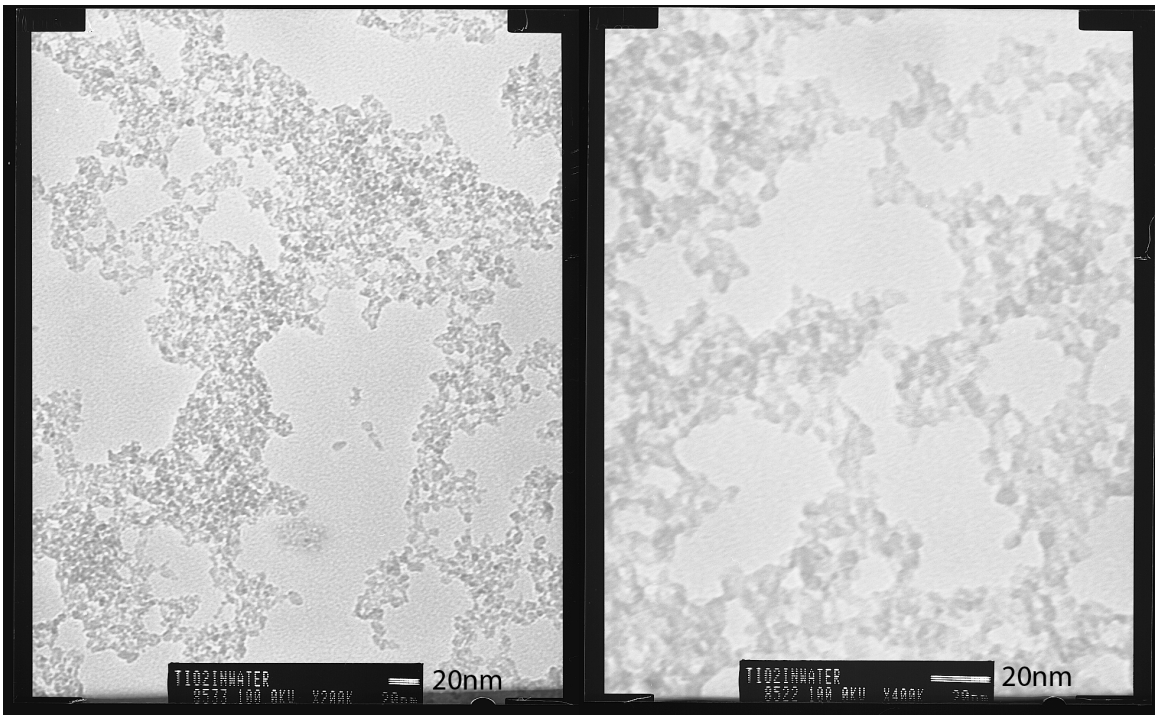

Figure A.6.4: TiO_2 nanoparticles dissolved into deionised water. (TEM pictures)

The TiO_2 nanoparticles are polydisperse (size below 10nm) and are aggregated (Figure A.6.4). They are polycrystalline (Figure A.6.5) and are made of anatase (Table A.6).

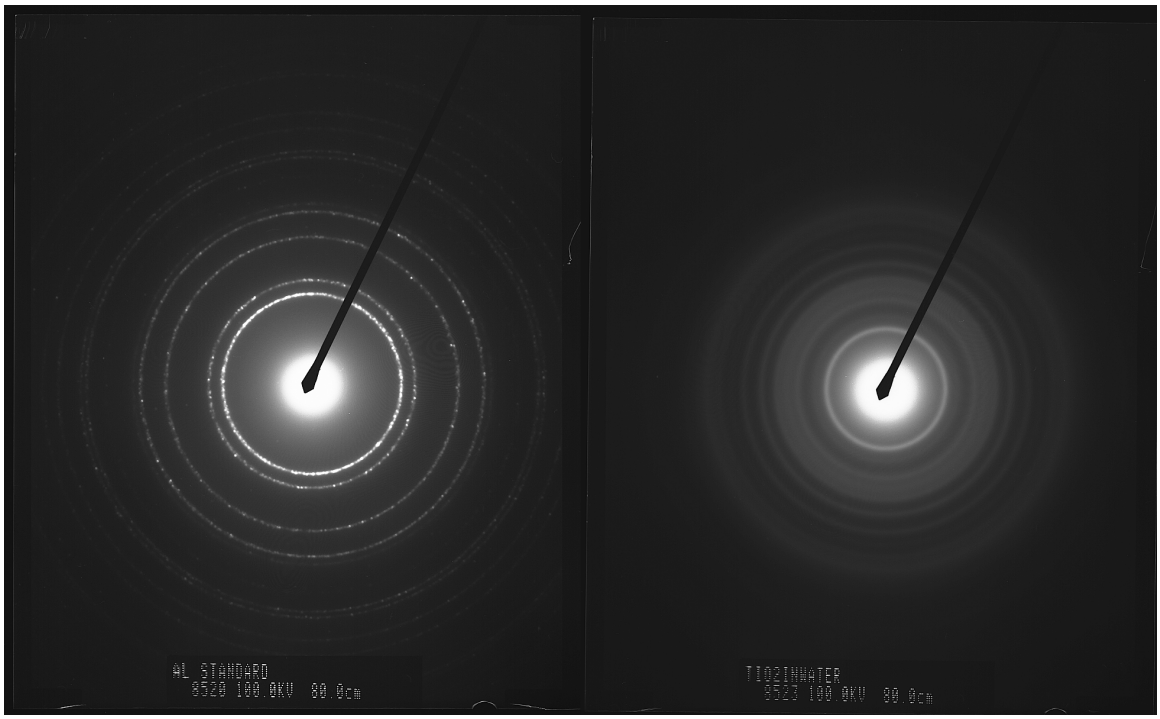

Figure A.6.5: Single Area Electron Diffraction patterns of the aluminium standard (left) and of the TiO_2 nanoparticles (right).

Al standard	diameter (cm)	known interplanar distance (Å)	K (cm.Å)
1st ring	2.56	2.338	5.9853
2nd ring	2.95	2.024	5.9708
3rd ring	4.19	1.431	5.9959
4th ring	4.92	1.221	6.0073
5th ring	5.13	1.169	5.9970
6th ring	6.47	1.0124	6.5502
7th ring	6.65	0.9289	6.1772
8th ring	7.28	0.9055	6.5920
		average	5.9913
		stdev	0.0138
		%	0.2310

TiO_2 NPs	diameter (cm)	calculated interplanar distance (Å)	JCPDS 21-1272 interplanar distance (Å)	anatase Intensity	hkl
1st ring	1.7	3.5243	3.52	100	101
2nd ring (hazy)	2.07	2.8943	2.431	10	103
3rd ring	2.53	2.3681	2.378	20	004
4th ring (hazy)	2.84	2.1096	2.332	10	112
5th ring	3.13	1.9141	1.892	35	200
6th ring	3.56	1.6829	1.6999	20	105
7th ring	4.09	1.4649	1.6665	20	211
8th ring	4.41	1.3586	1.493	4	213
			1.4808	14	204
			1.3641	6	116

Table A.6: Determination of the interplanar distances of the TiO_2 nanoparticles.

Appendix 7.

Color development.

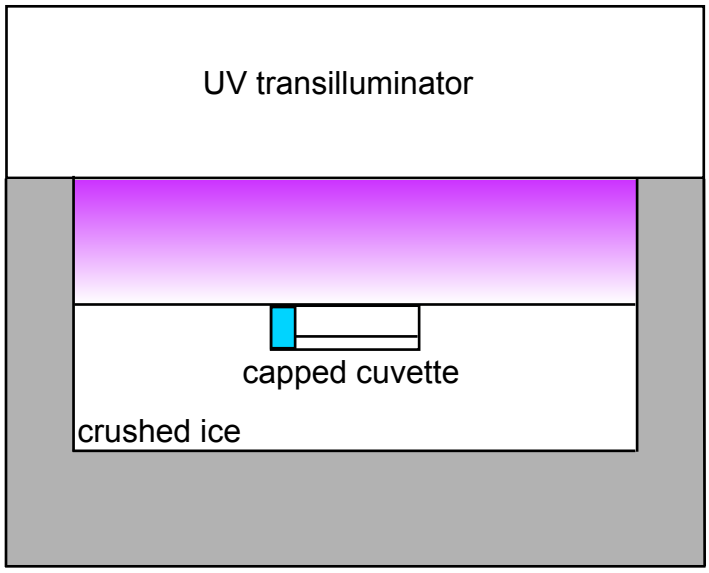

Figure A.7.1: Schema representing the longitudinal section of the experimental setup used to perform the color development.

An ultraviolet transilluminator (belonging to Professor Kawamura's laboratory, Hunter College, New York, USA) displaying six Sylvania lamps (15W each, 350nm) was used to excite our TiO_2 nanoparticles. Its upper cover is removable. The UV-light exposure time was set to be equal to the typical ELISA color-development time, i.e. 10 minutes. The UV-transparent cuvettes employed during our experiments are the ultra-micro Brand UV Cuvettes (15mm window height) on which a cap fits. Our developing solution (prepared right before the development) is made of methylviologen dichloride and sodium formate dissolved into sodium carbonate buffer pH~11. The solutions exposed to UV light are

composed of 1ml of sodium carbonate buffer pH~11 containing 10mM of methylviologen dichloride, 10mM of sodium formate and a given concentration of TiO_2 nanoparticles ($\leq 5.34 mg.ml^{-1}$). The volume of the solution exposed to UV light was set to 1ml leaving 1.4ml of air enclosed in the cuvette. It was a compromise between the dilution of the dye formed during the UV-light exposure and its consumption by O_2. During our experiments, no nitrogen gas was involved to facilitate them. The capped cuvettes were horizontally placed on crushed ice contained in a polystyrene box. The distance separating the cuvette from UV lamps was less than 10cm. The sample absorption was recorded right before the UV-light exposure, right after it, and after a certain time from 1100 to 190nm.

Appendix 8.

Protocol to covalently attach antibody to the surface of TiO_2 nanoparticles.

A.8.1. Information related to the chemicals and equipment needed.

Chemicals & equipment	Companies	Catalog numbers
NHS (N-Hydroxysuccinimide)	SigmaAldrich	130672-25G
EDC (N-(3-Dimethylaminopropyl)-N′-ethylcarbodiimide hydrochloride)	SigmaAldrich	E1769-25G
DOPAC (3,4-Dihydroxyphenylacetic acid)	SigmaAldrich	850217
Anti-mouse IgG (developed in goat)	SigmaAldrich	M8642
Mouse IgG	SigmaAldrich	I5381
Dialysis kit (dialysis cassettes, syringes)	Fisher Scientific Thermo Scientific	PI-66332 66332

Table A.8: Information related to the chemicals and equipemengt used to conjugate antibodies at the TiO_2-nanoparticle surface.

A.8.2. Reconstitution of the anti-mouse IgG in PBS buffer (antibody solution).

1. Add 8mg of NaCl into an Eppendorf tube.

2. Add 1ml of autoclaved deionized water into the Eppendorf tube.

3. Vortex it and centrifuge it for a few seconds to get all the solution at the bottom of the Eppendorf tube.

4. Add the mixture to the vial containing the antibody and gently rotate it until the powder dissolves.

Features of the antibody solution:

total volume = 1 ml, [antibody solution] = 1mg/ml or] ~ 6.67µM since MW (antibody) ~ 150kDa, [PBS] = 0.01M, [NaCl] = 0.150M and pH = 7.2.

A.8.3. Preparation of the 0.05M MES buffer solution pH ~ 5.2.

1. Put 4.88 g of MES in a glass bottle.

$m = 0.05M \times 0.5L \times 195.23g.mol^{-1} = 4.88g$

2. Add 500 ml of autoclaved water and a clean magnetic stirrer.

3. Stir the solution until the powder is dissolved.

4. Mix 5 NaOH pellets and 10ml of autoclaved deionized water in a Falcon tube and vortex it until the pellets are completely dissolved.

Add a given amount of NaOH solution to fix the pH at 5.2.

5. Filter the solution using a filtering unit.

A.8.4. Dialysis of the anti-mouse IgG against MES buffer.

1. Fill a plastic beaker with 300 ml of MES buffer prepared earlier.

2. Add a clean stirring magnet into the beaker and cover it with parafilm.

3. Fill the dialysis cassette with the antibody solution using the provided syringe.

4. Place the cassette within the plastic beaker and cover it with parafilm.

5. Place it inside a fridge containing a magnetic plate. (Laboratory of Dr. Dixie Goss, Hunter College, New York, USA)

6. Let the cassette incubate for 6 hours at 4°C.

7. Collect the solution trapped in the cassette and put it in an Eppendorf tube.

A.8.5. DOPAC/TiO_2 redispersed in MES buffer.

1. Take 1ml of native TiO_2 solution (1ml of TIP, 20ml of isopropanol and 50ml of water)

2. Centrifuge it at 14,000 rpm during 30 minutes and remove the supernatant. (you should see a deposit of a transparent material)

3. Add 100µl of MES buffer and redisperse it using the ultrasounds until there is no deposit.

4. Add 900µl of MES buffer.

5. Steps 2, 3 and 4 have to be repeated twice more.

6. Keep some sample for DLS and UV-Vis measurements.

7. Add 40mg of DOPAC in the Eppendorf tube, in other words five times the amount of Ti ions to completely saturate the surface of the TiO_2 nanoparticles.

$[TiO_2] = 0.003412mol / 71ml = 4.817 \times 10^{-5} mol.ml^{-1}$

$m_{DOPAC} = 4.817 \times 10^{-5} mol.ml^{-1} \times 1ml \times 168.15g.mol^{-1} = 8.1mg$

8. Let it incubate overnight at 4°C.

9. Centrifuge at 14,000rpm during 30min. and remove the supernatant.

10. Add 1ml of MES.

11. Steps 10 and 11 have to be repeated twice more.

12. Redisperse the DOPAC-coated TiO_2 nanoparticles in 80µl of MES buffer.

Keep some sample to perform some DLS and UV-vis measurements.

Provided that LPCT (ligand-to-particle charge transfer) band of DOPAC-coated TiO_2 nanoparticles should be visible at 420 nm, the grafting of DOPAC should be revealed by UV-Vis measurements.

A.8.6. Antibody conjugation to the DOPAC-coated TiO_2 nanoparticles via EDC/NHS process.

1. Mix 383.4mg of EDC and 10 ml of MES in a Falcon tube.

$m = 200mM \times 0.01L \times 191.71g.mol^{-1} = 0.038342g \sim 383.4mg$

2. Mix 920.7mg of NHS and 10 ml of MES in a Falcon tube.

$m = 800mM \times 0.01L \times 115.09g.mol^{-1} = 0.92072g \sim 920.7mg$

3. Add 10µl of EDC and 10µl of NHS into 80µl of DOPAC-coated TiO_2-nanoparticle solution to activate their carboxylic groups.

4. Let it incubate at room temperature during 10min.

5. Centrifuge it at 14,000rpm during 10min. and remove the supernatant in order to get rid of all of the EDC and NHS, which did not activate the carboxylic groups of DOPAC-coated TiO_2-nanoparticle. They could potentially activate the ones of the antibodies, resulting in their own attachment.

6. Add 100µl of MES to the activated DOPAC-coated TiO_2 nanoparticles and the entire volume of antibody solution.

7. Let it incubate for 3h at room temperature.

8. Centrifuge at 14,000rpm during 10min., remove the supernatant and add 200µl of MES. The step 6 has to be repeated twice more.

9. Store 10µl to perform DLS measurements. The attachment of the antibody should be revealed by the DLS measurements.

A.8.7. Dialysis of the TiO_2-labeled antibodies against PBS buffer.

1. Fill a plastic beaker with 300 ml of PBS buffer prepared earlier.

2. Add a clean stirring magnet into the beaker and cover it with parafilm.

3. Fill the dialysis cassette with the TiO_2-labeled antibody solution using the provided syringe.

4. Place the cassette within the plastic beaker and cover it with parafilm.

5. Place it inside a fridge containing a magnetic plate. (Laboratory of Dr. Dixie Goss, Hunter College, New York, USA)

6. Let the cassette incubate for 6 hours at 4°C.

7. Collect the solution trapped in the cassette and put it in an Eppendorf tube.

Appendix 9.

Optimization of the TiO_2-labeled antibody concentration.

A.9.1. Reconstitution of the mouse IgG in PBS buffer (antigen solution).

1. Add 8mg of NaCl into an Eppendorf tube.

2. Add 1 ml of autoclaved deionized water into the Eppendorf tube.

3. Vortex it and centrifuge it for a few seconds to get all the solution at the bottom of the Eppendorf tube.

4. Add the mixture to the vial containing the antibody and gently rotate it until the powder dissolves.

5. Store 900 ul of Ag solution and with the 100 left do serial dilutions.

$0.1 mg.ml^{-1}$, $10 \mu g.ml^{-1}$, $1 \mu g.ml^{-1}$, $0.1 \mu g.ml^{-1}$ (need of 400µl for each concentration).

A.9.2. Optimization of the TiO_2-labeled antibody concentration. (adapted from the ELISA protocol of Abcam [72])

Wash buffer: 0.05% Tween20 in PBS buffer.

Blocking buffer: 0.1% BSA in PBS buffer.

Two concentrations of antigen solutions are tried: 0 and 20μg.ml^{-1}.

Two relative concentrations of TiO_2-labeled antibodies (compared to the amount of TiO_2 present in 1ml) are tried: 1/10 and 1/2000.

Number of samples = 2 × 2 × 3 = 12

1. Add 100μl of antigen solution into each cuvette (3 trials) and cover them.

2. Let it incubate overnight at 4°C.

3. Remove the liquid with a pipet and rinse twice the cuvette with 100μl of wash buffer.

4. Flip dry on a stack of Kimwipes.

5. Add 200μl of blocking buffer, close the cuvette and let it incubate overnight at 4°C.

6. Remove the liquid with a pipet and rinse twice the cuvette with 100μl of wash buffer.

7. Flip dry on a stack of Kimwipes.

8. Add 100μl of TiO_2-labeled antibody solution.

9. Let it incubate overnight at 4°C.

11. Pipet the liquid to remove it and rinse twice the cuvette with 100μl of wash buffer.

12. Flip dry on a stack of Kimwipes.

13. Add 100μl of developing solution and measure the absorbance.

Appendix 10.

Notes.

1. Wootz: Piece of ancient Indian steel whose production required the use of wood from Cassia auriculata, the leaves from Calotropis gigantea and ores from given Indian mines.[2]

2. This expression refers to cells either subjected to genetic mutations, or infected by viruses or parasites, or affected by cancer.

3. Epidermal Growth Factor Receptor. The extent of the EGFR overexpression on the malignant-cell surface is cancer-type dependent.

4. Cetyltrimethylammonium bromide.

5. Receptor domain overexpressed by certain cancer cells such as glioblastoma multiforme.

6. 3,4-dihydroxyphenylacetic acid (dopamine derivative).

7. 3-sulfo-1-hydroxysuccinimide / 1-ethyl-3-[3-dimethylaminopropyl] carbodiimide hydrochloride.

8. NanoPhotonic Explorers for Biomedical use by Biologically Localized Embedding.

9. "Cancer cells pump the introduced drug molecules back out into the extracellular environment."[6]

10. N-isopropylacrylamide.

11. N,N'-methylenebisacrylamide.

12. Small interference RNA.

13. Poly(2-(dimethylamino)ethyl methacrylate).

14. Poly(2-(dimethylamino)ethyl methacrylate-b-poly(ethyleneglycol) α-methoxy, ω-methacrylate.

15. The hapten-labeled DNA oligonucleotides result from the hybridization of a long DNA oligonucleotide (called biobarcodes) and a short hapten-labeled DNA oligonucleotides.

Hapten: small molecule that can elicit an immune response when attached onto a larger carrier.

16. Complementary Metal-Oxide-Silicon.

17. Any two adjacent conductors can be considered as a capacitor, although the capacitance will be small unless the conductors are close together or long.

"Usually, the capacitance between two coplanar strips (…) is comparable to the stray capacitance of the leads (conductors that connect the electrodes with the electrical excitation source)."[26]

18. Heavily-doped polycrystalline silicon typically employed in CMOS technology.

19. Phosphoric acid (H_3PO_4) was mixed with NaOH to fix the pH at 7. This pH is supposed to be optimal for antibody/antigene binding interaction.

20. Poly(ethylene glycol acrylamide) and 800 refers to the molecular weight of the chain.

21. Fluorenylmethyloxycarbonyl. It is a fluorescent protection group.

22. 1mg of elastase is dissolved into 1ml of glycine/NaOH buffer whose pH is 8.4. (25ml of 0.2M glycine, 2ml of 0.2M NaOH and 73ml of deionised water are mixed to prepare 100ml of buffer solution.)

Bibliography.

1. Chang, K., *Tiny is beautiful: translating 'nano' into practical.* The New York Times, 2005.

2. Reibold, M., et al., *Materials: carbon nanotubes in an ancient Damascus sabre.* Nature, 2006. **444**: p. 286-286.

3. Tani, T., Photographic sensitivity: theory and mechanisms., 1995: p. 1-264.

4. Melancon, M.P., et al., *In vitro and in vivo targeting of hollow gold nanoshells directed at epidermal growth factor receptor for photothermal ablation therapy.* Molecular Cancer Therapeutics, 2008. **7**(6): p. 1730-1739.

5. Rozhkova, E.A., et al., *A high-performance nanobio photocatalyst for targeted brain cancer therapy.* Nano Letters, 2009. **9**(9): p. 3337-3342.

6. Kopelman, R., et al., *Multifunctional nanoparticle platforms for in vivo MRI enhancement and photodynamic therapy of a rat brain cancer.* Journal of Magnetism and Magnetic Materials, 2005. **293**: p. 404-410.

7. Samsam Bakhtiari, A.B., et al., *An efficient method based on the photothermal effect for the release of molecules from metal nanoparticle surface.* Angewandte Chemie International Edition, 2009. **48**: p. 4166-4169.

8. Li, D., et al., *Thermosensitive copolymer networks modify gold nanoparticles for nanocomposite entrapment.* Chemistry - a European Journal, 2007. **13**: p. 2224-2229.

9. Kong, W.-H., et al., *Efficient intracellular siRNA delivery strategy through rapid and simple two steps mixing involving noncovalent post-PEGylation.* Journal of Controlled Release, 2009. **138**: p. 141-147.

10. Xie, J., et al., *Ultrasmall c(RGDyK)-coated Fe_3O_4 nanoparticles and their specific targeting to integrin $\alpha_v\beta_3$-rich tumor cells.* Journal of the American Chemical Society, 2008. **130**(24): p. 7542-7543.

11. Schwartzberg, A.M., et al., *Synthesis, characterization, and tunable optical properties of hollow gold nanospheres.* Journal of Physical Chemistry B, 2006. **110**(40): p. 19935-19944.

12. Schild, H.G., *Poly(N-isopropylacrylamide): experiment, theory and application.* Progress in Polymer Science, 1992. **17**: p. 163-249.

13. Thornton, P.D., et al., *Enzyme-responsive hydrogel particles for the controlled release of proteins: designing peptide actuators to match payload.* Soft Matter, 2008. **4**: p. 821-827.

14. Bruchez, M.J., et al., *Semiconductor nanocrystals as fluorescent biological labels.* Science, 1998. **281**: p. 2013-2016.

15. Mirkin, C.A., et al., *A DNA-based method for rationally assembling nanoparticles into macroscopic materials.* Nature, 1996. **382**: p. 607-609.

16. Elghanian, R., et al., *Selective colorimetric detection of polynucleotides based on the distance dependent optical properties of gold nanoparticles.* Science, 1997. **277**: p. 1078-1080.

17. Nam, J.-M., S.-Y. Park, and C.A. Mirkin, *Bio-barcodes based on oligonucleotide-modified nanoparticles.* Journal of the American Chemical Society, 2002. **124**(15): p. 3820-3821.

18. Park, S.-Y., T.A. Taton, and C.A. Mirkin, *Array-based electrical detection of DNA with nanoparticle probes.* Science, 2002. **295**: p. 1503-1506.

19. de la Rica, R., C. Fernández-Sánchez, and A. Baldi, *Polysilicon interdigitated electrodes as impedimetric sensors.* Electrochemistry Communications, 2006. **8**: p. 1239-1244.

20. Varshney, M. and L. Yanbin, *Interdigitated array microelectrodes based impedance biosensors for detection of bacterial cells.* Biosensors and Bioelectronics, 2009. **24**: p. 2951-2960.

21. Van Gerwen, P., et al., *Nanoscaled interdigitated electrode arrays for biochemical sensors.* Sensors and Actuators B, 1998. **49**: p. 73-80.

22. de la Rica, R., A. Baldi, and C. Fernández-Sánchez, *Local detection of enzymatic ion generation with polycrystalline silicon interdigitated electrodes and its application to biosensing.* Applied Physics Letters, 2007. **90**(074102): p. 1-3.

23. Umetsu, M., et al., *Zinc oxide-binding antibody and use there of.* Patent application number: 20100173360 2010.

24. Lee, W.-Y., et al., *Microfabricated conductometric urea biosensor based on sol-gel immobilized urease.* Electroanalysis, 1999. **12**(1): p. 78-82.

25. de la Rica, R., et al., *Single-cell pathogen detection with a reverse-phase immunoassay on impedimetric transducers.* Analytical Chemistry, 2009. **81**(18): p. 7732-7736.

26. Mamishev, A.V., et al., *Interdigitated sensors and transducers.* Proceedings of the IEEE, 2004. **92**(5): p. 808-845.

27. Tesla, N., *Electrical condenser.* US Patent 464 667, 1891.

28. Webster, M.S., et al., *Computer aided modelling of an interdigitated microelectrode array impedance biosensor for the detection of bacteria.* IEEE Transactions on Dielectrics and Electrical Insulation, 2009. **16**(5): p. 1356-1363.

29. Berggren, C., B. Bjarnason, and G. Johansson, *Capacitive biosensors.* Electroanalysis, 2001. **13**(3): p. 173-180.

30. de la Rica, R., et al., *Selective detection of live pathogens via surface-confined electric field perturbation on interdigitated silicon transducers.* Analytical Chemistry, 2009. **81**(10): p. 3830-3835.

31. Fernández-Sánchez, C., et al., *Disposable noncompetitive immunosensor for free and total prostate-specific antigen based on capacitance measurement.* Analytical Chemistry, 2004. **76**(19): p. 5649-5656.

32. Rickert, J., et al., *A 'mixed' self-assembled monolayer for an impedimetric immunosensor.* Biosensors and Bioelectronics, 1996. **11**(8): p. 757-768.

33. de la Rica, R., et al., *Label-free cancer cell detection with impedimetric transducers.* Anal Chem, 2009. **81**(24): p. 10167-71.

34. de la Rica, R., et al., *Peptide-nanotube biochips for label-free detection of multiple pathogens.* Small, 2010. **6**(10): p. 1092-1095.

35. Segura-Quijano, F., et al., *Towards fully integrated wireless impedimetric sensors.* Sensors, 2010. **10**: p. 4071-4082.

36. de la Rica, R., C. Fernández-Sánchez, and A. Baldi, *Electric preconcentration and detection of latex beads with interdigitated electrodes.* Applied Physics Letters, 2007. **90**: p. 174104-1 -174104-3.

37. National Cancer Institute, http://www.cancer.gov/cancertopics/types/prostate, 2010.

38. Fujita, K., et al., *Specific detection of prostate cancer cells in urine by multiplex immunofluorescence cytology.* Hum Pathol, 2009. **40**(7): p. 924-33.

39. Markx, G.H. and C.L. Davey, *The dielectric properties of biological cells at radiofrequencies: applications in biotechnology.* Enzyme and Microbial Technology 1999. **25**(3-5): p. 161-171.

40. Wegener, J., A. Janshoff, and C. Steinem, *The quartz crystal microbalance as a novel means to study cell-substrate interactions in situ.* Cell Biochem Biophys, 2001. **34**(1): p. 121-51.

41. Arnold, L.J., Jr., et al., *Antineoplastic activity of poly(L-lysine) with some ascites tumor cells.* Proc Natl Acad Sci U S A, 1979. **76**(7): p. 3246-50.

42. Wittmer, C.R., et al., *Fibronectin terminated multilayer films: protein adsorption and cell attachment studies.* Biomaterials, 2007. **28**(5): p. 851-60.

43. Lavery, C.B., et al., *Purification of peroxidase from horseradish (Armoracia rusticana) roots.* Journal of Agricultural and Food Chemistry, 2010. **58**: p. 8471-8476.

44. Horseradish peroxidase product information (Sigma-Aldrich).

45. Xu, J., et al., *Photokilling cancer cells using highly cell-specific antibody-TiO_2 bioconjugates and electroporation.* Bioelectrochemistry, 2007. **71**: p. 217-222.

46. Larsen, S.T., et al., *Nano titanium dioxide particles promote allergic sensitization and lung inflammation in mice.* Basic & Clinical Pharmacology & Toxicology, 2009. **106**: p. 114-117.

47. Rajh, T., et al., *Surface modification of small particle TiO_2 colloids with cysteine for enhanced photochemical reduction: an EPR study* Journal of Physical Chemistry, 1996. **100**(11): p. 4538-4545.

48. 3,3',5,5'-Tetramethylbenzidine product information (Sigma-Aldrich).

49. Silverman, F.P., et al., *Salicylate activity. 1. Protection of plants from paraquat injury.* J Agric Food Chem, 2005. **53**(25): p. 9764-8.

50. Ebbesen, T.W., G. Levey, and L.K. Patterson, *Photoreduction of methyl viologen in aqueous neutral solution without additives.* Nature, 1982. **298**: p. 545-547.

51. Moser, J., et al., *Surface Complexation of Colloidal Semiconductors Strongly Enhances Interfacial Electron-Transfer Rates.* Langmuir, 1991. **7**(12): p. 3012-3018.

52. Prado, A.G.S. and L.L. Costa, *Photocatalytic decouloration of malachite green dye by application of TiO_2 nanotubes.* Journal of Hazardous Materials, 2009. **169**: p. 297-301.

53. Chen, C.-Y., *Photocatalytic degradation of azo dye reactive orange 16 by TiO_2.* Water Air Soil Pollution, 2009. **202**: p. 335-342.

54. Ogino, C., et al., *Recognition and effective degradation of 17β-Estradiol by anti-estradiol-antibody-immobilized TiO_2 nanoparticles.* Journal of Bioscience and Bioengineering, 2007. **104**(4): p. 339-342.

55. Zan, L., et al., *Photocatalysis effect of nanometer TiO_2 and TiO_2-coated ceramic plate on Hepatitis B virus.* Journal of Photochemistry and Photobiology B: Biology, 2007. **86**: p. 165-169.

56. Matsunaga, T., et al., *Photoelectrochemical sterilization of microbial cells by semiconductor powders.* FEMS Microbiology Letters, 1985. **29**: p. 211-214.

57. Triantaphylidès, C. and M. Havaux, *Singlet oxygen in plants: production, detoxification and signaling.* Trends in Plant Science, 2009. **14**(4): p. 219-228.

58. Tachikawa, T., et al., *Direct observation of the one-electron reduction of methyl viologen mediated by the CO_2 radical Anion during TiO_2 photocatalytic reactions.* Langmuir, 2004. **20**(22): p. 9441-9444.

59. Treguer, M., et al., *Enhanced yield of photoinduced electrons in doped silver halide crystals.* Nature, 1999. **402**(6764): p. 865-867.

60. Liu, S. and T. Saji, *Photocatalytic formations of patterning dye films with TiO_2 particles based on chromogenic development of photography.* Bulletin of the Chemical Society of Japan, 1997. **70**(4): p. 755-760.

61. Jones, R.W. and P.B. Garland, *Sites and specificity of the reaction of bipyridylium compounds with anaerobic respiratory enzymes of Escherichia coli. Effects of*

permeability barriers imposed by the cytoplasmic membrane. Biochem J, 1977. **164**(1): p. 199-211.

62. Ridley, H., et al., *Development of a viologen-based microtiter plate assay for the analysis of oxyanion reductase activity: Application to the membrane-bound selenate reductase from Enterobacter cloacae SLD1a-1.* Analytical Biochemistry, 2006. **358**: p. 289-294.

63. Gao, Y. and I. Kyratzis, *Covalent immobilization of proteins on carbon nanotubes using the cross-linker 1-ethyl-3-(3-dimethylaminopropyl)carbodiimide--a critical assessment.* Bioconjug Chem, 2008. **19**(10): p. 1945-50.

64. Qi, L., et al., *Redispersible hybrid nanopowders: cerium oxide nanoparticle complexes with phosphonated-PEG oligomers.* ACS Nano, 2008. **2**(5): p. 879-88.

65. Edwards, M.O.M., et al., *'Electric-paint display' with carbon counter electrodes* Electrochimica Acta, 2001. **46**(13-14): p. 2187-2193.

66. Ghica, M.E. and C.M.A. Brett, *A glucose biosensor using methyl viologen redox mediator on carbon film electrodes.* Analytica Chimica Acta, 2005. **532**(2): p. 145-151.

67. Pejoux, C., R. de la Rica, and H. Matsui, *Biomimetic crystallization of sulfide semiconductor nanoparticles in aqueous solution.* Small, 2010. **6**(9): p. 999-1002.

68. Watanabe, T. and K. Honda, *Measurement of the extinction coefficient of the methyl viologen cation radical and the efficiency of its formation by*

semiconductor photocatalysis. The Journal of Physical Chemistry, 1982. **86**(14): p. 2617-2619.

69. *Tryptan blue product information (Sigma Aldrich).* http://sigma-aldrich.custhelp.com/app/answers/list/p/21,82.

70. Ma, L., et al., *Oxidative stress in the brain of mice caused by translocated nanoparticulate TiO_2 delivered to the abdominal cavity.* Biomaterials, 2010. **31**(1): p. 99-105.

71. Mahshid, S., M. Askari, and M.S. Ghamsari, *Synthesis of TiO_2 nanoparticles by hydrolysis and peptization of titanium isopropoxide solution.* Journal of Materials Processing Technology, 2007. **189**(1-3): p. 296-300.

72. *Direct ELISA protocol (Abcam).*